Université de Montréal

Magnetic Properties of Paramagnetic Systems: Density Functional Studies

par
Seongho Moon

Département de Chimie
Faculté des Arts et des Sciences

Thèse présentée à la faculté des études supérieures
en vue de l'obtention du grade de
Philosophiae Doctor (Ph. D)
en Chimie

Mai 2003

Université de Montréal
Faculté des études supérieures

Cette thèse intitulée

Magnetic Properties of Paramagnetic Systems:
Density Functional Studies

présentée par:
Seongho Moon

a été évaluée par un jury composé des personnes suivantes:

Professeur Tucker Carrington, Président-rapporteur
Professeur Dennis R. Salahub, Directeur de recherche
Professeur Mathias Ernzerhof, Membre du jury
Professeur Vladimir G. Malkin, Examinateur externe
Michel Côté, représentant du doyen de la FES

RESUME

Le propos principal de cette thèse est d'étudier les propriétés magnétiques des espèces paramagnétiques possédant des électrons non appariés. Cette étude a été réalisée à l'aide de la théorie de la fonctionnelle de la densité (DFT).

Afin de simuler correctement les paramètres de résonance magnétique, nous proposons une approche combinée mécanique quantique/mécanique moléculaire (QM/MM). La région quantique est tronquée par des potentiels capuchons à un électron quantique (QCP) qui sont paramétrés de façon à reproduire les structures moléculaires comportant tous les électrons ainsi que les distributions de charge. Les effets de l'environnement sont modélisés en incluant le champ électrique, causé par le domaine MM, dans l'Hamiltonien DFT. Cette approche montre que les effets électrostatiques dus à la partie MM transfèrent principalement à la partie QM à travers les orbitales Kohn-Sham non soumises au champ et donc implicitement aux énergies correspondantes. Nous examinons plusieurs systèmes modèles partant de petites molécules organiques et allant jusqu'à des modèles biologiques. Grâce à la simplicité de l'implémentation, l'approche présentée ici nous permet d'étudier les paramètres magnétiques de modèles réalistes notamment des sites actifs biologiques.

Nous présentons une expression générale pour les déplacements RMN paramagnétiques qui est indépendante des paramètres empiriques et permet des applications de calculs. Pour un cas particulier (doublet Kramers spatialement non dégénéré) dans lequel il n'existe pas d'états excités accessibles thermiquement, l'équation exécutable pour les déplacements paramagnétiques est dérivée en utilisant un Hamiltonien effectif de spin et la statistique de Boltzmann. Les déplacements chimiques RMN paramagnétiques sont décomposés en trois contributions dans notre équation : une contribution orbitalaire, une contribution de contact de Fermi et enfin une contribution de pseudo-contact. Les contributions individuelles sont déterminées par les calculs ab initio des paramètres de résonance magnétique. Afin de valider ce travail, des calculs DFT ont été réalisés pour les déplacements chimiques RMN de certains complexes d'oxydes d'azote, de

protéine/cuivre bleu et d'imidazole cyanidrique ferrique. Les études théoriques, comparées avec les travaux expérimentaux, fournissent trois indications principales : (1) l'approche présentée ici dans le cadre de la DFT donne des simulations fiables et prometteuses. (2) les déplacements orbitalaires sont facilement approximés par les déplacements chimiques RMN dans des environnements à couche fermée similaires. (3) les déplacements de contact de Fermi dominent le déplacement chimique total et sont très sensibles aux changements structurels.

Mots-clés: théorie de la fonctionnelle de la densité, QM/MM, QCP, Hamiltonien effectif de spin, déplacement orbitalaire, déplacement de contact de Fermi, déplacement de pseudo-contact, paramètres de résonance magnétique.

ABSTRACT

The main concern of this thesis is to investigate the magnetic properties of paramagnetic species which have unpaired electrons. The present study is based on density functional theory (DFT).

In order to simulate magnetic resonance parameters efficiently, we propose a combined quantum mechanics/molecular mechanics (QM/MM) approach. The quantum region is truncated by one-electron quantum capping potentials (QCPs) which are parameterized to duplicate all-electron molecular structures and charge distributions. The effects from the surroundings are modeled by including the electric field, due to the MM domain, in the DFT Hamiltonian. This approach shows that the electrostatic effects from the MM part mainly transfer to the QM part implicitly through the field-free Kohn-Sham orbitals and through the corresponding energies. We examine several model systems ranging from small organic molecules to biological models. Because of the simplicity of the implementation, the present approach enables us to investigate the magnetic parameters of large, realistic models of biological active sites.

For paramagnetic NMR shifts, we provide a general expression which is independent of empirical parameters and give the recipe for practical calculations. For a special case (spatially non-degenerate Kramers doublet) with no thermally accessible excited states, the working equation for the paramagnetic shifts is derived by using an effective spin Hamiltonian and Boltzmann statistics. The paramagnetic NMR shifts are decomposed into the three contributions within the equation: the orbital, Fermi contact, and pseudocontact contributions. The individual contributions are determined by the first-principles calculations of the magnetic resonance parameters. For validation, the DFT calculations are carried out for the NMR chemical shifts of some nitroxides, blue copper proteins, and ferric cyanide-imidazole complexes. The theoretical studies, compared with the experimental works, indicate mainly three things: (1) the present approach within the DFT framework provides reliable and promising simulations; (2) the orbital shifts are readily approximated by the NMR chemical shifts in similar, closed-shell environments;

(3) the Fermi contact shifts dominate the total shifts and they are very sensitive to structural changes.

Key words: Density functional theory, QM/MM, QCP, effective spin Hamiltonian, orbital shift, Fermi contact shift, pseudocontact shift, magnetic resonance parameters.

ACKNOWLEDGEMENTS

During my study, I have realized that I am a really tiny existence in the vast ocean of science. I am sure that I would lose my way there without the guidance of my supervisor, Professor Dennis R. Salahub. I cannot but thank you for expanding my horizons in science and making me scientist. The driving force that I could overcome adversity in the days arose from the fact that I wanted to be your real student.

I would like to thank Dr. Serguei Patchkovskii for letting me understand the big picture and details of magnetic properties (specially, paramagnetic NMR theory). I cannot forget happy moments while doing science and sports together.

I am grateful to Dr. Gino DiLabio for providing carbon capping potentials and for fruitful discussions of QM/MM theories.

I wish to acknowledge the present and past members of Salahub group, Mark, Steeve, Sébastian, Elisa, Delphine and the present and past members of SIMS theory group, John, Dennis, Raphael, Hilaire, Sergei, Nelaine, Luciano, Gwang-Soo, Yoshii for your kind support and stimulating discussions.

For my wife Ge Won and my daughter Yejin .....

TABLE OF CONTENTS

LIST OF TABLES

LIST OF FIGURES

LIST OF ABBREVIATIONS

DFT	Density Functional Theory
HK	Hohenberg and Kohn
KS	Kohn and Sham
XC	Exchange-Correlation
LDA	Local Density Approximation
LSDA	Local Spin Density Approximation
GGA	Generalized Gradient Approximation
PW86	Perdew-Wang86
B88	Becke88
PW91	Perdew-Wang91
LYP	Lee, Yang, and Parr
OEP	Optimized Effective Potential
KLI	Krieger, Li, and Iafrate
BP	Breit-Pauli
UDFT	Uncoupled Density Functional Theory
FPT	Finite Perturbation Theory
NMR	Nuclear Magnetic Resonance
EPR	Electron Paramagnetic Resonance
ESR	Electron Spin Resonance
GIAO	Gauge Including Atomic Orbital
IGLO	Individual Gauge for Localized Orbital
LMO	Localized Molecular Orbital
CO	Canonical Orbital
SOS-DFPT	Sum-Over-State Density Functional Perturbation Theory
FC	Fermi Contact
QM/MM	Quantum Mechanics/Molecular Mechanics
QCP	Quantum Capping Potential
LA	Link Atom
LSCF	Localized Self-Consistent Field

GHO	Generalized Hybrid Orbital
ECP	Effective Core Potential
MO	Molecular Orbital
CMP	Cytosine MonoPhosphate
deMon	density-functional Montreal
DZVP	Double Zeta plus Polarization
PDB	Protein Data Bank
RESP	Restrained ElectroStatic Potential
PPDME	ProtoPorphyrinIX DiMethyl Ester
Mb	Myoglobin
Hb	Hemoglobin
Cyt-c	Cytochrome
HRP	HorseRadish Peroxidase
revPBE	revised Perdew, Burke, and Ernzerhof
STO	Slater Type Orbital

INTRODUCTION

Most fields of magnetic resonance parameters (e.g. NMR chemical shifts, nuclear spin-spin coupling constants, ESR A-tensors and g-tensors) have already been conquered by first-principles electronic structure methods [1-5]. Therefore, the thesis focuses on two major, related subjects which are beyond the limit of the present methods. One is a combined quantum mechanics/molecular mechanics (QM/MM) approach which enables us to simulate the magnetic resonances of macromolecules including proteins and nucleic acids. The other is NMR chemical shifts of paramagnetic species (open-shell systems) which have not been explored properly yet by first-principles methods.

Despite remarkable progress in computational chemistry in recent years, first-principles calculations for the magnetic resonance parameters of large biological and chemical systems are still far from routine. However, since most magnetic properties are local, we can divide the large system into the small reactive parts which are treated by high level quantum mechanics (QM) and the bulk which is treated by molecular mechanics (MM). This hybrid method has two intrinsic problems: (1) how to partition the system into the QM and MM regions; (2) how to treat interactions between two regions. Here, we propose a QM/MM method to overcome the problems and to keep the balance between accuracy and expediency for evaluation of the magnetic resonance parameters of large systems such as proteins and nucleic acids. In the present approach, the frontier bonds between QM and MM regions are capped by one-electron quantum capping potentials (QCPs) which are parameterized to mimic the electronic character of a methyl group at the QM/MM boundary [6]. The advantages of this approach is that QCPs can be incorporated in most DFT programs with minimal code modification since they follow the format and concept of conventional effective core potentials (ECP) [7]. Furthermore, some artificial effects of the link atom methods [8] and the special basis set manipulations of the localized self-consistent field (LSCF) [9] and the generalized hybrid orbital (GHO) [10] methods can be avoided and the number of electrons in the QM boundary can be reduced greatly compared to with the pseudobond approach [11]. In this approach, the QM parts are influenced by the the electrostatic effect of the environment

represented by MM partial atomic charges. This description appears to be adequate in calculation of magnetic resonance parameters, as long as the MM part is not directly connected to the magnetic nuclei, and polarization effects of the QM part by MM partial charges dominate interactions between the QM and MM subsystems.

The importance of nuclear magnetic resonance (NMR) spectroscopy for studies of paramagnetic species (open-shell system), particularly in biomolecules, cannot be overestimated [12-14]. Paramagnetic NMR spectra serve as the source of long-range structural data [15-17] and provide a sensitive probe of the magnitudes and signs of the spin density distributions [18,19]. Unique features of paramagnetic spectra are represented by spectral line broadening and a huge expansion of the chemical shift scale. These result from the fact that the magnetic nuclei of paramagnetic species are strongly influenced by local magnetic fields arising from unpaired electrons. For the proper interpretation of the spectra, theoretical studies, which can give the direct relationship between the spectra and molecular and electronic structures, should be accompanied by experiments. So far, many theoretical approaches have been carried out to investigate the spectra [19-23]. However, frankly speaking, they are not pure theoretical approaches because they strongly depend on empirical parameters. Recent dramatic progress in the first-principles calculation of magnetic resonance parameters finally gives us a possibility to predict the spectra without any help of empirical factors. Hence, in the thesis, in order to achieve the goal, first, we derive a complete, general expression for the paramagnetic NMR shielding and give the recipe for practical calculations and, second, for a special case (spatially non-degenerate Kramers doublet) with no thermally populated excited states, the working formalisms for the paramagnetic shift are derived by using an effective spin Hamiltonian and Boltzmann statistics.

The rest of thesis is organized as follows: In Chapter 1, we provide a short review of the unit systems and general theories for electromagnetism. The general features of DFT are also explained, especially for exchange-correlation functionals, since this work is based on the DFT method. Finally, the theories and equations of various magnetic resonance parameters (such as NMR chemical shielding tensors, nuclear spin-spin coupling tensors,

electron-nuclear hyperfine tensors, and EPR g-tensors) are reviewed. We focus on the non-relativistic, one-component case, where magnetic parameters are treated as second-order properties, for practical reasons. In Chapter 2, we provide basic theories about QCPs and demonstrate how QCPs and MM charges can be handled in Kohn-Sham (KS) equations and how magnetic parameters are affected by them and this approach is applied to the magnetic parameter calculation for several model systems. In Chapter 3, we provide a complete, general expression for the paramagnetic chemical shifts using the Boltzmann statistics and derive working equations, which purely depend on the first-principles calculations, for an isolated Kramers doublet state. This approach is applied to the chemical shift calculations of several organic radicals and metalloprotein models. Finally in last chapter, some global conclusions are presented and possible future works are discussed.

References

1. Helgaker, T., Jaszuński M., Ruud, K., *Chem. Rev.* **1999**, 99, 293.
2. Malkin, V. G., Malkina, O. L., Erisson, L. A., Salahub, D. R., In *Modern Density Functional Theory: A Tool for Chemistry; Theoretical and Computational Chemistry*; Seminario, J. M., Politzer, P., Eds.; Elsevier, Amsterdam, 1995.
3. Malkina, O. L., Vaara, J., Schimmelpfennig, B., Munzarová, M., Malkin, V. G., Kaupp, M., *J. Am. Chem. Soc.* **2000**, 122, 9206.
4. Schreckenbach, G., Ph. D. Thesis, The University of Calgary, Canada, 1996.
5. Lenthe, E. van; Wormer, P. E. S.; Avoird, A. van der *J. Chem. Phys.* **1997**, 107, 2488.
6. DiLabio, G. A.; Hurley, M. M.; Christiansen, P. A. J. *Chem. Phys.* **2002**, 116, 9578.
7. (a) Christiansen, P. A.; Lee, Y. S.; Pitzer, K. S. *J. Chem. Phys.* **1979**, 71, 4445. (b) Christiansen, P. A.; Ermler, W. C.; Pitzer, K. S. *Ann. Rev. Phys. Chem.* **1985**, 36, 407. (c) Berger, A.; Dolg, M.; Küchle, W.; Stoll, H.; Preuss, H. *Mol. Phys.* **1993**, 80, 1431.
8. Singh, U.C.; Kollman, P.A. *J. Comput. Chem.* **1986**, 7, 718.
9. Assfeld, X.; Rivail, J.-L. *Chem. Phys. Lett.* **1996**, 263, 100.
10. Gao, J.; Amara, P.; Alhambra, C.; Field, M. J. *J. Phys. Chem. A* **1998**, 102, 4714.
11. Zhang, Y.; Lee, T.-S.; Yang, W. *J. Chem. Phys.* **1998**, 110, 46.
12. Bertini, I.; Luchinat, C., *NMR of Paramagnetic Molecules in Biological Systems*, Benjamin/Cummings, Menlo Park, CA, 1986.
13. Bertini, I.; Turano, P.; Vila, A. J., *Chem. Rev.* **1996**, 93, 2833.
14. Bertini, I; Luchinat, C.; Parigi, G., *Solution NMR of Paramagnetic Molecules*, Elsevier, Amsterdam, 2001.
15. Bertini, I.; Luchinat, C.; Piccoioli, *Methods Enzymol.* **2001**, 339, 314.
16. Bertini, I.; Luchinat, C.; Piccioli, M., *Concepts in Magn. Reson.* **2002**, 14, 259.
17. Allegrozzi, M.; Bertini, I.; Choi, S.-N.; Lee, Y.-M, Luchinat, C, *Eur. J. Inorg. Chem.* **2002**, 2121.

18. Bertini, I., Luchinat, C., *In Physical Methods*: *for Chemistrs*, edited by Drago, R. S., 2nd ed., HBJ, 1992, p. 500.

19. Lar Mar, G. N., Horrocks, Jr., W. D., *NMR of Paramagnetic Molecules: Principles and Applications*, Academic Press, New York and London, 1973.

21. McGarvey, B. R., *Coord. Chem. Rev.* **1998**, 170, 75.

22. McGarvey, B. R.; Batista, N. C.; Bezerra, C. W. B.; Schultz, M. S.; Franco, D. W., *Inorg. Chem.* **1998**, 37, 2865.

23. Lohr, L. L.; Miller, J. C.; Sharp, R. R. *J. Chem. Phys.* **1999**, 111, 10148.

Chapter 1. Theoretical Background

1.1. Electromagnetism

1.1.1. Units in Electromagnetism

Prior to exploring magnetic properties in quantum mechanics, the system of units should be mentioned. In spite of the attempted standardization to the MKS-SI system of units, the cgs-Gaussian system of units is often used in electromagnetism [1]. Conversions between the two systems may not be achieved easily because of the different definition for the electric charge q. Electromagnetic units are based on two relationships; Coulomb's law for the electric charge and the law of Biot and Savart for the electric current.

Coulomb's law (electrostatic system)

MKS	cgs	Gaussian-cgs
$F = \frac{1}{4\pi\varepsilon_0}\frac{q_1 q_2}{r^2}$	$F = \frac{q_1 q_2}{r^2}$	$F = \frac{q_1 q_2}{r^2}$

where q is electric charge and r is the distance between charges. The constant ε_0 is the permittivity of the vacuum and has the value of $10^7/4\pi c^2$ C^2/Nm^2.

The law of Biot and Savart (electromagnetic system)

MKS	cgs	Gaussian-cgs
$F = \frac{\mu_0}{2\pi}\frac{i_1 i_2}{r}L$	$F = 2\frac{i_1 i_2}{r}L$	$F = 2\frac{i_1 i_2}{c^2 r}L$

which relates the force F per length L between long, parallel conductors to the currents i_1 and i_2 at the distance r. The constant μ_0 is the permeability of the vacuum and has the value of $4\pi \times 10^{-7}$ N/A^2.

In the MKS system the unit of electric charge is the Coulomb (C) which is defined from Ampere's law (1C = 1A·1s) not from Coulomb's law. Since the unit of electric charge is decided, the constants ε_0 and μ_0 are fixed by the related laws.

In the cgs system there is no fundamental unit of electric charge q. By Coulomb's law the unit of electric charge q may be measured in dyne$^{1/2}$·cm. The unit of the electric field E is given in dyne$^{1/2}$/cm by the relationship $F = qE$, and the electric potential V is dyne$^{1/2}$ by the relationship $E = \nabla V$. However, the square of the potential V^2 is clearly not force (dyne). This means that the units can not show how many factors of the charge occur in a given equation. This defect can be removed by the consistent use of the unit 'esu' although it is not fundamental like the unit 'Coulomb' in the MKS system. Once the unit 'esu' is introduced, the unit of electric field E is dyne/esu and that of electric potential V is esu/cm (= erg/esu = statvolt). The magnetic field B has its own unit 'Gauss' rather than dyne$^{1/2}$/cm. This serves the same purpose as the introduction of the unit 'esu' on the electric side. In the cgs system the unit of electric current is abampere and this is not equal to statampere (= esu/sec). Therefore the relationship between the two units must be determined. By experiment or by theory relating it to other fundamental constants 'abampere' is equal to 'statamp·c' (where c is the velocity of light). The Gaussian-CGS system uses statampere and hence the constant c is included explicitly. The fundamental equations are readily reduced to dimensionless form.

In quantum mechanics, the Gaussian units are often combined with the atomic units where $\hbar$ (Planck's constant divided by 2π), m (electronic mass) and e (electronic charge) are all numerically unity. By the definition, the units of energy and length are redefined as "Hartree" ($E_0 = 4.3598 \times 10^{-11}$ erg) and "Bohr" ($a_0 = 5.2918 \times 10^{-9}$ cm), repectively. Since in the Gaussian system electromagnetic units depend on mechanical units, they are

also redefined as: (1) electronic charge (e = force$^{-1/2}$/distance = $(E_0/a_0)^{-1/2}/a_0$ = 4.80325 × 10^{-10} esu) (2) electric field (e/a_0^2 = 1.715272 × 10^7 esu/cm^{-2}) (3) magnetic field (e/a_0^2c = 2.350540 × 10^9 G).

Table 1.1 Conversions of some units and expressions between MKS-SI and Guassian-cgs Systems.

Quantity	MKS-SI	Gaussian-cgs
Distance	Meter	10^2 cm
Force	Newton	10^5 dyne
Energy	Joule	10^7 erg
Charge	Coulomb	2.998×10^9 esu
Current	Ampere	2.998×10^9 statampere(esu/sec)
Electric Potential	Volt	1/299.8 statvolt
Electric Field	Volt/meter	1/29980 statvolt/cm
Magnetic Field	Tesla	10^4 gauss
	μ_0	$4\pi/c^2$
	$4\pi\varepsilon_0$	1
	B	**B**/c

1.1.2. Charged Particles in a Magnetic Field ; Minimal Coupling [2]

The electric field **E** and the magnetic field **B** are governed by Maxwell's equations. The explicit forms of the equations are given by:
(in the MKS-SI system)

$$\nabla\cdot\mathbf{B}=0 \qquad \nabla\times\mathbf{B}=\mu_0\varepsilon_0\frac{\partial\mathbf{E}}{\partial t}+\mu_0\mathbf{j} \tag{1.1a}$$

$$\nabla\cdot\mathbf{E}=\frac{\rho}{\varepsilon_0} \qquad \nabla\times\mathbf{E}=-\frac{\partial\mathbf{B}}{\partial t} \tag{1.1b}$$

(In the Gaussian-cgs system)

$$\nabla \cdot \mathbf{B} = 0 \qquad \nabla \times \mathbf{B} = \frac{1}{c}\frac{\partial \mathbf{E}}{\partial t} + \frac{4\pi \mathbf{j}}{c} \tag{1.2a}$$

$$\nabla \cdot \mathbf{E} = 4\pi\rho \qquad \nabla \times \mathbf{E} = -\frac{1}{c}\frac{\partial \mathbf{B}}{\partial t} \tag{1.2b}$$

where μ_0 is the permeability of free space, ε_0 is the permittivity of free space, ρ is the charge density and **j** is the current density. The first terms of Eqs. (1.1a, 1.2a) show that all magnetic field lines which enter a particular closed surface must eventually leave the surface; thus there are no magnetic monopoles or sources of 'magnetic charge'. The second terms of Eqs. (1.1a, 1.2a) show that a time-varying electric field and a current density generate a magnetic field. The first terms of Eqs. (1.1b and 1.2b) indicate that the amount of total electric flux through a given closed surface is proportional to the amount of electric charge in the volume contained by that surface. The second terms of Eqs. (1.1b, 1.2b) indicate that a magnetic field changing in time acts as a source for a electric field.

A scalar potnetial ϕ and a vector potential **A** can be introduced in terms of the fields **E** and **B** (in the Gaussian system):

$$\mathbf{E} = -\frac{1}{c}\frac{\partial \mathbf{A}}{\partial t} - \nabla\phi \qquad \mathbf{B} = \nabla \times \mathbf{A} \tag{1.3}$$

An electron (negatively charged particle) at a position **r** in the fields **E** and **B** will experience a force (the Lorentz force)

$$\mathbf{F} = -e\left[\mathbf{E}(\mathbf{r}) + \frac{1}{c}\dot{\mathbf{r}} \times \mathbf{B}(\mathbf{r})\right] = -e\left[-\frac{1}{c}\frac{\partial \mathbf{A}}{\partial t} - \nabla\phi(\mathbf{r}) + \frac{1}{c}\dot{\mathbf{r}} \times (\nabla \times \mathbf{A}(\mathbf{r}))\right] = -\nabla U \tag{1.4}$$

The generalized potential U in the fields **E** and **B** can be obtained from the eq (1.4):

$$U = \frac{e}{c}(\dot{\mathbf{r}} \cdot \mathbf{A}) + e\phi \tag{1.5}$$

The Lagrangian is

$$L = T - U = \frac{1}{2}m\dot{\mathbf{r}}^2 - \frac{e}{c}\dot{\mathbf{r}} \cdot \mathbf{A} - e\phi \tag{1.6}$$

and the momentum becomes

$$\mathbf{p} = \frac{\partial L}{\partial \dot{\mathbf{r}}} = m\dot{\mathbf{r}} - \frac{e}{c}\mathbf{A} \tag{1.7}$$

Finally, the Hamiltonian is given by:

$$H = \dot{\mathbf{r}} \cdot \mathbf{p} - L = \frac{1}{2}m\dot{\mathbf{r}}^2 + e\phi = \frac{1}{2m}(\mathbf{p} + \frac{e}{c}\mathbf{A})^2 + e\phi \tag{1.8a}$$

If atomic units are introduced, the Hamiltonian can be expressed as:

$$H = \frac{1}{2}(\mathbf{p} + \alpha\mathbf{A})^2 + \phi \tag{1.8b}$$

where $\alpha(=1/c)$ is the fine structure constant.

From now on, the atomic units based on the Gaussian system are employed in all equations. All systems concerned here are time-independent.

1.2. Density Functional Theory

In quantum mechanics, the conventional wave function based methods are very complicated to be used because the wave function cannot be probed experimentally and depends on 4N variables, three spatial and one spin variables for each of the N electrons. In fact, they cannot handle the interesting systems in biology and material science, which contain many atoms and electrons. The complexity can be diminished by replacing the wave function and its associated Schrödinger equation with the electron density and its associated calculational scheme since the electron density depends only on the three spatial variables (x, y, z) and that can be measured by X-ray diffraction.

The density functional theory (DFT) [3] uses the electron density as the main variable. The electron density is defined as

$$\rho(\mathbf{r}_1) = N\int\cdots\int |\Psi(\mathbf{r}_1\sigma_1\mathbf{x}_2...\mathbf{x}_N)|^2\, d\sigma_1 d\mathbf{x}_2...d\mathbf{x}_N \tag{1.9}$$

This function determines the probability of finding any of the N electrons within the volume element $\mathrm{d}\mathbf{r}_1$ while the other N-1 electrons have arbitrary positions and spins in the state represented by Ψ. Electrons are indistinguishable and the probability of finding any electron at this position is, therefore, just N times the probability for one particular electron. The electron density is a positive function and goes to zero at infinity ($\mathbf{r} \to \infty$) and gives the total number of electrons when integrated over all space,

$$\int \rho(\mathbf{r}_1) d\mathbf{r}_1 = N \tag{1.10}$$

In 1964, Hohenberg and Kohn justified theoretically the electron density as fundamental quantity within quantum mechanics [4]. In their paper, they showed that a unique mapping between the ground state electron density and the external potential V_{ext} exists based on the variational principle. This is the first Hohenberg-Kohn (HK) theorem. It implies that given a density, only one potential and wave function correspond to that

density, so all properties are functionals of the ground state density. This is indeed the case since any property may be determined as the expectation value of the corresponding operator and the wave function is determined by the density.

From now on, we will be concerned with systems of electrons moving in the field of fixed nuclei, so the external potential V_{ext} is just the nuclear field. In this case, the Hamiltonian is

$$\hat{H} = \hat{T} + \hat{V}_{Ne} + \hat{V}_{ee} \tag{1.11}$$

$$\hat{T} = \sum_{i=1}^{N} -\frac{1}{2}\nabla^2(i); \hat{V}_{Ne} = \sum_{i=1}^{N}\sum_{A=1}^{M}\frac{-Z_A}{|r_A - r_i|}; \hat{V}_{ee} = \sum_{i<j}^{N}\frac{1}{r_{ij}}$$

where A runs over the M nuclei while i and j denote the N electrons in the system. The operator $\hat{T}$ describes the kinetic energy of the electrons and the remaining two operators $\hat{V}_{Ne}$ and $\hat{V}_{ee}$ represent the attractive electrostatic interaction between the nuclei and the electrons and the repulsive potential due to the electron-electron interaction, respectively. If the external potential V_{Ne} is taken for each density $\rho(\mathbf{r})$ according to the first HK theorem, a functional E[ρ] yields the ground state energy of the system having this ρ as its ground state density. On the other hand, if a fixed external potential V_{Ne} is chosen, for which Ψ_0 is the ground state and E_0 the corresponding ground state energy, and we evaluate for each $\rho(\mathbf{r})$ the expectation value of the Hamiltonian with the fixed V_{Ne} for $\Psi_0(\rho)$, a functional E_v[ρ] will have E_0 as lower bound according to the variational principle

$$E_v[\rho] = <\Psi[\rho]|\ \hat{T} + \hat{V}_{ee} + \hat{V}_{Ne}\ |\Psi[\rho]> = T[\rho] + V_{ee}[\rho] + \int V_{Ne}\rho(\mathbf{r})d\mathbf{r} \geq E_0 \tag{1.12}$$

This is usually refered to as the second HK theorem. It is cleary shown by the HK theorems that the electron density can replace the complicated wave function if one seeks to calculate the ground state energy. However, it should be noted that the HK threoms are

only of importance from a theoretical point of view since the theorems are based on the exact functionals. In reality, we do not know the exact functionals and the theorems do not give any information about the unknown functionals. In 1965, Kohn and Sham provided a creative and practical way to solve many intrinsic problems of the DFT [5].

1.2.1. Kohn-Sham Approach

In fact, so far, many pragmatic DFT models have been developed such as Thomas-Fermi [6] and related models [3] that are based on the ideal uniform electron gas system and in which all parts are expressed as pure functionals of the electron density. Unfortunately, it turns out that all methods based on the Thomas-Fermi scheme are not successful in chemical applications because it is hard to obtain the relationship between the spatial distribution of the electrons and their velocities which are needed for the kinetic energy.

In order to overcome the kinetic energy functional problem, Kohn and Sham introduced the orbital concept of a corresponding non-interacting system into DFT. In the Schrödinger equation ($\hat{H}\Psi = E\Psi$: time-independent, non-relativistic case) [7], the Hamiltonian is fixed and the wave function is the only variable. Hence, in the full interacting system, all information on the interactions is in the wave function. The wave functions can be described by a linear combination of Slater determinants Ψ_S.

$$\Psi = \sum_{i=1}^{\infty} C_i \Psi_S^i \tag{1.12}$$

In this system, the electron density and the kinetic energy can be represented using the natural spin orbitals ϕ_i which are the elements of the orthonormal set in which one-electron density matrix (vide infra) is diagonal and their occupation numbers n_i. The explicit forms are given by

$$\rho(\mathbf{r}) = \sum_{i=1}^{\infty} \sum_{s} n_i \, |\phi_i(\mathbf{r},s)|^2 \tag{1.13}$$

and

$$T = \sum_{i=1}^{\infty} n_i \, \langle \phi_i | -\frac{1}{2}\nabla^2 | \phi_i \rangle \tag{1.14}$$

On the other hand, in a non-interacting system, the Hamiltonian $\hat{H}_S$ does not have the electron-electron interaction terms and therefore the wave funtion Ψ_S can be described by a single Slater determinant.

$$\hat{H}_S = \sum_{i=1}^{N} \left(-\frac{1}{2}\nabla_i^2 \right) + \sum_{i=1}^{N} V_S \tag{1.15}$$

and

$$\Psi_S = \frac{1}{\sqrt{N!}} | \phi_1 \phi_2 ... \phi_N | \tag{1.16}$$

In the Schrödinger equation of the non-interacting system ($\hat{H}_S \Psi_S = E\Psi_S$), the external potential V_S ($=V_{eff}$) can be adjusted in order to have the same ground state properties (energy, density,...) as those of the full interacting system. In this system, the electron density and the kinetic energy can be represented by

$$\rho_s(\mathbf{r}) = \sum_{i=1}^{N} |\phi_i(\mathbf{r})|^2 \tag{1.17}$$

and

$$T_S = \sum_{i=1}^{N} < \phi_i | -\frac{1}{2}\nabla^2 | \phi_i > \tag{1.18}$$

The N lowest eigenstates ϕ_i are determined by the self-consistent solution of the one-electron Kohn-Sham equation which is derived by the variational search for the minimum of the energy functional $E[\rho]$ in the space of orbitals ϕ_i with the constraint of orthonormal orbitals. The Kohn-Sham (KS) orbital equation can be obtained,

$$\hat{h}_{KS}\phi_i = \left[-\frac{1}{2}\nabla^2 + V_{eff}\right]\phi_i = \sum_{j}^{N} \varepsilon_{ij}\phi_j \tag{1.19}$$

and after the diagonalization of the Hermitian matrix ε_{ij} by a unitary transformation of the orbitals the cannonical form of KS equation is

$$\hat{h}_{KS}\phi_i = \left[-\frac{1}{2}\nabla^2 + V_{eff}\right]\phi_i = \varepsilon_i\phi_i \tag{1.20}$$

To get the explicit form of V_{eff}, the energy functional $E[\rho]$ can be rewritten as

$$\begin{aligned} E[\rho] &= < \Psi_S | \hat{H}_S | \Psi_S > \\ &= T_S[\rho] + J[\rho] + E_{XC}[\rho] + E_{Ne}[\rho] \\ &= \sum_{i=1}^{N} < \phi_i | -\frac{1}{2}\nabla_i^2 | \phi_i > + \frac{1}{2}\iint \frac{\rho(\mathbf{r}_1)\rho(\mathbf{r}_2)}{|\mathbf{r}_1 - \mathbf{r}_2|} d\mathbf{r}_1 d\mathbf{r}_2 + E_{XC}[\rho] + \int V_{ext}(\mathbf{r}_1)\rho(\mathbf{r}_1) d\mathbf{r}_1 \end{aligned} \tag{1.21}$$

The KS effective potential is defined by

$$\begin{aligned} V_{eff}(\mathbf{r}_1) &= \frac{\delta J[\rho]}{\delta\rho(\mathbf{r}_1)} + \frac{\delta E_{XC}[\rho]}{\delta\rho(\mathbf{r}_1)} + V_{ext}(\mathbf{r}_1) \\ &= \int \frac{\rho(\mathbf{r}_2)}{|\mathbf{r}_1 - \mathbf{r}_2|} d\mathbf{r}_2 + V_{XC}(\mathbf{r}_1) + V_{ext}(\mathbf{r}_1) \end{aligned} \tag{1.22}$$

In KS theory, the kinetic energy $T_S[\rho]$ is not the true kinetic energy $T[\rho]$ and there are non-classical electron-electron repulsion terms. The kinetic energy correction and the non-classical contributions are treated in the exchange-correlation functional.

$$F[\rho] = T_S[\rho] + J[\rho] + E_{XC}[\rho] \tag{1.23}$$

and

$$E_{XC}[\rho] = T[\rho] - T_S[\rho] + V_{ee}[\rho] - J[\rho] \tag{1.24}$$

If we know the exact form of $E_{XC}[\rho]$, the KS equation is exact. In principle, the exact ground state properties can be obtained from the solution of the equation. Unfortunately, it is impossible to know the exact form of the $E_{XC}[\rho]$. However, so far, many accurate functionals have been developed and now the DFT methods are comparable to post Hartree-Fock methods.

1.2.2. Approximate Exchange-Correlation Functionals

From the KS formalism, it is shown that most of contributions to the energy can be treated exactly, including the major fraction of the kinetic energy. All remaining unknown parts are collected into $E_{XC}[\rho]$. To make the KS equation feasible, the only thing to be done is to build the approximate functionals as accurate as possible.

1.2.2.1. Density Matrices and Pair Correlation Functions

In the Schrödinger equation, the Hamiltonian operator contains only one- and two-electron operators so that the total energy can be expressed in terms of the probabilty of finding one electron and pairs of electrons in space. Here, we introduce the concepts of

density matrices including the concepts of first and second order spinless density matrices [8]. The density matrix

$$\gamma_N(\mathbf{x}_1\mathbf{x}_2...\mathbf{x}_N,\mathbf{x}'_1\mathbf{x}'_2...\mathbf{x}'_N)=\Psi(\mathbf{x}_1\mathbf{x}_2...\mathbf{x}_N)\Psi^*(\mathbf{x}'_1\mathbf{x}'_2...\mathbf{x}'_N) \tag{1.26}$$

represents the probabilty distribution associated with a solution of the Schrödinger equation with the Hamiltonian operator $\hat{H}$. In the above equation, $\mathbf{x}_i$ denotes the spatial, $\mathbf{r}_i$, and the spin, σ_i, coordinates of electron *i*. The first order spinless reduced density matrix is obtained by integrating the product $\Psi\Psi^*$ over all variables, except the spatial coordinates of one electron, and summing over spin,

$$\rho_1(\mathbf{r}_1,\mathbf{r}'_1)=N\int\cdots\int\Psi(\mathbf{r}_1\sigma_1\mathbf{x}_2\mathbf{x}_3...\mathbf{x}_N)\Psi^*(\mathbf{r}'_1\sigma_1\mathbf{x}_2\mathbf{x}_3...\mathbf{x}_N)\mathrm{d}\sigma_1\mathrm{d}\mathbf{x}_2\mathrm{d}\mathbf{x}_3...\mathrm{d}\mathbf{x}_N \tag{1.26}$$

The electron density (1.9) is the diagonal element of this matrix,

$$\rho(\mathbf{r}_1)=\rho_1(\mathbf{r}_1,\mathbf{r}_1)=N\int\cdots\int|\Psi(\mathbf{r}_1\sigma_1\mathbf{x}_2\mathbf{x}_3...\mathbf{x}_N)|^2\,\mathrm{d}\sigma_1\mathrm{d}\mathbf{x}_2\mathrm{d}\mathbf{x}_3...\mathrm{d}\mathbf{x}_N \tag{1.27}$$

The second order spinless density matrix can be defined as:

$$\rho_2(\mathbf{r}_1\mathbf{r}_2,\mathbf{r}'_1\mathbf{r}'_2)=\frac{N(N-1)}{2}\int\cdots\int\Psi(\mathbf{r}_1\sigma_1\mathbf{r}_2\sigma_2\mathbf{x}_3...\mathbf{x}_N)\Psi^*(\mathbf{r}'_1\sigma_1\mathbf{r}'_2\sigma_2\mathbf{x}_3...\mathbf{x}_N)\mathrm{d}\sigma_1\mathrm{d}\sigma_2\mathrm{d}\mathbf{x}_3...\mathrm{d}\mathbf{x}_N \tag{1.28}$$

The pair density is

$$\begin{aligned}\rho_2(\mathbf{r}_1,\mathbf{r}_2)&=\rho_2(\mathbf{r}_1\mathbf{r}_2,\mathbf{r}_1\mathbf{r}_2)\\&=\frac{N(N-1)}{2}\int\cdots\int|\Psi(\mathbf{x}_1\mathbf{x}_2\mathbf{x}_3...\mathbf{x}_N)|^2 d\sigma_1 d\sigma_2 d\mathbf{x}_3...d\mathbf{x}_N\end{aligned} \tag{1.29}$$

the diagonal element of the second order density matrix and corresponds to the probability of finding a pair of electrons simultaneously within two volume element $d\mathbf{r}_1$ and $d\mathbf{r}_2$, while the remaining N-2 electrons have arbitrary positions and spins. This probability distribution contains all information about electron correlation and gives the total number of distinct pairs of electrons when integrated over the whole space with respect to $\mathbf{r}_1$ and $\mathbf{r}_2$. From the antisymmetry of the wave function, it is found that the probabilty of finding two electrons with the same spin at the same point in space is zero, which is a statement of the Pauli principle. This property gives an effect on the movement of electrons and it is known as exchange or Fermi correlation. The electrons of antiparallel spins also move in a correlated fashion, which prevent the electrons from coming too close to each other and this effect is known as Coulomb correlation. The influence of the Fermi and Coulomb correlation can be expressed on the pair density by separating the pair density into two parts:

$$\rho_2(\mathbf{r}_1,\mathbf{r}_2) = \rho(\mathbf{r}_1)\rho(\mathbf{r}_2)[1 + f(\mathbf{r}_1;\mathbf{r}_2)] \tag{1.30}$$

where $f(\mathbf{r}_1;\mathbf{r}_2)$ is often called the correlation factor. The hole function is defined as the difference between the conditional probability $\Omega(\mathbf{r}_1;\mathbf{r}_2)$ and the uncorrelated probability of finding an electron at $\mathbf{r}_2$, where $\Omega(\mathbf{r}_1;\mathbf{r}_2)$ is the probability of finding any electron at $\mathbf{r}_2$ if one electron exists already at $\mathbf{r}_1$. The hole function takes the form:

$$\begin{aligned} h_{XC}(\mathbf{r}_1;\mathbf{r}_2) &= \Omega(\mathbf{r}_1;\mathbf{r}_2) - \rho(\mathbf{r}_2) \\ &= \frac{\rho_2(\mathbf{r}_1,\mathbf{r}_2)}{\rho(\mathbf{r}_1)} - \rho(\mathbf{r}_2) = \rho(\mathbf{r}_2) f(\mathbf{r}_1;\mathbf{r}_2) \end{aligned} \tag{1.31}$$

The name 'hole' originates from the fact that correlation leads to a depletion of the electron density for $\mathbf{r}_2$ closer to $\mathbf{r}_1$ compared to the uncorrelated case. From (1.31) we can see the important result that the integration of the hole function at $\mathbf{r}_2$ gives rise to the charge of one electron:

$$\int h_{XC}(\mathbf{r}_1;\mathbf{r}_2)d\mathbf{r}_2 = -1 \tag{1.32}$$

1.2.2.2. Fermi and Coulomb Holes

The electrons in an external field move in a correlated way which means that they always keep a certain distance to each other. This can be pictorially described by the introduction of the idea of the exchange-correlation hole. With the concept of the hole function the electron-electron repulsion potential energy can be defined as:

$$\begin{aligned} E_{ee} &= <\Psi|\sum_{i<j}^{N}\frac{1}{r_{ij}}|\Psi> \\ &= \frac{1}{2}\int\frac{\rho_2(\mathbf{r}_1;\mathbf{r}_2)}{r_{12}}d\mathbf{r}_1 d\mathbf{r}_2 \\ &= \frac{1}{2}\int\frac{\rho(\mathbf{r}_1)\rho(\mathbf{r}_2)}{r_{12}}d\mathbf{r}_1 d\mathbf{r}_2 + \frac{1}{2}\int\frac{\rho(\mathbf{r}_1)h_{XC}(\mathbf{r}_1;\mathbf{r}_2)}{r_{12}}d\mathbf{r}_1 d\mathbf{r}_2 \end{aligned} \tag{1.33}$$

In the above equation, the first term represents the classical Coulomb interaction. Here it should be noted that this term has the unphysical self-interaction which has to be removed. (For example, this Coulomb term still exists in a one-electron system but it will be cancelled by the Fermi hole.) The second term denotes the interaction between the charge density and the charge distribution of the hole. The hole function contains the correction for the self-interaction as well as the non-classical correlation effects [9]. The hole function can be expressed as a sum of the Fermi hole and the Coulomb hole:

$$h_{XC}(\mathbf{r}_1;\mathbf{r}_2) = h_X(\mathbf{r}_1;\mathbf{r}_2) + h_C(\mathbf{r}_1;\mathbf{r}_2) \tag{1.34}$$

The function $h_X(\mathbf{r}_1;\mathbf{r}_2)$ represents the hole in the probability density of electrons with same spin due to the Pauli principle and the function $h_C(\mathbf{r}_1;\mathbf{r}_2)$ denotes the hole resulting from the electrostatic interaction which has contributions for electrons of either spin.

First, let us focus on the Fermi hole. If the total hole is just governed by the Fermi hole, the pair density can be expressed as:

$$\rho_2(\mathbf{r}_1,\mathbf{r}_2) = \rho(\mathbf{r}_1)[\rho(\mathbf{r}_2) + h_X(\mathbf{r}_1;\mathbf{r}_2)] \tag{1.35}$$

The Fermi hole has an important property:

$$\int h_X(\mathbf{r}_1;\mathbf{r}_2)d\mathbf{r}_2 = -1 \tag{1.36}$$

If there is one electron of spin σ is already known to be at $\mathbf{r}_1$, the conditional probability of electrons of the same spin at $\mathbf{r}_2$ integrates to N-1. Hence, the reference electron is removed from the distribution. The Fermi hole function has for $2 \rightarrow 1$ (implying same spins) a depth equal ro the density of electrons with the same spin as the reference electron

$$h_X(\mathbf{r}_2 \rightarrow \mathbf{r}_1;\mathbf{r}_1) = -\rho(\mathbf{r}_1) \tag{1.37}$$

and zero depth for opposite spin electrons

$$h_X(\mathbf{r}_2 \rightarrow \mathbf{r}_1, \sigma_2 \neq \sigma_1;\mathbf{r}_1) = 0 \tag{1.38}$$

As a result, the Fermi hole removes the unphysical self-interaction of the Coulomb repulsion and confirms the Pauli principle that two electrons of the same spin cannot be at the same position in space. In addition, this leads to a considerable advantage when we define the Coulomb hole.

The Coulomb hole is defined as the difference between total exchange-correlation hole and the Fermi hole

$$h_C(\mathbf{r}_1;\mathbf{r}_2) = h_{XC}(\mathbf{r}_1;\mathbf{r}_2) - h_X(\mathbf{r}_1;\mathbf{r}_2) \tag{1.39}$$

From equations (1.32) and (1.36), the definition is obvious that the Coulomb hole integrates to zero over all space:

$$\int h_C(\mathbf{r}_1;\mathbf{r}_2)d\mathbf{r}_2 = 0 \tag{1.40}$$

Electrons with opposite spins are correlated to each other by the Coulomb hole. The Coulomb hole is negative at the postion $\mathbf{r}_1$ of the reference electron since it originates from the electrostatic repulsion which keeps electrons apart. On the other hand, the Coulomb hole is positive and largest at the position $\mathbf{r}_2$ of the probe electron, which is confirmed by the condition (1.40).

1.2.2.3. The Adiabatic Connection

In the KS theory, the kinetic energy is derived from the non-interacting system and thus the kinetic energy difference between the real and the reference systems should be included in the exchange-correlation functional $E_{XC}[\rho]$. This can be achieved by the adiabatic connection process [10]. Two extreme systems (the non-interacting reference system and the fully interacting real system) are connected smoothly by the coupling strength parameter λ which ranges from 0 to 1. In this case, the Hamiltonian takes the form:

$$\hat{H}_\lambda = \hat{T} + \hat{V}_{ext}^{\lambda} + \lambda \sum_{i<j} \frac{1}{r_{ij}} \tag{1.41}$$

The electron density is not changed by λ since the external potential $\hat{V}_{ext}^{\lambda}$ is adjusted for each value of λ. For the case of λ=0, the system is non-interacting ($\hat{V}_{ext}^{\lambda=0} = \hat{V}_S$), while λ=1 denotes that the system is fully interacting ($\hat{V}_{ext}^{\lambda=1} = \hat{V}_{ext}$). In terms of the adiabatic connection the energy of the fully interacting system can be expressed as:

$$E_{\lambda=1} = E_{\lambda=0} + \int_0^1 dE_\lambda \tag{1.42}$$

Here, the infinitesimal energy change dE_λ is the expectation value of the corresponding Hamiltonian:

$$d\hat{H}_\lambda = d\hat{V}_{ext}^{\lambda} + d\lambda \sum_{i<j} \frac{1}{r_{ij}} \tag{1.43}$$

and, using the hole formalism, takes the form:

$$dE_\lambda = \int \rho(\mathbf{r}) d\hat{V}_{ext}^{\lambda} d\mathbf{r} + \frac{1}{2} d\lambda \int \frac{\rho(\mathbf{r})\rho(\mathbf{r}')}{|\mathbf{r}-\mathbf{r}'|} d\mathbf{r}d\mathbf{r}' + \frac{1}{2} d\lambda \int \frac{\rho(\mathbf{r}) h_{XC}^{\lambda}(\mathbf{r};\mathbf{r}')}{|\mathbf{r}-\mathbf{r}'|} d\mathbf{r}d\mathbf{r}' \tag{1.44}$$

From the equations (1.42 and 1.44), the explicit energy expression of the fully interacting system can be taken as:

$$E_{\lambda=1} = T_S + \int \rho(\mathbf{r}) d\hat{V}_{ext} d\mathbf{r} + \frac{1}{2} \int \frac{\rho(\mathbf{r})\rho(\mathbf{r}')}{|\mathbf{r}-\mathbf{r}'|} d\mathbf{r}d\mathbf{r}' + \frac{1}{2} \int \frac{\rho(\mathbf{r}) \bar{h}_{XC}(\mathbf{r};\mathbf{r}')}{|\mathbf{r}-\mathbf{r}'|} d\mathbf{r}d\mathbf{r}' \tag{1.45}$$

where $\bar{h}_{XC}$ is the coupling-strength integrated exchange-correlation hole and can be defined as:

$$\bar{h}_{XC}(\mathbf{r};\mathbf{r}') \equiv \int_0^1 h_{XC}^{\lambda}(\mathbf{r};\mathbf{r}') d\lambda \tag{1.46}$$

In consequence, from eq (1.45), it is shown that the energy of the fully interacting system can be obtained based on the kinetic energy of the non-interacting system if the explicit form of $\overline{h}_{XC}$ is defined.

1.2.2.4. Local Spin Density Approximation (LSDA)

It is impossible to find an exact exchange-correlation functional form of the true electron density. Hence, the pragmatic goal of DFT is to find a good approximate functional. All approximations start from the ideal model system, the homogeneous electron gas system, where electrons move on a uniformly distributed positive charge background. In this model, the electron density is a constant everywhere, which means that any local density can represent the electron density of the whole system. In the local density approximation (LDA), the exchange-correlation energy can be obtained from the electron density at a point in space. In the local spin density approximation (LSDA), the electron density is simply replaced by the spin density ($\rho^{\alpha}(\mathbf{r})$ and $\rho^{\beta}(\mathbf{r})$), which gives additional flexibility to the functional.

From the homogenous electron gas model, the exchange functional has a simple, explicit form:

$$E_X^{LSDA} = -\frac{3}{2}\left(\frac{3}{4\pi}\right)^{1/3}\int(\rho^{\alpha}(\mathbf{r})^{4/3} + \rho^{\beta}(\mathbf{r})^{4/3})d\mathbf{r} \qquad (1.47)$$

which was derived by Dirac [11]. On the other hand, there is no explicit form of the correlation functional derived by mathematics. The most popular functional was made by Vosko, Wilk and Nusair (VWN) [12] who used a Padé approximation to interpolate the results from a Monte-Carlo simulations carried out by Ceperly and Alder [13]. The VWN correlation functional takes the form:

$$E_C^{LSDA}[\rho^\alpha, \rho^\beta] = \int \rho(\mathbf{r}) \varepsilon_C(\rho^\alpha, \rho^\beta) d\mathbf{r} \tag{1.48}$$

and

$$\varepsilon_C(r_S) = A\left\{ \ln\left(\frac{x^2}{X(x)}\right) + \frac{2b}{Q}\tan^{-1}\left(\frac{Q}{2x+b}\right) - \frac{bx_0}{X(x_0)}\left[\ln\left(\frac{(x-x_0)^2}{X(x)}\right) + \frac{2(b+2x_0)}{Q}\tan^{-1}\left(\frac{Q}{2x+b}\right)\right]\right\} \tag{1.49}$$

Here, $X(x) = x^2 + bx + c$, $Q = (4c - b^2)^{1/2}$, x_0, b and c are constants. The Wigner-Seitz radius r_S is related to the density:

$$r_S = \left(\frac{3}{4\pi\rho}\right)^{1/3} \tag{1.50}$$

In spite of the drastic approximation (the use of the uniform electron gas model), LSDA gives fairly good results for equilibrium structures and vibrational frequencies for covalently coordinated molecules, which are comparable to or even better than the Hartree-Fock approximation. Part of the success of LSDA seems to be that the exchange-correlation hole of the uniform electron gas satisfies most of the important properties (in eqs 1.36 and 1.37) established for the exact exchange-correlation hole [10(b)] and the spherically averaged LSDA hole is a good approximation to the exact one in the bonding region where the exact hole becomes more symmetric with respect to the reference electron than in the separated atoms [14]. In an atom, the exact hole is displaced toward the nucleus, while the LSDA hole still remains in the bond since it is always attached to the reference electron. This causes significant deviation from the exact differential exchange energy upon bond formation. The LSDA hole will have a good accuracy for small distance between the reference and the probe electrons because in the local density approximation the exchange-correlation hole is around the reference electron as if the neighborhood were part of a uniform electron gas of constant density. However, in real

system with considerably varying charge density, the LSDA results will get worse the larger the distance between two electrons. From the reasons, LSDA results show a overbinding tendency which makes the molecules overstabilized compared to the separated atoms [15] and can not treat long-range interaction such as hydrogen bonding [16] and van der Waals interaction.

1.2.2.5. Generalized Gradient Approximation (GGA)

Inhomogeneities of the electron density can be taken into account by including the higher derivatives of the density into the functional. The GGA functional can be generally written as:

$$\begin{aligned} E_{XC}^{GGA}[\rho_\alpha,\rho_\beta] &= \int f(\rho_\alpha,\rho_\beta,\nabla\rho_\alpha,\nabla\rho_\beta)d\mathbf{r} \\ &= E_X^{GGA} + E_C^{GGA} \end{aligned} \tag{1.51}$$

The GGA exchange energy takes the form:

$$E_X^{GGA} = E_X^{LDA} - \sum_{\sigma=\alpha,\beta}\int F(s_\sigma)\rho_\sigma^{4/3}(\mathbf{r})d\mathbf{r} \tag{1.52}$$

where s_σ is the reduced density gradient for spin σ:

$$s_\sigma(\mathbf{r}) = \frac{|\nabla\rho_\sigma(\mathbf{r})|}{\rho_\sigma^{4/3}(\mathbf{r})} \tag{1.53}$$

s_σ is to be understood as a local inhomogeneity parameter.

For the function F, there are two main classes. The first one is based on the GGA exchange energy functional devised by Becke (B88) [17].

$$F^{B88} = \frac{\beta s_\sigma^2}{1 + 6\beta s_\sigma \sinh^{-1}(s_\sigma)} \tag{1.54}$$

Becke imposed the correct –1/r asymptotic behavior for the exchange energy density and used one parameter β fitted on the exact atomic HF exchange energy of noble gas atoms. The Perdew-Wang91 (PW91) functional is also related to this approach.

The second class of GGA exchange functionals uses a rational function of the reduced density gradient for F. Perdew used the second-order expansion with a cut-off radius to impose conditions (1.36) and (1.37) to the exchange hole function [18]. With this procedure, he was able to compute atomic exchange energies within 1% of the exact HF exchange energy. Further simplification of the model led to the well-known Perdew-Wang86 (PW86) exchange functional [19]:

$$F^{PW86} = \left\{1 + 1.296\left(\frac{s_\sigma}{(24\pi^2)^{1/3}}\right)^2 + 14\left(\frac{s_\sigma}{(24\pi^2)^{1/3}}\right)^4 + 0.2\left(\frac{s_\sigma}{(24\pi^2)^{1/3}}\right)^6\right\}^{1/15} \tag{1.55}$$

which is parameter free. The B86 functional and the PBE functional are also in this class.

The corresponding GGA correlation functionals have more complicated mathematical forms and no physical significance [20]. Becke showed that the inclusion of GGA exchange and correlation functionals using the combination of B88 for exchange and PW91 [21] for correlation reduced the absolute error and the overbinding tendency of LSDA [22]. The GGA functionals give better results for hydrogen bonded systems and for thermochemistry than the LSDA.

However, still there are obstacles that the GGA can not overcome. Since the LDA exchange-correlation potential dose not have the right asymptotic behavior at long distance, adding the gradient correction does not lead to significant improvement. The bad asymptotic behavior of LDA is not greatly corrected by the addition of gradient corrections [23].

1.2.2.6. meta-Generalized Gradient Approximation (meta-GGA)

To improve the GGA approximation, more factors can be included into the functional. In the meta-GGA functionals, the Laplacian of the density $\nabla^2\rho(\mathbf{r})$ and the kinetic energy density $\tau_\sigma(\mathbf{r})$ are added to the GGA [24]. By the definition of Becke [25], the kinetic energy density takes the form:

$$\tau_\sigma(\mathbf{r}) = \sum_i^{occ} |\nabla \phi_i^\sigma(\mathbf{r})|^2 \tag{1.56}$$

The meta-GGA functional can be generally expressed as:

$$E_{XC}^{meta-GGA}[\rho(\mathbf{r})] = \int f(\rho(\mathbf{r}), \nabla\rho(\mathbf{r}), \nabla^2\rho(\mathbf{r}), \tau(\mathbf{r}))d\mathbf{r} \tag{1.57}$$

These types of functionals give better results than the pure GGA functionals for many chemical systems. Part of the success comes from the orbital-dependent exchange-correlation energy. However, to add the kinetic energy density into the exchange-correlation energy, extra computational work is needed since $\tau_\sigma(\mathbf{r})$ is an implicit functional of the density.

1.2.2.7. Hybrid Functionals

Generally, the exchange contributions are much larger than the corresponding correlation effects. If the exchange energy of a Slater determinant is used in DFT which can be computed exactly, the error due to the LSDA or GGA exchange approximation can be reduced. The direct sum of the exact KS exchange energy and the LSDA or GGA correlation energy are unphysical by definition. Becke proposed an idea where the exact KS exchange energy is mixed with a traditional exchange-correlation functional using some parameters [26]. He introduced the adiabatic connection concept into this problem.

At $\lambda = 0$, the non-interacting limit, the exchange-correlation energy is the exact KS exchange energy without correlation. Hence, the exact KS exchange energy is used at $\lambda = 0$ and LSDA or GGA is used at $\lambda = 1$. With this idea, Becke introduced hybrid functionals:

$$E_{XC}^{B3PW91} = E_{XC}^{LSDA} + a(E_X^{Exact} - E_X^{LSDA}) + b\Delta E_X^{B88} + c\Delta E_C^{PW91} \tag{1.58}$$

where a=0.20, b=0.72 and c=0.81. The three paremeters were determined by a linear least-squares fit on an experimental reference data set [27]. The first parameter a represents the correction for the LSDA or GGA exchange energy near $\lambda = 0$ limit. A fraction of about 20-25 % exact exchange is reasonable for all hybrid schemes on purely theoretical grounds [28]. The most popular hybrid functional, B3LYP [29], can be obtained by the replacement of the PW91 correlation functional by the LYP correlation functional in (1.58). B3LYP gives better results than B3PW91 and other pure GGA functionals for organic molecules. In particular, hybrid methods represent a significant improvement over GGA and LSDA functionals for transition metal compounds and systems including hydrogen bonds since they provide better asymptotic behavior of exchange functionals.

1.2.2.8. Optimized Effective Potential (OEP) method

If the exact KS exchange energy form is incorporated into the KS energy formula, the only approximation of this case comes from the correlation energy functional:

$$\begin{aligned} E_{KS}^{OEP}[\{\phi_{i\alpha},\phi_{j\beta}\}] = T_S[\{\phi_{i\alpha},\phi_{j\beta}\}] + J[\{\phi_{i\alpha},\phi_{j\beta}\}] + \int v_{ext}\rho(\mathbf{r})d\mathbf{r} \\ + E_X^{exact}[\{\phi_{i\alpha},\phi_{j\beta}\}] + E_C[\{\phi_{i\alpha},\phi_{j\beta}\}] \end{aligned} \tag{1.59}$$

where the exact KS exchange energy takes the form:

$$E_X^{exact} = -\frac{1}{2}\sum_{\sigma=\alpha,\beta}\sum_{ij}^{N_\sigma}\int \frac{\phi_{i\sigma}^*(\mathbf{r})\phi_{j\sigma}^*(\mathbf{r}')\phi_{j\sigma}(\mathbf{r})\phi_{i\sigma}(\mathbf{r}')}{|\mathbf{r}-\mathbf{r}'|}d\mathbf{r}d\mathbf{r}' \tag{1.60}$$

The spin orbitals of (1.59) are obtained by the self-consistent solution of the KS equation:

$$\hat{h}_{OEP}\phi_{i\sigma} = \left[-\frac{1}{2}\nabla^2 + V_\sigma^{OEP}\right]\phi_{i\sigma} = \varepsilon_{i\sigma}\phi_{i\sigma} \tag{1.61}$$

Here, the optimized effective potential V_σ^{OEP} is obtained by the requirement [30]:

$$\frac{\delta E_{KS}^{OEP}[\{\phi_{i\alpha},\phi_{j\beta}\}]}{\delta V_\sigma^{OEP}(\mathbf{r})} = 0 \tag{1.62}$$

The physical idea of the OEP method is simple, while equation (1.62) leads to an integral equation that is computationally impractical to solve. Recently, Krieger, Li and Iafrate (KLI) have developled an approximate but fairly accurate procedure to overcome this problem, reducing the determination of V_σ^{OEP} to the solution of simple linear equations [31]. However, this method still needs much more computational efforts compared to GGA and meta-GGA functionals and has the problems related to finding a suitable correlation functional in which there is no cancellation of errors between exchange and correlation contributions which makes the success of LDA. However, all properties that depends on the KS orbitals can be obtained with higher accuracy than other type of functional.

1.3. Magnetic Resonance Parameters

In the presence of a homogeneous magnetic field, the mechanical and spin motions of electrons related to magnetic interactions can be described by the relativistic four-component Dirac equation [32]. In many cases, however, it is almost impossible to deal with a fully relativistic theory. Most relativistic effects are quite small compared in magnitude to the total quantities involved for light elements. Hence, it is feasible to use perturbation theory based on the Breit-Pauli (BP) Hamiltonian which is composed of the spin-free, non-relativistic Hamiltonian and the spin-dependent and spin-free perturbation terms arising from the relativistic treatment. The explicit forms of the BP perturbation terms can be derived from a careful reduction of a relativistic theory to a nonrelativistic form. For magnetic property calculations, the terms related to the external magnetic field should be considered in this perturbation treatment and this can be achieved by the minimal coupling principle in Eq. (1.8b).

In this study, electron spin-spin interactions (zero-field splittings) and relativistic corrections (the mass-velocity and the Darwin operators) to the nonrelativistic kinetic and potential operators will not be covered since we focus on the paramagnetic systems which have one unpaired electron and relatively light atoms. We just focus on spatially non-degenerate Kramers doublet states. As vector potential, the Coulomb gauge [33, 32(c)] is chosen which is divergence free:

$$\nabla \cdot \mathbf{A} = 0 \tag{1.63}$$

and

$$\mathbf{A} = \frac{1}{2}\mathbf{B} \times (\mathbf{r} - \mathbf{R}_O) \tag{1.64}$$

where $\mathbf{R}_O$ represents a gauge origin.

In the presence of the external magnetic field **B**, the nuclear magnetic moment **M** and the electronic magnetic moment **m**, the full quantum mechanical Hamiltonian of the system can be expanded in powers of the parameters as small perturbations [34]:

$$\begin{aligned} \mathrm{H}(\mathbf{B},\mathbf{M},\mathbf{m}) = {} & \mathrm{H}^{(0)} + \mathbf{B}\cdot\mathbf{H}^{(100)} + \mathbf{B}^{T}\mathbf{H}^{(200)}\mathbf{B} \\ & + \sum_{N}\mathbf{M}_{N}\cdot\mathbf{H}_{N}^{(010)} + \sum_{N}\mathbf{B}^{T}\mathbf{H}_{N}^{(110)}\mathbf{M}_{N} + \sum_{M}\sum_{N}\mathbf{M}_{M}^{T}\mathbf{H}_{MN}^{(020)}\mathbf{M}_{N} \\ & + \sum_{j}\mathbf{m}_{j}\cdot\mathbf{H}_{j}^{(001)} + \sum_{j}\mathbf{B}^{T}(-\mathbf{1}+\mathbf{H}_{j}^{(101)})\mathbf{m}_{j} + \sum_{j}\sum_{N}\mathbf{m}_{j}^{T}\mathbf{H}_{jN}^{(011)}\mathbf{M}_{N} \end{aligned} \tag{1.63}$$

with

$$\mathbf{M}_{N} = g_{N}\beta_{N}\mathbf{I}_{N} \tag{1.64}$$

$$\mathbf{m} = \sum_{j}\mathbf{m}_{j} = -g_{e}\beta\sum_{j}\mathbf{s}_{j} \tag{1.65}$$

where g_N and g_e are the nuclear and the free-electron g-values, β_N (=α/2M_p, M_p : proton mass) and β (=α/2) are the nuclear and the Bohr magnetons, $\mathbf{I}_N$ and **S** are the nuclear and the electron spin angular momenta. The $\mathbf{H}^{(nlm)}$ is an operator representing interactions *n*-linear in **B**, *l*-linear in **M** and *m*-linear in **m**. The subscript *j* denotes electron *j* and the subscript N represents nucleus N. The one-electron perturbation operators of the Hamiltonian are as follows:

$$\mathbf{H}^{(100)} = \frac{\alpha}{2}\sum_{j}\mathbf{l}_{jO} \tag{1.66}$$

$$\mathbf{H}^{(200)} = \frac{\alpha^{2}}{8}\sum_{j}|\mathbf{r}_{jO}|^{2}\,\mathbf{1} - \mathbf{r}_{jO}\mathbf{r}_{jO}^{T} \tag{1.67}$$

$$\mathbf{H}_{N}^{(010)} = \alpha\sum_{j}\frac{\mathbf{r}_{jN}\times\mathbf{p}_{j}}{|\mathbf{r}_{jN}|^{3}} = \alpha\sum_{j}\frac{\mathbf{l}_{jN}}{|\mathbf{r}_{jN}|^{3}} \tag{1.68}$$

$$\mathbf{H}_N^{(110)} = -\mathbf{1} + \frac{\alpha^2}{2}\sum_j \frac{(\mathbf{r}_{jO}^T \mathbf{r}_{jN})\mathbf{1} - \mathbf{r}_{jO}\mathbf{r}_{jN}^T}{|\mathbf{r}_{jN}|^3} \tag{1.69}$$

$$\mathbf{H}_N^{(020)} = \frac{|\mathbf{r}_{MN}|^2\,\mathbf{1} - 3\mathbf{r}_{MN}\mathbf{r}_{MN}^T}{|\mathbf{r}_{MN}|^5} + \alpha^2 \sum_j \frac{(\mathbf{r}_{jM}^T \mathbf{r}_{jN})\mathbf{1} - \mathbf{r}_{jM}\mathbf{r}_{jN}^T}{|\mathbf{r}_{jM}|^3 |\mathbf{r}_{jN}|^3} \tag{1.70}$$

$$\mathbf{H}_j^{(001)} = \frac{\alpha}{2}\left(-\sum_N Z_N \frac{\mathbf{l}_{jN}}{|\mathbf{r}_{jN}|^3} + \sum_{k\neq j} \frac{\mathbf{l}_{jk} + 2\mathbf{l}_{kj}}{|\mathbf{r}_{jk}|^3} \right) \tag{1.71}$$

$$\begin{aligned} \mathbf{H}_j^{(101)} = & -\frac{\alpha^2}{4}\sum_N Z_N \frac{(\mathbf{r}_{jO}^T \mathbf{r}_{jN})\mathbf{1} - \mathbf{r}_{jO}\mathbf{r}_{jN}^T}{|\mathbf{r}_{jN}|^3} \\ & + \frac{\alpha^2}{4}\sum_{k\neq j}\left(\frac{(\mathbf{r}_{jO}^T \mathbf{r}_{kj})\mathbf{1} - \mathbf{r}_{jO}\mathbf{r}_{kj}^T}{|\mathbf{r}_{jk}|^3} + 2\frac{(\mathbf{r}_{kO}^T \mathbf{r}_{jk})\mathbf{1} - \mathbf{r}_{kO}\mathbf{r}_{jk}^T}{|\mathbf{r}_{jk}|^3} \right) \end{aligned} \tag{1.72}$$

$$\mathbf{H}_{jN}^{(011)} = -\frac{8\pi}{3}\delta(\mathbf{r}_{jN}) + \frac{|\mathbf{r}_{jN}|^2\,\mathbf{1} - 3\mathbf{r}_{jN}\mathbf{r}_{jN}^T}{|\mathbf{r}_{jN}|^5} \tag{1.73}$$

where $\mathbf{r}_{jO} = \mathbf{r}_j - \mathbf{R}_O$ and $\mathbf{l}_{jO} = \mathbf{r}_{jO} \times \mathbf{p}_j$ and $\delta(\mathbf{r}_{jN})$ represents the Dirac delta function. In this Hamiltonian (1.66) represents the orbital Zeeman interaction, (1.67) the diamagnetic response of the electrons to the magnetic field, (1.68) the orbital hyperfine interaction, (1.69) the nuclear Zeeman and the electronic nuclear Zeeman corrections, (1.70) the electron coupled nuclear spin-spin interaction, (1.71) the electron spin-orbit interaction and the electron-electron spin-orbit interaction and the electron spin-other-orbit interaction, (1.72) the electron spin-orbit Zeeman gauge correction and the electron-electron spin-orbit gauge correction and the electron spin-other-orbit Zeeman gauge correction. Finally, (1.73) corresponds to the Fermi contact interaction and the dipolar hyperfine interaction.

Since the magnetic spectral transitions are just due to the spin states, the magnetic resonance can be investigated in terms of the spin Hamiltonian. The spin Hamiltonian is

derived by replacing the full Hamiltonian by an effective operator acting on only spin space:

$$\begin{aligned} \mathrm{H}_{spin} = &-\sum_N g_N \beta_N \mathbf{I}_N^T (\mathbf{1} - \boldsymbol{\sigma}_N)\mathbf{B} + \frac{1}{2}\sum_M \sum_N g_M \beta_N g_N \beta_N \mathbf{I}_M^T (\mathbf{D}_{MN} + \mathbf{K}_{MN})\mathbf{I}_N \\ &+ \sum_j \beta \mathbf{S}_j^T (g_e \mathbf{1} + \Delta\mathbf{g})\mathbf{B} - \sum_j \sum_N \mathbf{S}_j^T (A_{iso,N}\mathbf{1} + \mathbf{A}_{dip,N})\mathbf{I}_N \end{aligned} \tag{1.74}$$

where $\boldsymbol{\sigma}_N$ is the shielding tensor of the nucleus N, $\mathbf{D}_{MN}$ is the nuclear dipole-dipole coupling tensor for nuclei M and N, $\mathbf{K}_{MN}$ is the electron coupled (or reduced) nuclear spin-spin coupling tensor for nuclei M and N, $\Delta\mathbf{g}$ is the change from the free electron g-tensor, $A_{iso,N}$ is the isotropic hyperfine constant and $\mathbf{A}_{dip,N}$ is the anisotropic hyperfine tensor. In (1.74) the zero-field splitting can be neglected (in the high-field limit) and for a rapidly tumbling molecule, the direct spin-spin coupling constants $\mathbf{D}_{MN}$ vanish due to a rotational averaging of the spin Hamiltonian. The analysis of magnetic resonance spectra can be performed by the calculation of the magnetic resonance parameters in terms of the molecular electronic structure of the system.

The magnetic parameters can be derived in terms of the second derivatives of the total molecular energy E with respect to perturbation parameters, **a** and **b**:

$$\mathbf{E}_{\mathbf{ab}}^{(11)} = \left(\frac{\partial^2 \mathrm{E}}{\partial \mathbf{a} \partial \mathbf{b}} \right)_{\mathbf{a}=\mathbf{b}=0} \tag{1.75}$$

In quantum mechanics, the magnetic resonance parameters may be determined by the second derivatives of the energy expectation value of the complete Hamiltonian with respect to perturbation parameters:

$$\mathbf{E}_{\mathbf{ab}}^{(11)} = \left(\frac{\partial^2 < \Psi(\mathbf{a},\mathbf{b}) \mid \mathrm{H}(\mathbf{a},\mathbf{b}) \mid \Psi(\mathbf{a},\mathbf{b}) >}{\partial \mathbf{a} \partial \mathbf{b}} \right)_{\mathbf{a}=\mathbf{b}=0} \tag{1.76}$$

where the Hamiltonian $\mathbf{H(a,b)}$ contains the perturbation terms depending on **a** and **b**, and $\mathbf{\Psi(a,b)}$ is the ground state wavefunction of this Hamiltonian. Using the Hellmann-Feynman theorem, we can transform Eq. (1.75) to the form:

$$\begin{aligned} \mathbf{E}_{\mathbf{ab}}^{(11)} &= \frac{\partial}{\partial \mathbf{a}}\left(< \Psi(\mathbf{a}) | \left(\frac{\partial \mathbf{H(a,b)}}{\partial \mathbf{b}} \right)_{\mathbf{b}=0} | \Psi(\mathbf{a}) > \right)_{\mathbf{a}=0} \\ &= \frac{\partial}{\partial \mathbf{b}}\left(< \Psi(\mathbf{b}) | \left(\frac{\partial \mathbf{H(a,b)}}{\partial \mathbf{a}} \right)_{\mathbf{a}=0} | \Psi(\mathbf{b}) > \right)_{\mathbf{b}=0} \end{aligned} \tag{1.77}$$

In the above equation, the parameters **a** and **b** can exchange freely and hence it is often referred to as the exchange theorem of double perturbation theory [35, 33]. Here, it should be noted that the wavefunction in Eq. (1.77) depends on only one parameter up to first order. This approach enables us to treat the magnetic parameters within a single framework and to make the mathematical processes simple since many terms that are independent of the parameters under consideration can be removed.

1.3.1. Perturbation Theory

Among the second-order magnetic properties, the diamagnetic part depends only on the ground state wave function and the calculation is straightforward:

$$\mathbf{E}_{\mathbf{ab}}^{(11),dia} = < \Psi^{(0)} | \mathbf{H}^{(11)} | \Psi^{(0)} > \tag{1.78}$$

But, the paramagnetic part depends on the first-order perturbed wave function and there are a number of methods to calculate this term efficiently:

$$\mathbf{E}_{\mathbf{ab}}^{(11),para} = < \Psi^{(10)} | \mathbf{H}^{(01)} | \Psi^{(0)} > + < \Psi^{(0)} | \mathbf{H}^{(01)} | \Psi^{(10)} > \tag{1.79}$$

Here, we will focus on the two methods: the uncoupled DFT (UDFT) [34,37] and the finite perturbation theory (FTP) [36].

In the KS-DFT scheme where current density is not involved and only one electron operators of magnetic fields are considered, a magnetic property can be defined as:

$$\mathbf{E}_{\mathbf{ab}}^{(11)} = \sum_{k\sigma}^{occ} \frac{\partial}{\partial \mathbf{a}} \left(< \phi_{k\sigma}(\mathbf{a}) \,|\, \mathbf{H}^{(01)} + \mathbf{a}^T \mathbf{H}^{(11)} \,|\, \phi_{k\sigma}(\mathbf{a}) > \right)_{\mathbf{a}=0} \tag{1.80}$$

where $\phi_{k\sigma}$ refers to KS molecular orbitals with spin σ (hereafter, the label KS will be dropped to simplify the notation). Since the first order operator $\mathbf{H}^{(10)}$ is purely imaginary (see, Eqs. (1.66, 68, 71)), the KS orbitals can be expanded in a power series for the imaginary perturbation parameter $i\mathbf{a}$ to make the second-order properties observable:

$$\phi_{k\sigma}(\mathbf{a}) = \phi_{k\sigma}^{(0)} + (i\mathbf{a})\phi_{k\sigma}^{(1)} + (i\mathbf{a})^2 \phi_{k\sigma}^{(2)} + \ldots \tag{1.81}$$

The first-order perturbed molecular orbitals $\phi_{k\sigma}^{(1)}$ can be obtained from the KS orbital equation for a system in the presence of a perturbation parameter **a**:

$$\begin{aligned} &\mathbf{F}_\sigma(\mathbf{a})\phi_{k\sigma}(\mathbf{a}) \\ &= [-\frac{1}{2}\nabla^2 + v_{eff}^{\sigma}(\mathbf{a}) + \mathbf{a}\mathbf{H}^{(1)}]\phi_{k\sigma}(\mathbf{a}) \\ &= \varepsilon_{k\sigma}(\mathbf{a})\phi_{k\sigma}(\mathbf{a}) \end{aligned} \tag{1.82}$$

In the finite perturbation theory (FPT) [36], Eq. (1.82) is solved self-consistently with a finite value ($\mathbf{a} \ll 1$) of the perturbation parameter **a**. The additional matrix elements corresponding to $\mathbf{a}\mathbf{H}^{(1)}$ are added to the Fock matrix. The implementation of this method is simple and the Fermi contact contribution of the nuclear spin-spin coupling is usually solved by this method. However, the finite value should be reasonably chosen to avoid the quadratic effect (if it is too large) and to separate it from the numerical noise (if it is

too small). Furthermore, if the perturbation is purely imaginary or complex, the FPT will be much more time-comsuming.

In the uncoupled DFT (UDFT) [34,37], Eq (1.82) is expanded in terms of the perturbation parameter a up to first-order and collecting terms of the first-order (in this case, the equation sets free from the perturbation parameters and there are no imaginary terms):

$$[-\frac{1}{2}\nabla^2 + v_{eff}^{\sigma,(0)}]\ \phi_{k\sigma}^{(1)} + [\mathbf{H}^{(1)} + v_{eff}^{\sigma,(1)}]\ \phi_{k\sigma}^{(0)} = \varepsilon_{k\sigma}^{(0)}\phi_{k\sigma}^{(1)} \tag{1.83}$$

To obtain $\phi_{k\sigma}^{(1)}$, the unperturbed KS equation has to be solved, first. In this case, the first order corrections to the orbitals are purely imaginary and the first-order change in the electron density vanishes:

$$\boldsymbol{\rho}^{(1)} = \left(\frac{\partial\rho(\mathbf{a})}{\partial\mathbf{a}}\right)_{\mathbf{a}=0} = \sum_{k\sigma}^{occ}(-i\mathbf{a} < \phi_{k\sigma}^{(1)} \mid \phi_{k\sigma}^{(0)} > + i\mathbf{a} < \phi_{k\sigma}^{(0)} \mid \phi_{k\sigma}^{(1)} >) = 0 \tag{1.84}$$

This is an important point in UDFT-NMR calculations because the first order change in the exchange-correlation (XC) potential $v_{eff}^{(1)}$ in Eq (1.83) can be removed under the approximation that the XC functional only depends on the electron density. In fact, the exact XC functional depends on the paramagnetic current density as well as the electron density in the external magnetic field. However, its contribution to magnetic properties would be rather small and can be neglected (this was proved for chemical shielding [38]).

In UDFT, the KS orbitals in a perturbation can be expanded in terms of the linear combination of field free atomic orbitals $\chi_{\mu}^{(0)}$ (for simplicity, a common origin or a natural origin is only considered here):

$$\phi_{k\sigma}(\mathbf{a}) = \sum_{\mu}^{basis} C_{\mu k\sigma}(\mathbf{a})\chi_{\mu}^{(0)} \tag{1.84}$$

and the atomic density matrix element $\mathbf{P}_{\mu\nu}$ is defined as:

$$\mathbf{P}_{\mu\nu}(\mathbf{a}) = \sum_{k\sigma}^{occ} C_{\mu k\sigma}^{*}(\mathbf{a})C_{\nu k\sigma}(\mathbf{a}) \tag{1.85}$$

Here, a set of $C_{\mu k\sigma}(\mathbf{a})$ denotes field-dependent molecular orbital coefficients. The first order corrections of the atomic density matrix elements are obtained by the field-dependent Roothaan equation (in a matrix form) [39]:

$$\mathbf{F(a)C(a) = S(a)C(a)E(a)} \tag{1.86}$$

where all terms have conventional meanings. The field-dependent molecular coefficient matrix **C(a)** is redefined with the field-dependent expansion coefficient matrix **U(a)** and the field-free molecular coefficient matrix **C(0)** in the first order perturbation approximation [40]:

$$\mathbf{C(a)=C(0)d(a)} \tag{1.87}$$

The Roothaan equation in terms of **d(a)** is:

$$\mathbf{F'(a)U(a)=S'(a)d(a)E(a)} \tag{1.88}$$

with

$$\mathbf{F'(a) = C^{\dagger}(0)F(a)C(0)} \tag{1.89}$$

and

$$\mathbf{S'(a) = C^{\dagger}(0)S(a)C(0)} \tag{1.90}$$

The orthonormal condition gives the diagonal elements of the first order expansion coefficient matrix element $d_{kk}^{(1)}$ and for the common gauge origin (center of charge) or natural origin (position of a nucleus of interest), this term goes to zero since the atomic basis functions are field free:

$$d_{kk}^{(1)} = -\frac{1}{2} S_{kk}^{\prime(1)} = 0 \tag{1.91}$$

where k refers to the occupied orbitals. If the field dependent Roothaan equation is solved to first order in the field, the off-diagonal elements of the first-order expansion coefficient $d_{ak}^{(1)}$ can be derived as:

$$d_{ak}^{(1)} = \frac{F_{ak}^{\prime(1)} - S_{ak}^{\prime(1)}\varepsilon_k^{(0)}}{\varepsilon_k^{(0)} - \varepsilon_a^{(0)}} = \frac{F_{ak}^{\prime(1)}}{\varepsilon_k^{(0)} - \varepsilon_a^{(0)}} = \frac{<\phi_a|\mathbf{H}^{(1)}|\phi_k>}{\varepsilon_k^{(0)} - \varepsilon_a^{(0)}} \tag{1.92}$$

where $\varepsilon_k^{(0)}$ and $\varepsilon_a^{(0)}$ represent the occupied and the virtual orbital KS orbital energies in the absence of fields, respectively. In UDFT ($v_{eff}^{(1)}$ =0), the perturbed Roothaan equation is not coupled and thus the first-order perturbed KS orbitals can be obtained by a single calculation after the self-consistent calculation of the unperturbed KS equations.

1.3.2. NMR Chemical Shielding Tensors

The NMR shielding tensors can be defined as the second-order response of the electronic energy to the external magnetic moment $\mathbf{B}$ and the nuclear magnetic moment $\mathbf{M}_N$:

$$\begin{aligned}\boldsymbol{\sigma}_N &= \left[\frac{\partial^2 \mathrm{E}(\mathbf{B},\mathbf{M}_N)}{\partial \mathbf{B}\partial \mathbf{M}_N}\right]_{\mathbf{B}=\mathbf{M}_N=0} \\ &= \sum_{k\sigma}^{occ}\left(\frac{\partial}{\partial \mathbf{B}} < \phi_{k\sigma}(\mathbf{B}) \mid \mathbf{H}_N^{(010)} + \mathbf{B}^T \mathbf{H}_N^{(110)} \mid \phi_{k\sigma}(\mathbf{B}) >\right)_{\mathbf{B}=0}\end{aligned} \tag{1.93}$$

Here, it is shown that the KS orbitals $\phi_{k\sigma}$ are perturbed only by $\mathbf{B}$ and it is sufficient to determine them up to first order with respect to $\mathbf{B}$ for the shielding calculation. The explicit forms of the one-electron operators $\mathbf{H}_N^{(010)}$ and $\mathbf{H}_N^{(110)}$ are given in Eqs (1.68, 69).

Physical observables such as the energy and the current density should be gauge independent. In fact, the calculated NMR shielding tensor with the finite basis sets depends on the choice of the gauge origin. For the vector potential $\mathbf{A}_N$ relating to the magnetic moment of the nucleus N, $\mathbf{R}_N$ is an obvious natural gauge origin because the position of the nucleus N is the origin of the magnetic moment. On the other hand, for the vector potential $\mathbf{A}_O$ relating to the homogeneous external magnetic moment, $\mathbf{R}_O$ is an arbitrary gauge origin because we don't know the explicit origin of the homogeneous external magnetic field. So far, many ways to solve the gauge problem have been developed [41]. In this study, we focus on two methods: the "gauge including atomic orbitals" (GIAO) [41(a)] and the "individual gauge for localized orbitals (IGLO) [41(b)].

In the GIAO ansatz, the atomic basis functions are taken to be field dependent:

$$\begin{aligned}\chi_\mu(\mathbf{B}) &= \exp[-i\mathbf{B}\cdot\boldsymbol{\Lambda}_\mu]\cdot\chi_\mu^{(0)} \\ &= \mathbf{F}_\mu(\mathbf{B})\cdot\chi_\mu^{(0)}\end{aligned} \tag{1.94}$$

where

$$\boldsymbol{\Lambda}_\mu = \frac{\alpha}{2}(\mathbf{R}_\mu - \mathbf{R}_O)\times\mathbf{r} \tag{1.95}$$

Here, $\chi_\mu^{(0)}$ represents standard (field free) Gaussian atomic orbitals and $\mathbf{R}_\mu$ is the position vector of the atom where the orbital χ_μ is centered. In Eq (1.94) the field dependent phase factor gauarantees that the expectation values are gauge invariant. In this case, in Eqs. (1.91 and 1.92), the first order corrections of the overlap integrals $\mathbf{S}_{\mathbf{kk}}^{\prime(1)}$ and $\mathbf{S}_{\mathbf{ak}}^{\prime(1)}$ do not disappear. The GIAO shielding tensors have a more complex form due to the field-dependent basis functions. The shielding tensors can be separated into diamagnetic and paramagnetic contributions ($\sigma = \sigma^d + \sigma^p$) where both are gauge invariant and are expectation values of Hermitian operators [42].

In the UDFT-GIAO scheme, the diamagnetic term can be described as:

$$\begin{aligned}\boldsymbol{\sigma}_N^d &= \sum_{k\sigma}^{occ} < \phi_{k\sigma}^{(0)} \mid \tilde{\mathbf{H}}_N^{(110)} + \tilde{\mathbf{H}}_{N,d}^{(010)} \mid \phi_{k\sigma}^{(0)} > \\ &= \sum_{k\sigma}^{occ} \sum_{\mu\nu}^{basis} C_{\mu k\sigma}^{(0)} C_{\nu k\sigma}^{(0)} < \chi_\mu^{(0)} \mid \tilde{\mathbf{H}}_N^{(110)} + \tilde{\mathbf{H}}_{N,d}^{(010)} \mid \chi_\nu^{(0)} >\end{aligned} \tag{1.96}$$

where

$$\tilde{\mathbf{H}}_N^{(110)} = \frac{\alpha^2}{2} \frac{(\mathbf{r}_\nu^T \mathbf{r}_N)\mathbf{1} - \mathbf{r}_\nu \mathbf{r}_N^T}{|\mathbf{r}_N|^3} \tag{1.97}$$

and

$$\tilde{\mathbf{H}}_{N,d}^{(010)} = \frac{\alpha}{2} i(\mathbf{R}_{\mu\nu} \times \mathbf{r}_{k\nu})(\mathbf{H}_N^{(010)})^T \tag{1.98}$$

The operator $\tilde{\mathbf{H}}_N^{(110)}$ is gauge-transformed from the arbitrary origin $\mathbf{R}_O$ to the GIAO origin $\mathbf{R}_\nu$. The last term in Eq (1.96) depends on the gauge factors and makes $\boldsymbol{\sigma}_N^d$ Hermitian.

The paramagnetic terms $\boldsymbol{\sigma}_N^p$ can be decomposed to the three individual contributions and described as:

$$\boldsymbol{\sigma}_N^p = \boldsymbol{\sigma}_N^{p0} + \boldsymbol{\sigma}_N^{p1} + \boldsymbol{\sigma}_N^{p2} \tag{1.99a}$$

$$\begin{aligned}\boldsymbol{\sigma}_N^{p0} &= \sum_{k\sigma}^{occ} < \phi_{k\sigma}^{(0)} \mid \widetilde{\mathbf{H}}_{N,p}^{(010)} \mid \phi_{k\sigma}^{(0)} > \\ &= \sum_{\mu\nu}^{basis} \sum_{k\sigma}^{occ} C_{\mu k\sigma}^{(0)} C_{\nu k\sigma}^{(0)} < \chi_\mu^{(0)} \mid \widetilde{\mathbf{H}}_{N,p}^{(010)} \mid \chi_\nu^{(0)} >\end{aligned} \tag{1.99b}$$

$$\begin{aligned}\boldsymbol{\sigma}_N^{p1} &= \sum_{kj\sigma}^{occ} < \phi_{k\sigma}^{(0)} \mid \mathbf{H}_N^{(010)} \mid \phi_{j\sigma}^{(0)} >< \phi_{j\sigma}^{(0)} \mid (\boldsymbol{\Lambda}_{\mu\nu})^T \mid \phi_{k\sigma}^{(0)} > \\ &= \sum_{\mu\nu}^{basis} \sum_{kj\sigma}^{occ} C_{\mu k\sigma}^{(0)} C_{\nu k\sigma}^{(0)} < \phi_{k\sigma}^{(0)} \mid \mathbf{H}_N^{(010)} \mid \phi_{j\sigma}^{(0)} >< \chi_\mu^{(0)} \mid (\boldsymbol{\Lambda}_{\mu\nu})^T \mid \chi_\nu^{(0)} >\end{aligned} \tag{1.99c}$$

$$\begin{aligned}\boldsymbol{\sigma}_N^{p2} &= -2 \sum_{k\sigma}^{occ} \sum_{a}^{vir} < \phi_{k\sigma}^{(0)} \mid \mathbf{H}_N^{(010)} \mid \phi_{a\sigma}^{(0)} > \left(\frac{< \phi_{a\sigma}^{(0)} \mid \left(\widetilde{\mathbf{H}}^{(100)}\right)^T \mid \phi_{k\sigma}^{(0)} >}{\varepsilon_{k\sigma}^{(0)} - \varepsilon_{a\sigma}^{(0)}} \right) \\ &= -2 \sum_{\mu\nu}^{basis} \sum_{k\sigma}^{occ} \sum_{a}^{vir} C_{\mu k\sigma}^{(0)} C_{\nu k\sigma}^{(0)} < \phi_{k\sigma}^{(0)} \mid \mathbf{H}_N^{(010)} \mid \phi_{a\sigma}^{(0)} > \left(\frac{< \chi_\mu^{(0)} \mid \left(\widetilde{\mathbf{H}}^{(100)}\right)^T \mid \chi_\nu^{(0)} >}{\varepsilon_{k\sigma}^{(0)} - \varepsilon_{a\sigma}^{(0)}} \right)\end{aligned} \tag{1.99d}$$

where the operator $\mathbf{H}_N^{(010)}$ is shown in Eq (1.68) and the operators $\boldsymbol{\Lambda}_{\mu\nu}$ and $\widetilde{\mathbf{H}}_{N,p}^{(010)}$ are given by:

$$\boldsymbol{\Lambda}_{\mu\nu} = i(\boldsymbol{\Lambda}_\mu - \boldsymbol{\Lambda}_\nu) \tag{1.100}$$

and

$$\widetilde{\mathbf{H}}_{N,p}^{(010)} = -\frac{\alpha}{2} i(\mathbf{R}_\mu \times \mathbf{R}_\nu)(\mathbf{H}_N^{(010)})^T \tag{1.101}$$

and, at last, the operator $\widetilde{\mathbf{H}}^{(100)}$ takes the form:

$$\widetilde{\mathbf{H}}^{(100)} = \mathbf{H}^{(100)} + \mathbf{\Lambda}_{\mu\nu}\mathbf{F}^{(0)}_{k\sigma} - \varepsilon^{(0)}_{k\sigma}\mathbf{\Lambda}_{\mu\nu} \tag{1.102}$$

where the operator $\mathbf{H}^{(100)}$ is described in Eq. (1.66), $\mathbf{F}^{(0)}_{k\sigma}$ and $\varepsilon^{(0)}_{k\sigma}$ denote the unperturbed KS operator and orbital energies of spin σ, respectively.

In the IGLO ansatz, the field dependent phase factor which gauarantees the gauge invariance of physical observables is included into the localized KS molecular orbitals (LMO) $\widetilde{\phi}_k$ [43]:

$$\widetilde{\phi}'_k(\mathbf{B}) = \mathbf{exp}[-i\mathbf{B}\cdot\mathbf{\Lambda}_k]\cdot\widetilde{\phi}_k\,(\mathbf{B}) \tag{1.103}$$

where

$$\mathbf{\Lambda}_k = \frac{\alpha}{2}(\mathbf{R}_k - \mathbf{R}_O)\times\mathbf{r} \tag{1.104}$$

where $\mathbf{R}_k$ is the centroid of the charge (dipole moment) of the LMO $\widetilde{\phi}_k$. The LMOs can obtained by the unitary transformation of the canonical KS orbitals (COs) ϕ_p:

$$\widetilde{\phi}_k = \sum_p^{occ} U_{pk}\phi_p \tag{1.105}$$

For a single determinant wave function, any expectation value is invariant under a unitary transformation. Since the spin orbitals that make the electronic energy stationary are not unique, no particular physical significance can be given to a particular set of spin orbitals. Hence, the COs ϕ_k of Eq. (1.82) can be replaced with the LMOs $\widetilde{\phi}'_k$ without any change

of the shielding but since the LMOs are not the eigenfunction of the KS operator they can be mixed among themselves without changing the expectation value.

$$\boldsymbol{\sigma}_N = \sum_{kj\sigma}^{occ} \frac{\partial}{\partial \mathbf{B}} \left(< \tilde{\phi}'_{k\sigma}(\mathbf{B}) \,|\, \mathbf{H}_N^{(010)} + \mathbf{B}^T \mathbf{H}_N^{(110)} \,|\, \tilde{\phi}'_{j\sigma}(\mathbf{B}) > < \tilde{\phi}'_{j\sigma}(\mathbf{B}) \,|\, \tilde{\phi}'_{k\sigma}(\mathbf{B}) > \right)_{\mathbf{B}=0} \tag{1.106}$$

In the UDFT scheme with the orbital energy correction term in the paramagnetic shielding, the explicit form of shielding tensor using the IGLO method can be derived ,which is often called the sum-over-state density functional perturbation theory (SOS-DFTP) [34].

The diamagnetic term $\boldsymbol{\sigma}_N^d$ which just depends on the unperturbed KS orbitals is defined as:

$$\boldsymbol{\sigma}_N^d = \sum_{k\sigma}^{occ} < \tilde{\phi}_{k\sigma}^{(0)} \,|\, \tilde{\mathbf{H}}_N^{(110)} \,|\, \tilde{\phi}_{k\sigma}^{(0)} > \tag{1.107}$$

where

$$\tilde{\mathbf{H}}_N^{(110)} = \frac{\alpha^2}{2} \frac{(\mathbf{r}_k^T \mathbf{r}_N)\mathbf{1} - \mathbf{r}_k \mathbf{r}_N^T}{|\mathbf{r}_N|^3} \tag{1.108}$$

where the operator $\tilde{\mathbf{H}}_N^{(110)}$ is gauge-transformed from the arbitrary origin $\mathbf{R}_O$ to the IGLO origin $\mathbf{R}_k$.

The paramagnetic terms $\boldsymbol{\sigma}_N^p$ are usually decomposed to the two contributions and expressed by:

$$\boldsymbol{\sigma}_N^p = \boldsymbol{\sigma}_N^{p0} + \boldsymbol{\sigma}_N^{p1} \tag{1.109a}$$

where

$$\boldsymbol{\sigma}_N^{p0} = \sum_{kj\sigma}^{occ} < \tilde{\phi}_{k\sigma}^{(0)} \mid \mathbf{H}_N^{(010)} \mid \tilde{\phi}_{j\sigma}^{(0)} \succ\prec \tilde{\phi}_{j\sigma}^{(0)} \mid \boldsymbol{\Lambda}_{jk} \mid \tilde{\phi}_{k\sigma}^{(0)} > \tag{1.109b}$$

and

$$\boldsymbol{\sigma}_N^{p1} = 2\sum_{k\sigma}^{occ}\sum_{a}^{vir} < \tilde{\phi}_{k\sigma}^{(0)} \mid \mathbf{H}_{N\sigma}^{(010)} \mid \tilde{\phi}_{a\sigma}^{(0)} > \tilde{\mathrm{d}}_{\mathrm{ak}\sigma}^{(1)} \tag{1.109c}$$

where the operator $\mathbf{H}_N^{(010)}$ can be seen in Eq. (1.68) and the operator $\boldsymbol{\Lambda}_{jk}$ is defined as:

$$\boldsymbol{\Lambda}_{jk} = i(\boldsymbol{\Lambda}_j - \boldsymbol{\Lambda}_k) \tag{1.110}$$

and the off-diagonal elements of the first-order expansion coefficient is given by:

$$\begin{aligned} \tilde{\mathrm{d}}_{\mathrm{ak}\sigma}^{(1)} = & \sum_{m\sigma}^{occ} \left[\frac{\sum_{n}^{occ} < \phi_{a\sigma}^{(0)} \mid \left(\mathbf{H}_N^{(100)}\right)^T \mid \tilde{\phi}_{n\sigma}^{(0)} > U_{nm}}{\varepsilon_{m\sigma}^{(0)} - \varepsilon_{a\sigma}^{(0)} - \Delta E_{m\to a}^{XC}} \right] U_{km} \\ & + \sum_{m\sigma}^{occ} \left[\frac{\sum_{nj}^{occ} < \phi_{a\sigma}^{(0)} \mid (\boldsymbol{\Lambda}_{jk})^T \mid \tilde{\phi}_{j\sigma}^{(0)} \succ\prec \tilde{\phi}_{j\sigma}^{(0)} \mid \mathbf{F}_{\sigma}^{(0)} \mid \tilde{\phi}_{n\sigma}^{(0)} > U_{nm}}{\varepsilon_{m\sigma}^{(0)} - \varepsilon_{a\sigma}^{(0)} - \Delta E_{m\to a}^{XC}} \right] U_{km} \end{aligned} \tag{1.111}$$

where index "m" refers to the COs and indices "n", "j" and "k" correspond to the LMOs. The explicit forms of the orbital energy correction $\Delta E_{m\to a}^{XC}$ can be seen in ref [34] and by this correction the current density dependence of the XC functionals can be taken into account indirectly.

1.3.3. NMR Nuclear Spin-Spin Coupling Tensors

The reduced nuclear spin-spin coupling tensors $\mathbf{K}_{MN}$ is defined as the second derivative of the total energy of the system to the magnetic moments of the nuclei M and N:

$$\begin{aligned}\mathbf{K}_{MN} &= \left[\frac{\partial^2 \mathrm{E}(\mathbf{M}_M,\mathbf{M}_N)}{\partial \mathbf{M}_M \partial \mathbf{M}_N}\right]_{\mathbf{M}_N=\mathbf{M}_M=0} \\ &= \sum_{k\sigma}^{occ}\left(\frac{\partial}{\partial \mathbf{M}_M} < \phi_{k\sigma}(\mathbf{M}_M) \mid \mathbf{H}_N^{(010)} + \mathbf{M}_M^T \mathbf{H}_{MN}^{(020)} - g_e \beta_e \mathbf{s}_k^T \mathbf{H}_N^{(011)} \mid \phi_{k\sigma}(\mathbf{M}_M) > \right)_{\mathbf{M}_M=0}\end{aligned} \tag{1.112}$$

The reduced coupling tensors are related to the experimentally detectable coupling tensors by the formula [44]:

$$\mathbf{J}_{MN} = g_M \beta_N g_N \beta_N \mathbf{K}_{MN} \tag{1.113}$$

The reduced coupling tensors $\mathbf{K}_{MN}$ are independent of the nuclear g-values and the nuclear magneton and just depends on the electronic structure of the system. From Eq (1.112), it is shown that there are four contributions to the coupling.

The first operator $\mathbf{H}_N^{(010)}$ of the Hamiltonian in Eq (1.112) represents the paramagnetic spin-orbit (PSO) contribution. In the UDFT scheme with the additional orbital energy correction, this PSO contribution takes the form:

$$\mathbf{K}_{MN}^{PSO} = -2\sum_{k\sigma}^{occ}\sum_{a}^{vir} \frac{< \phi_{k\sigma}^{(0)} \mid \mathbf{H}_M^{(010)} \mid \phi_{a\sigma}^{(0)} >< \phi_{a\sigma}^{(0)} \mid \left(\mathbf{H}_N^{(010)}\right)^T \mid \phi_{k\sigma}^{(0)} >}{\varepsilon_{k\sigma}^{(0)} - \varepsilon_{a\sigma}^{(0)} - \Delta E_{k\to a}^{XC}} \tag{1.114}$$

where the factor of two arises because of the presence of two equivalent energy terms which differ in that the two nuclei M and N are permuted [44].

The second operator $\mathbf{H}_{MN}^{(020)}$ in Eq. (1.112) represents the diamagnetic spin-orbit (DSO) contribution. The DSO term has a bilinear dependence on $\mathbf{M}_M$ and $\mathbf{M}_N$, and this contribution only depends on the unperturbed ground state wave function:

$$\mathbf{K}_{MN}^{DSO} = 2\sum_{k\sigma}^{occ} < \phi_{k\sigma}^{(0)} | \mathbf{H}_{MN}^{(020)} | \phi_{k\sigma}^{(0)} > \tag{1.115}$$

where the factor of two has the same meaning as in the case of the PSO term.

The Fermi contact (FC) arises from the first term of the operator $\mathbf{H}_N^{(011)}$ in Eq. (1.73). This is the most important of all the contributions and the most sensitive to geometry changes [45]. The FC term takes the form:

$$\mathbf{K}_{MN}^{FC} = \sum_{k\sigma}^{occ} \left(\frac{\partial}{\partial \mathbf{M}_M} < \phi_{k\sigma}(\mathbf{M}_M) | \frac{\alpha}{2} \left(\frac{g_e}{2} \right) \frac{8\pi}{3} \delta(\mathbf{r}_{kN}) \mathbf{s}_k \mathbf{1} | \phi_{k\sigma}(\mathbf{M}_M) > \right)_{\mathbf{M}_M = 0} \tag{1.116}$$

This term can be solved self-consistently using the finite perturbation theory (FPT) [36]. The FPT method is equivalent to a complete solution of the infinitesimal perturbation in the limit of small perturbations. In this theory, the matrix element of the Hamiltonian is:

$$H_{\mu\nu}^{\alpha}(\mathbf{M}_M) = H_{\mu\nu}^{\alpha}(0) + \lambda < \chi_{\mu}^{(0)} | \delta(\mathbf{r}_M) | \chi_{\nu}^{(0)} > \tag{1.117}$$

for spin α and

$$H_{\mu\nu}^{\beta}(\mathbf{M}_M) = H_{\mu\nu}^{\beta}(0) - \lambda < \chi_{\mu}^{(0)} | \delta(\mathbf{r}_M) | \chi_{\nu}^{(0)} > \tag{1.118}$$

for spin β, where λ denotes the perturbation parameter. The final expression of the reduced FC coupling constant is:

$$\mathbf{K}_{MN}^{FC} = \left(\frac{8\pi}{3}\right)^2 \left(\frac{\alpha}{2}\right)^2 \left(\frac{g_e}{2}\right)^2 (\lambda)^{-1} \sum_{\mu\nu} P_{\mu\nu}^{\alpha-\beta}(\lambda) < \chi_\mu^{(0)} \mid \delta(\mathbf{r}_N)\mathbf{1} \mid \chi_\nu^{(0)} > \qquad (1.119)$$

where

$$P_{\mu\nu}^{\alpha-\beta}(\lambda) = \sum_k^{occ(\alpha)} C_{k\mu}^{(0)*}(\lambda) C_{k\nu}^{(0)}(\lambda) - \sum_k^{occ(\beta)} C_{k\mu}^{(0)*}(\lambda) C_{k\nu}^{(0)}(\lambda) \qquad (1.120)$$

The second term of $\mathbf{H}_N^{(011)}$ in Eq (1.73) leads the spin-dipolar (SD) contribution. The calculation of the SD contribution is the most time-consuming of the second-order terms due to the electron spin and position vector coupling term ($\mathbf{s}_k \cdot \mathbf{r}_{kN}$) but its contribution to the total spin coupling is relatively small (the details of this term are in ref [44]). Hence, this term is normally not taken into account. In addition to the four contributions, the FC-SD (Fermi contact-spin-dipolar) cross term should be considered because the anisotropy of the nuclear spin coupling tensor is dominated by this cross term. The term can be calculated by the FPT as in the case of the Fermi contact coupling [34].

1.3.4. Hyperfine Coupling Tensors

The reduced hyperfine (hf) coupling tensors $\mathbf{T}_N$, which are independent of $g_e\beta g_N\beta_N$, can be explained as the second order derivatives of the electronic energy to the nuclear magnetic momentum and the electronic magnetic momentum:

$$\begin{aligned}
\mathbf{T}_N &= \left[\frac{\partial^2 \mathrm{E}(\mathbf{M}_N, \mathbf{m})}{\partial \mathbf{M}_N \partial \mathbf{m}}\right]_{\mathbf{m}=\mathbf{M}_N=0} \\
&= \langle \mathbf{S}_Z \rangle^{-1} \sum_{k\sigma}^{occ} < \phi_{k\sigma}^{(0)} \mid \mathbf{s}_k^T \mathbf{H}_N^{(011)} \mid \phi_{k\sigma}^{(0)} > \qquad (1.121) \\
&+ \langle \mathbf{S}_Z \rangle^{-1} \sum_{k\sigma}^{occ} \left(\frac{\partial}{\partial \mathbf{M}_N} < \phi_{k\sigma}(\mathbf{M}_N) \mid \mathbf{s}_k^T \mathbf{H}_k^{(001)} + \mathbf{B}^T \mathbf{H}_k^{(101)} \mathbf{s}_k \mid \phi_{k\sigma}(\mathbf{M}_N) > \right)_{\mathbf{M}_N=0}
\end{aligned}$$

In the above equation, the integrals with the operators $\mathbf{H}_k^{(001)}$ and $\mathbf{H}_k^{(101)}$ represent the spin-orbit interactions and the spin-orbit gauge corrections, respectively. The contributions of these terms to the total hf coupling is, however, relatively small and we just focused on the Fermi contact (isotropic) and the spin dipolar (anisotropic) interactions which arise from the operator $\mathbf{H}_{kN}^{(011)}$. The Fermi contact interaction is purely quantum mechanical and arises when there is a non-zero probability of finding the electron at a magnetic nucleus. This is the case when the singly occupied molecular orbital has s-character on the target nucleus. The Fermi contact term, $\mathbf{A}_N^{iso} = g_e \beta g_N \beta_N \mathbf{T}_N^{iso}$, takes the form:

$$\mathbf{A}_N^{iso} = \frac{4\pi}{3} g_e \beta g_N \beta_N \langle S_z \rangle^{-1} \sum_{\mu\nu}^{basis} P_{\mu\nu}^{\alpha-\beta} < \chi_\mu^{(0)} \mid \delta(\mathbf{r}_{kN})\mathbf{1} \mid \chi_\nu^{(0)} > \qquad (1.122)$$

The second term of the operator $\mathbf{H}_N^{(011)}$ in Eq (1.73) represents the spin dipolar interactions, $\mathbf{A}_N^{dip} = g_e \beta g_N \beta_N \mathbf{T}_N^{dip}$, between the nuclear and the electron spins:

$$\mathbf{A}_N^{dip} = \frac{1}{2} g_e \beta g_N \beta_N \langle S_z \rangle^{-1} \sum_{\mu\nu}^{basis} P_{\mu\nu}^{\alpha-\beta} < \chi_\mu^{(0)} \mid \frac{\mid \mathbf{r}_{kN} \mid^2 \mathbf{1} - 3\mathbf{r}_{kN}\mathbf{r}_{kN}^T}{\mid \mathbf{r}_{kN} \mid^5} \mid \chi_\nu^{(0)} > \qquad (1.123)$$

In general, the experimental values of $A_{\parallel}$ and $A_{\perp}$ components of the hyperfine coupling can be obtained. In the case of axially symmetric systems, $A_{\parallel} = (A_{N,zz}^{dip} + A_N^{iso})$ and $A_{\perp} = [1/2(A_{N,xx}^{dip} + A_{N,yy}^{dip}) + A_N^{iso}]$.

1.3.5. EPR g-tensors

Here, we limit the g-tensor theories on one-component case to treat them in the frame of the perturbation theory. In this case, we assume the spin-orbit coupling may be weak. In a

view of non-relativistic DFT, the two-electron spin-orbit coupling operator might be related to the exchange-correlation functionals which include the current dependent term. Since the exact form of the functionals have been not found, we focus only on UDFT method.

The electronic g-tensors are defined as:

$$\mathbf{g} = g_e \mathbf{1} + \Delta\mathbf{g} \tag{1.124}$$

and the g-shift tensors $\Delta\mathbf{g}$ which are the deviations from the free-electron value g_e. The g-tensors can be defined as the second order response of the electronic energy of the system to the external magnetic field **B** and the effective electron spin **S**:

$$\begin{aligned}\Delta\mathbf{g} &= \frac{1}{\beta}\left[\frac{\partial^2 \mathrm{E}(\mathbf{B},\mathbf{S})}{\partial\mathbf{B}\partial\mathbf{S}}\right]_{\mathbf{S}=\mathbf{B}=0} \\ &= g_e \langle \mathbf{S}_z \rangle^{-1} \sum_{k\sigma}^{occ} \left(\frac{\partial}{\partial \mathbf{B}} < \phi_{k\sigma}(\mathbf{B}) | \mathbf{s}_{kz}^T \mathbf{H}_k^{(001)} + \mathbf{B}^T \mathbf{H}_k^{(101)} \mathbf{s}_{kz} | \phi_{k\sigma}(\mathbf{B}) > \right)_{\mathbf{B}=0}\end{aligned} \tag{1.125}$$

The paramagnetic contributions come from the first term of Eq (1.125) related to the spin-orbit operator $\mathbf{H}_k^{(001)}$. In this case, the ground state wave function is perturbed by the external magentic field up to first order and the final expression of the paramagnetic second-order spin-orbit/orbital Zeeman cross term in the common origin approach is:

$$\begin{aligned}\Delta\mathbf{g}_{SO/OZ}^{para} = g_e \sum_k^{occ(\alpha)} \sum_a^{vir(\alpha)} \frac{< \phi_k^{(0)} | \mathbf{H}_k^{(100)} | \phi_a^{(0)} >< \phi_a^{(0)} | \left(\mathbf{H}_k^{(001)}\right)^T | \phi_k^{(0)} >}{\varepsilon_k^{(0)} - \varepsilon_a^{(0)}} \\ - g_e \sum_k^{occ(\beta)} \sum_a^{vir(\beta)} \frac{< \phi_k^{(0)} | \mathbf{H}_k^{(100)} | \phi_a^{(0)} >< \phi_a^{(0)} | \left(\mathbf{H}_k^{(001)}\right)^T | \phi_k^{(0)} >}{\varepsilon_k^{(0)} - \varepsilon_a^{(0)}}\end{aligned} \tag{1.126}$$

Here, it should be noted that the above equation is only valid for the one-electron operator of $\mathbf{H}_k^{(001)}$ and its two electron operators should be modified as the effective one-

electron operators to be included in this approach. In general, this paramagnetic term $\Delta\mathbf{g}_{SO/OZ}^{para}$ dominates the whole g-tensors and the one-electron spin-orbit term in the operator $\mathbf{H}_k^{(001)}$ have the largest contribution to the tensors.

The diamagnetic spin-Zeeman gauge correction term is represented by the second operator $\mathbf{H}_k^{(101)}$ of Eq (1.125). The diamagnetic term just depends on the unperturbed ground state wave function:

$$\Delta\mathbf{g}_{GC}^{dia} = g_e \sum_{k\sigma}^{occ} < \phi_{k\sigma}^{(0)} \mid \mathbf{H}_k^{(101)} \mid \phi_{k\sigma}^{(0)} > \tag{1.127}$$

The operator $\mathbf{H}^{(101)}$ in Eq (1.72) includes the one- and two-electron terms but generally the two-electron contributions are neglected or consider approximately due to the small effect and the computational complexity.

At the Breit-Pauli level of relativistic treatments up to second order (α^2), the relativistic mass correction $\Delta\mathbf{g}_{RMC}$ to the electron spin Zeeman interaction arises from the magnetic field dependence of the spin-orbit Hamiltonian:

$$\Delta\mathbf{g}_{RMC} = -\frac{1}{2}\alpha^2 g_e \sum_{\mu\nu} P_{\mu\nu}^{\alpha-\beta} < \chi_\mu^{(0)} \mid p^2\mathbf{1} \mid \chi_\nu^{(0)} > \tag{1.128}$$

This term makes a small, isotropic contribution to the g-tensors and can be calculated straightforwardly since it is the expectation value of the unperturbed KS orbitals. It notes that the g-tensors are much less dependent on the gauge origin than chemical shifts [46] and thus only the common gauge origin approach is used here.

1.4. References

1. (a) Purcell, E. M., *Electricity and Magnetism*, McGraw-Hill, New York, 1985.
   (b) Jackson, J. D., *Classical electrodynamics*, Wiley, New York, 1975.
2. Harriman, J. E., *Theoretical Foundations of Electron Spin Resonance*, Academic Press, New York, 1978.
3. (a) Parr. R. G.; Yang, W., *Density Functional Theory of Atoms and Molecules*, Oxford, University Press, Oxford, 1989.
   (b) Koch, W.; Holthausen, M. C., *A Chemist's Guide to Density Functional Theory*, Wiley-VCH, New York, 2000.
4. Hohenberg, P.; Kohn, W. *Phys. Rev.* **1964**, 136, B864.
5. Kohn, W.; Sham, L. J. *Phys. Rev.* **1965**, 140, A1133.
6. (a) Thomas, L. H. *Proc. Camb. Phil. Soc.* **1926**, 23, 542.
   (b) Fermi, E. *Z. Phys.* **1928**, 48, 73.
7. Schrödinger, E. *Ann. Phys.* **1926**, 79, 361.
8. Davidson, E. R., *Reduced Density Matrices in Quantum Chemistry*, Academic Press, New York, 1976.
9. Baerends, E. J.; Gritsenko, O. V. *J. Phys. Chem. A*, 1997, 101, 5853
10. (a) Harris, J.; Jones, R. O. *J. Phys. F: Metal Phys.* **1974**, 4, 1170.
    (b) Gunnarsson, O.; Lundqvist, B. I. *Phys. Rev. B* **1976**, 13, 4274.
    (c) Langreth, D. C.; Perdew, J. P. *Phys. Rev. B* **1977**, 15, 2884.
    (d) Harris, J. *Phys. Rev. A* **1974**, 29,1648.
    (e) Ziegler, T. *Chem. Rev.* **1991**, 91, 651.
11. Dirac, P. *Proc. Camb. Philos. Soc.* **1930**, 26, 376.
12. Vosko, S. H.; Wilk, L.; Nusair, M. *Can. J. Phys.* **1980**, 58, 1200.
13. Ceperley, D. M.; Alder, B. J. *Phys. Rev. Lett.* **1980**, 45, 566.
14. Gunnarsson, O.; Jonson, M.; Lundqvist, B. I. *Phys. Rev. B* **1979**, 20, 3136.
15. Ernzerhof, M.; Perdew, J. P.; Burke, K. *Int. J. Quant. Chem.*, **1997**, 64, 285.
16. Sim, F.; St-Amant, A.; Papai, I.; Salahub, D. R. *J. Am. Chem. Soc.* **1992**, 114, 4391.

17. Becke, A. D. *Phys. Rev. A* **1988**, 38, 3098.

18. Perdew, J. P. *Phys. Rev. Lett.* **1985**, 55, 1665.

19. Perdew, J. P.; Yue, W. *Phys. Rev. B* **1986**, 33, 8800.

20. (a) Perdew, J. P. *Phys. Rev. B* **1986**, 33, 8822.
(b) Perdew, J. P. *Phys. Rev. B* **1986**, 34, 7406E.

21. (a) Perdew, J. P.; Chevary, J. A.; Vosko, S. H.; Jackson, K. A.; Pederson, M. R.; Singh, D. J.; Fiolhais, C. *Phys. Rev. B* **1992**, 46, 6671.
(b) Perdew, J. P.; Chevary, J. A.; Vosko, S. H.; Jackson, K. A.; Pederson, M. R.; Singh, D. J.; Fiolhais, C. *Phys. Rev. B* **1993**, 48, 4978E.
(c) Perdew, J. P.; Burke, K.; Yue, W. *Phys. Rev. B* **1996**, 54, 16533.

22. Becke, A. D. *J. Chem. Phys.* **1992**, 97, 9173.

23. (a) Umrigar, C. J.; Gonze, X. *Phys. Rev. A* **1994**, 50, 3827.
(b) Umrigar, C. J.; Gonze, X., High Performance Computing and its Applications in the Physical Sciences: Proceedings of the Mardi Gras 1993 Conference, edited by D. A. Browne et al., World Scientific, Singapore, **1994**, p. 43.

24. (a) Becke A. D., Roussel, M. R. *Phys. Rev. A* **1989**, 39, 3761.
(b) Perdew, J. P.; Kurth, S.; Zupan, A.; Blaha, P. *Phys. Rev. Lett.* **1999**, 82, 2544.
(c) van Voorhis, T.; Scuseria, G. E. *J. Chem. Phys.* **1998**, 109, 400.
(d) Proynov, E. I.; Chermette, H.; Salahub, D. R. *J. Chem. Phys.* **2000**, 113, 10013.
(d) Lee, C.; Yang, W.; Parr, R. G. *Phys. Rev. B* **1988**, 37, 785.

25. Becke, A. D. *J. Chem. Phys.* **1996**, 104, 1040.

26. (a) Becke, A. D. *J. Chem. Phys.* **1993**, 98, 1372.
(b) Becke, A. D. *J. Chem. Phys.* **1993**, 98, 5648.

27. (a) Curtiss, L. A.; Raghavachari, K.; Trucks, G. W.; Pople, J. A. *J. Chem. Phys.* **1991**, 94, 7221.
(b) Gill, P. M. W.; Johnson, B. G.; Pople, J. A.; Frisch, M. J. *Int. J. Quant. Chem. Quant. Chem. Symp.* **1992**, 26, 319.

28. (a) Perdew, J. P.; Ernzerhof, M.; Burke, K. *J. Chem. Phys.* 1996, 105, 9982.
(b) Ernzerhof, M.; Perdew, J. P.; Burke, K. *Int. J. Quant. Chem.* 1997, 64, 285.

29. Stephens, P. J.; Devlin, F. J.; Chabalowski, C. F.; Frisch, M. J. *J. Phys. Chem.* **1994**, 98, 11623.

30. (a) Sharp, R. T.; Horton, G. K. *Phys. Rev.* 1953, 90, 317.
(b) Talman, J. D.; Shadwick, W. F. *Phys. Rev. A* **1976**,14, 36.

31. Krieger, J. B.; Li, Y.; Iafrate, G. J. *Phys. Rev. A* **1992**, 46, 5453.

32. (a) Dirac, P. A. M. *Proc. R. Soc. London, Ser. A* **1929**, 117,610.
(b) Dirac, P. A. M. *Proc. R. Soc. London, Ser. A* **1929**, 118,351.
(c) Moss, R. E., *Advanced Molecular Quantum mechanics*; 2nd ed., Academic Press, London, New York, 1989.

33. McWeeny,R., *Methods of Molecular Quantum Mechanics*; 2nd ed., Academic Press, London, New York, 1989.

34. Malkin, V. G.; Malkina, O. L.; Eriksson, L. A.; Salahub, D. R., In *Modern Density Functional Theory: A Tool for Chemistry; Theoretical and Computational Chemistry*; Seminario, J. M.; Politzer, P., Eds.; Elsevier, Amsterdam, 1995., Vol. 2.

35. Epstein, S. T., *The Variation Method in Quantum Chemistry*, Academic Press, New York, 1974.

36. Pople, J. A.; McIver Jr., J. W.; Ostlund, N. S. *J. Chem. Phys.* **1968**, 49, 2965.

37. Schreckenbach, G., Ph. D. Thesis, The University of Calgary, Canada, 1996.

38. Lee, A. M.; Handy, N. C.; Colewell, S. M. *J. Chem. Phys.* **1995**, 103, 10095.

39. Roothaan, C. C. J. *Rev. Mod. Phys.* **1951**, 23, 69.

40. Pople, J. A.; Krishnan, R.; Schlegel, H. B.; Binkley, J. S. *Int. J. Quantum Chem. Symp.* **1979**, 13, 225.

41. (a) Ditchfield, R. *Mol. Phys.* **1974**, 27, 789.
(b) Kutzelnigg, W.; Fleischer, U.; Schindler, M. In *NMR-Basic Principles and Progress*, Springer, Heidelberg, 1990, Vol. 23, p.165.
(c) Hansen, A. E.; Bouman, T. D. *J. Chem. Phys.* **1985**, 82, 5035.

42. Fukui, H. *Magn. Res. Rev.* **1987**, 11, 205.

43. (a) Edmiston, C.; Ruedenberg, K. *Rev. Mod. Phys.* **1963**, 35, 457.
(b) Boys, S. F., In *Quantum Science of Atoms, Molecules, and Solids*, Löwdin, P. O. Eds., Academic Press, New York, 1966.
(c) Pipek, J.; Mezey, P. Z. *J. Chem. Phys.* **1989**, 90, 4916.
44. Kowalewski, J., *Progr. NMR Spectroscopy*, **1977**, 11, 1.
45. Geertsen, J.; Oddershede, J.; Scuseria, G. *J. Chem. Phys.* **1987**, 87, 2138.
46. Malkina, O. L.; Vaara, J.; Schimmelpfennig, B.; Munzarová, M.; Malkin, V. G.; Kaupp, M. *J. Am. Chem. Soc.* **2000**, 122, 9206.

Chapter 2. QM/MM Approach for Magnetic Properties

The aim of this chapter is to provide theoretical grounds and applications of a QM/MM approach, in which the QM subspace is embedded in the MM partial charges and the dangling bond is capped by simple one-electron quantum capping potentials (QCPs) [1], for various magnetic properties such as NMR chemical shielding tensors, NMR spin-spin coupling constants, and hyperfine structures [2-4].

2.1. Introduction

Most detectable paramagnetic compounds for high resolution NMR experiments are metalloproteins. Accurate theoretical approaches using DFT methods are indispensible to investigate the electronic structure and magnetic properties of the active site of metalloproteins. (In this thesis, we focus on DFT methods because they include electron correlation effects and have comparable computational cost to HF methods.) Despite tremendous advances in computer technology and computational techniques, DFT calculations on transition metal compound models containing around 100 atoms using basis sets of moderate quality still represent substantial undertakings. For example, the calculation of the model of the active site including additional backbone residues and environment effects would be computationally expensive at the ab initio or DFT level. However, since the magnetic properties are rather local, it is feasible to use a hybrid method in which quantum mechanical (QM) techniques apply to the small regions of interest but molecular mechanics (MM) to the bulk [5].

In the present QM/MM partition approach, two issues are critical for the success of the simulations: separation of the model into the QM and MM parts (boundary problem), and handling of the long-range interactions between the subsystems. Up to now, several methods to treat the broken covalent bond in a QM/MM partition have been issued. The most common method is the link atom (LA) method [6] where the valency is saturated by any univalent atom (H or halogen) or a methyl group. This method is very simple to use

but the results are sensitive to the placement of the link atom and it introduces some double counting of the interactions and also introduces distortion of the electron density of the QM part [7,8]. An advanced method for this problem is the localized self-consistent field (LSCF) method [9] where frozen localized orbitals are used to truncate the QM treatment at the frontier bond. The frozen localized orbitals are not included in the QM SCF procedure and their electron density are determined from model studies for the system. Although the assumption about transferability of the frozen bond orbitals for use in proteins seems valid, for each new system the frozen orbitals have to be determined anew. This approach has been refined by the generalized hybrid orbital (GHO) method [10] in which the bonds of boundary MM atoms are described by localized orbitals. In this approach, the localized orbitals (one active and three auxiliary orbitals) are included in the QM SCF procedure but only the active orbital between the QM and MM regions is optimized during SCF. Since the auxiliary orbitals are treated as the effective core potentials, the atomic parameters are general and transferable. However, both methods, LSCF and GHO, require substantial programming for implementation and lead to large errors in energy if large MM charges exist near the frontier orbitals [11]. Furthermore, GHO is only implemented at the semiempirical level. The other method for handling the QM/MM boundary is the pseudobond approach of Yang [12] where the effective potentials form a pseudobond with an adjacent carbon in the QM subsystem. In this approach, seven valence electrons are included in the QM SCF procedure and the effects of core electrons and the sp^3 σ carbon-carbon bond are included in the effective core potentials. Since it uses a conventional effective potential formulation, minimal programming is required for implementation. Here, we adopt the one-electron quantum capping potential (QCP) approach of DiLabio et al. [1], which is similar to the pseudobond method. In this technique, the QCPs are designed to model the electronic character of a methyl group at the QM/MM boundary. This approach is implemented using conventional effective core potential (ECP) [13] expansions and can be incorporated in most DFT programs with minimal code modification. By this approach, some artificial effects of the LA method and the special basis set manipulations of the LSCF and GHO methods can be avoided and the number of electrons in the QM boundary can be reduced greatly compared to with the pseudobond approach of Yang.

In general, the interactions (electrostatic, polarization, and exchange repulsion/charge-transfer) between the subsystems can be described by introducing additional one-electron terms in the Hamiltonian of the QM region [14]. Recently, Cui *et al.* have shown that the electrostatic effect of the environment can be represented by MM partial charges [15]. This description appears to be adequate in NMR chemical shielding calculations, as long as the MM part is not directly connected to the NMR nucleus, and polarization effects of the QM part by MM partial charges dominate interactions between the QM and MM subsystems. In this chapter, this idea will be adopted and validated beyond NMR chemical shielding calculations to all other magnetic properties.

2.2. Theory

2.2.1. Quantum Capping Potentials (QCPs)

The QCPs that are used in this thesis are designed based on Stuttgart semilocal pseudopotentials. (The QCPs were provided by Gino A. DiLabio). The atomic valence Hamiltonian for the pseudopotentials is given by:

$$H = -\frac{1}{2}\sum_i \nabla_i^2 + \sum_{i<j}\frac{1}{r_{ij}} + \sum_i V_{pp}(i) \tag{2.1}$$

where the indices i and j refer to valence electrons. The V_{pp} represents a semilocal pseudopotential of the form:

$$V_{pp}(i) = -\frac{Q}{r_i} + \sum_{l=0}^{l_{max}}\sum_k A_{kl}\,\mathbf{exp}(-a_{kl}r_i^2)P_l \tag{2.2}$$

Here, Q denotes the core charge (effective nuclear charge) of the atom and P_l is the projection operator onto the Hibert subspace with angular symmetry l.

$$P_l = \sum_{m=-l}^{l} | Y_{lm} \rangle\langle Y_{lm} | \qquad (2.3)$$

The A_{lk} and a_{kl} in Eq. (2.2) are the adjustable parameters to reproduce the electronic energy of the all electron system.

Since molecular bond orbitals are different from atomic orbitals, the QCPs include additional spherical shielding (one Gaussian $A_{kl}\,\mathbf{exp}(-a_{kl}r_i^2)$) and optional Pauli terms (three Gaussians) to reproduce model molecular properties. The parameters A_{lk} and a_{kl} of the additional Gaussians are adjusted by fitting the Mulliken charge of C^{QCP} for CH_3 group charge [1].

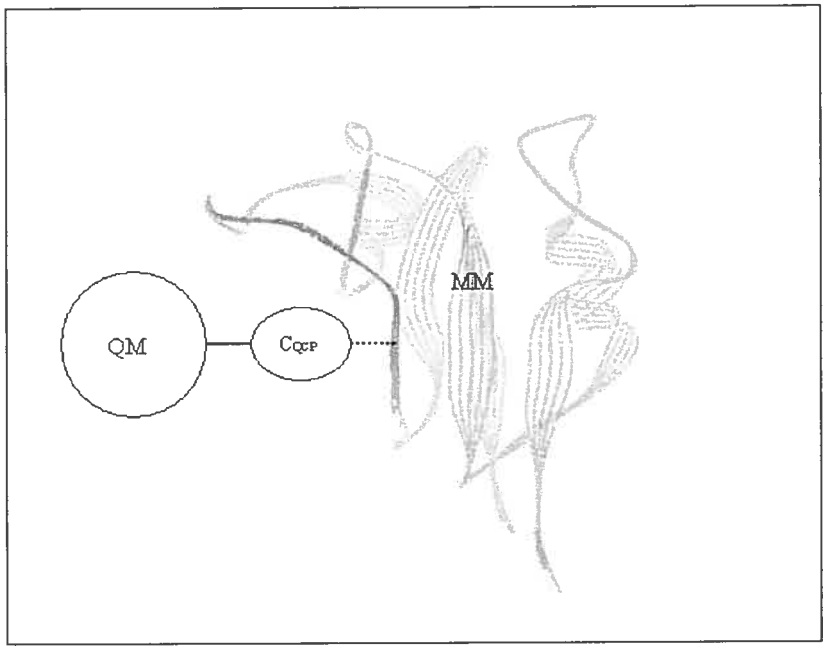

Figure 2.1. Schematic description of the partition into QM and MM regions using one-electron quantum capping potentials

2.2.2. Kohn-Sham (KS) Electronic Energy in Quantum Capping Potentials (QCPs) and MM Electrostatic Fields

In the simple electronic embedding model of the QM region, using QCPs, the KS electronic energy of the QM region is given by:

$$E^{tot} = E^{QM} + E^{QM/MM} \tag{2.4}$$

where

$$\begin{aligned} E^{QM} = &\sum_{k\sigma}^{occ} \sum_{C \in QCP} < \phi_{k\sigma} | \frac{\mathbf{p}^2}{2} + V_C^{QCP}(r_{kC}) | \phi_{k\sigma} > \\ &+ \int v(\mathbf{r})(\rho_\alpha + \rho_\beta) d\mathbf{r} + J[\rho_\alpha + \rho_\beta] + E_{XC}[\rho_\alpha, \rho_\beta] \end{aligned} \tag{2.5}$$

and

$$E^{QM/MM} = \sum_{k\sigma}^{occ} < \phi_{k\sigma} | - \sum_{J \in MM} \frac{q_J}{r_{kJ}} | \phi_{k\sigma} > \tag{2.6}$$

Here, $\phi_{k\sigma}$ ($\sigma = \alpha$ or β spin) denotes the KS molecular orbitals (MO) under the influence of QCPs, V_C^{QCP}, and MM charges, q_J, the operator $\mathbf{p}_k$ refers to the momentum of the kth electron, $v(\mathbf{r})$ represents the nuclear potential, J and E_{XC} are the Coulomb and exchange-correlation energies, ρ_α and ρ_β are the spin-up and spin-down electron densities.

The KS molecular orbitals $\phi_{k\sigma}$ are chosen to minimize the energy E^{tot}. Consequently, the orbitals are determined as solution of the following KS equations:

$$\begin{aligned} \mathbf{F}_\sigma \phi_{k\sigma} &= \left\{ \frac{\mathbf{p}^2}{2} + v_{eff}^\sigma + \sum_{C \in QCP} V_C^{QCP}(r_{kC}) - \sum_{J \in MM} \frac{q_J}{r_{kJ}} \right\} \phi_{k\sigma} \\ &= \varepsilon_{k\sigma} \phi_{k\sigma} \end{aligned} \tag{2.7}$$

where

$$v_{eff}^{\sigma} = v(\mathbf{r}) + \int \frac{\rho^{\sigma}(\mathbf{r}')}{|\mathbf{r}-\mathbf{r}'|} d\mathbf{r}' + \frac{\delta E_{XC}[\rho_{\alpha}^{tot}, \rho_{\beta}^{tot}]}{\delta \rho_{\sigma}^{tot}} \tag{2.8}$$

In Eq. (2.8) the first term represents the nuclear potential, the second term the Coulomb potential, and the last term the exchange-correlation potential. From Eq. (2.7), it is shown that the effects from MM partial charges and QCPs are involved in the QM subsystem through the KS molecular orbitals $\phi_{k\sigma}$, corresponding energies $\varepsilon_{k\sigma}$ .and electron density ρ.

2.2.3. Electrostatic Contribution to Magnetic Resonance Paramters

The present QM/MM approach is designed for the time-independent, non-relativistic case and the uncoupled DFT (UDFT) scheme with the standard exchange-correlation functionals (current density independent) [16,19]. It should be noted that the fomulas of magnetic parameters are already derived and explained in Chapter 1 and the terms related to QM/MM are only discussed in this section.

The magnetic resonance parameters can be expressed by the second-order response of the total KS electronic energy E, which includes the QCPs of boundary carbons and the electrostatic interactions with MM charges, with respect to two perturbation parameteres **a** and **b**:

$$\begin{aligned} \mathbf{E}_{\mathbf{ab}}^{(11)}(\mathbf{QM/MM}) &= \left(\frac{\partial^2 \mathrm{E}(\mathbf{a},\mathbf{b})}{\partial \mathbf{a} \partial \mathbf{b}} \right)_{\mathbf{a}=\mathbf{b}=0} \\ &= \sum_{k\sigma}^{occ} < \phi_{k\sigma}^{(0)} \mid \mathbf{H}_{\mathbf{ab}}^{(11)} \mid \phi_{k\sigma}^{(0)} > + \sum_{k\sigma}^{occ} \frac{\partial}{\partial \mathbf{a}} \left(< \phi_{k\sigma}(\mathbf{a}) \mid \mathbf{H}_{\mathbf{b}}^{(01)} \mid \phi_{k\sigma}(\mathbf{a}) > \right)_{\mathbf{a}=0} \end{aligned} \tag{2.9}$$

From Eq. (2.9), we can see that the two terms related to the QCPs and MM charges are independent of magnetic fields in this uncoupled DFT (UDFT) procedure and they will vanish upon differentiation of the total KS energy with respect to magnetic fields. As a result, the QCPs and MM charges affect the magnetic resonance parameters only through changes to the field-free KS orbitals and the first-order perturbed KS orbitals of the QM subsystem.

NMR chemical shielding tensors and electronic g-tensors depend on the external magnetic fields explicitly and therefore, by the choice of gauge origin [16,17], MM atoms and QCPs will contribute to the magnetic parameters in a different way. However, since the g-tensors are not sensitive to gauge origin (in this case, the common origin approach is comparable with other sophiscated methods) [18], the gauge-origin dependence of the QM/MM method will be only focused on chemical shielding tensors. On the other hand, nuclear spin-spin coupling tensors and hyperfine tensors are independent of a magnetic field and the nucleus of interest is a natural gauge origin. Hence, the QM/MM approach for nuclear spin-spin coupling constants, hyperfine tensors and g-tensors will be explained at the same time.

2.2.3.1 NMR Chemical Shielding Tensors

NMR shielding tensors $\boldsymbol{\sigma}_N$ in the influence of MM charges and QCPs can be defined in terms of the second derivatives of the total molecular energy $E_{KS}(\mathbf{B},\mathbf{M}_N)$ with respect to the external magnetic field $\mathbf{B}$ and nuclear magnetic moment $\mathbf{M}_N$:

$$\begin{aligned}\boldsymbol{\sigma}_N &= \left(\frac{\partial^2 E(\mathbf{B},\mathbf{M}_N)}{\partial \mathbf{B}\partial \mathbf{M}_N}\right)_{\mathbf{B}=\mathbf{M}_N=0} \\ &= \sum_{k\sigma}^{occ} \langle \phi_{k\sigma}^{(0)} | \mathbf{H}_N^{(110)} | \phi_{k\sigma}^{(0)} \rangle + \sum_{k\sigma}^{occ} \frac{\partial}{\partial \mathbf{B}} \left(\langle \phi_{k\sigma}(\mathbf{B}) | \mathbf{H}_N^{(010)} | \phi_{k\sigma}(\mathbf{B}) \rangle \right)_{\mathbf{B}=0}\end{aligned} \tag{2.10}$$

where the operators $\mathbf{H}_N^{(010)}$ (1.68) and $\mathbf{H}_N^{(110)}$ (1.69) and other notations are already defined in Chpater 1.

In order to investigate the effects on the chemical shielding of the QM subsystem from QCPs and MM charges, it is indispensible to know the detail solution of Eq. (2.10) which depends on the choice of the gauge origin. Here, we focus on the two methods: the "gauge including atom orbital" (GIAOs) [20] and the "individual gauge for localized orbital" [21] methods.

In the GIAO approach

In the UDFT scheme with GIAOs [16], the diamagnetic contribution $\boldsymbol{\sigma}_N^d$ to the shielding in MM charges and QCPs is given by (refer to Eqs. (1.96-1.98)):

$$\boldsymbol{\sigma}_N^d = \sum_{\mu\nu}^{basis} P_{\mu\nu}^{(0)} < \chi_\mu^{(0)} \mid \tilde{\mathbf{H}}_N^{(110)} + \tilde{\mathbf{H}}_{N,d}^{(010)} \mid \chi_\nu^{(0)} > \tag{2.11}$$

Here, $\chi_\mu^{(0)}$ represents orbital basis functions in the absence of magnetic fields. The magnetic field-free atomic density matrix element $P_{\mu\nu}^{(0)}$ in the QCPs and MM electric fields is defined as:

$$P_{\mu\nu}^{(0)} = \sum_{k\sigma}^{occ} C_{\mu k\sigma}^{(0)} C_{\nu k\sigma}^{(0)} \tag{2.12}$$

The paramagnetic shielding $\boldsymbol{\sigma}_N^p$ can be decomposed into the three individual contributions (see, Eqs (1.99-1.102)). The first contribution $\boldsymbol{\sigma}_N^{p0}$ is defined as:

$$\boldsymbol{\sigma}_N^{p0} = \sum_{\mu\nu}^{basis} P_{\mu\nu}^{(0)} < \chi_\mu^{(0)} \mid \tilde{\mathbf{H}}_{N,p}^{(010)} \mid \chi_\nu^{(0)} > \tag{2.13}$$

The second contribution $\boldsymbol{\sigma}_N^{p1}$ is given by:

$$\begin{aligned}\boldsymbol{\sigma}_N^{p1} &= \sum_{kj\sigma}^{occ}\sum_{\lambda\varpi}^{basis} C_{\lambda j\sigma}^{(0)} C_{\varpi k\sigma}^{(0)} < \phi_{KS,k\sigma}^{(0)} \mid \mathbf{H}_N^{(010)} \mid \phi_{KS,j\sigma}^{(0)} >< \chi_\lambda^{(0)} \mid (\boldsymbol{\Lambda}_{\lambda\varpi})^T \mid \chi_\varpi^{(0)} > \\ &= \sum_{\mu\nu\lambda\varpi}^{basis} P_{\mu\varpi}^{(0)} P_{\lambda\nu}^{(0)} < \chi_\mu^{(0)} \mid \mathbf{H}_N^{(010)} \mid \chi_\nu^{(0)} >< \chi_\lambda^{(0)} \mid (\boldsymbol{\Lambda}_{\lambda\varpi})^T \mid \chi_\varpi^{(0)} >\end{aligned} \tag{2.14}$$

The last contribution $\boldsymbol{\sigma}_N^{p2}$ is expressed as:

$$\begin{aligned}\boldsymbol{\sigma}_N^{p2} &= -2\sum_{k\sigma}^{occ}\sum_{a}^{vir}\sum_{\lambda\varpi}^{basis} C_{\lambda a\sigma}^{(0)} C_{\varpi k\sigma}^{(0)} < \phi_{k\sigma}^{(0)} \mid \mathbf{H}_N^{(010)} \mid \phi_{a\sigma}^{(0)} > \left(\frac{< \chi_\lambda^{(0)} \mid \left(\tilde{\mathbf{H}}^{(100)}\right)^T \mid \chi_\varpi^{(0)} >}{\varepsilon_{k\sigma}^{(0)} - \varepsilon_{a\sigma}^{(0)}} \right) \\ &= -2\sum_{k\sigma}^{occ}\sum_{a}^{vir}\sum_{\mu\nu\lambda\varpi}^{basis} X^{(0)} < \chi_\mu^{(0)} \mid \mathbf{H}_N^{(010)} \mid \chi_\nu^{(0)} > \left(\frac{< \chi_\lambda^{(0)} \mid \left(\mathbf{H}^{(100)} + \boldsymbol{\Lambda}_{\lambda\varpi}\mathbf{F}_\sigma^{(0)} - \varepsilon_{k\sigma}^{(0)}\boldsymbol{\Lambda}_{\lambda\varpi}\right)^T \mid \chi_\varpi^{(0)} >}{\varepsilon_{k\sigma}^{(0)} - \varepsilon_{a\sigma}^{(0)}} \right)\end{aligned} \tag{2.15}$$

where $X^{(0)} = C_{\mu k\sigma}^{(0)} C_{\nu a\sigma}^{(0)} C_{\lambda a\sigma}^{(0)} C_{\varpi k\sigma}^{(0)}$ and $\mathbf{F}_{k\sigma}^{(0)}$ denotes the magnetic field-free KS operator including MM charges and QCPs, while $\varepsilon_{k\sigma}^{(0)}$ and $\varepsilon_{a\sigma}^{(0)}$ represent corresponding KS energies of occupied and virtual orbitals, respectively.

From Eqs. (2.11, 2.13, and 2.14), it is shown that the core integrals, with field-free orbital basis functions $\chi^{(0)}$, of $\boldsymbol{\sigma}_N^{d}$, $\boldsymbol{\sigma}_N^{p0}$ and $\boldsymbol{\sigma}_N^{p1}$ are not modified in the present QM/MM approach and all influences from MM charges and QCPs are merged into the shieldings through the field-free atomic density elements $P_{\mu\nu}^{(0)}$. In Eq. (2.15), MM charges and QCPs give an effect on $\boldsymbol{\sigma}_N^{p2}$ in two ways: through $X^{(0)}$, $\varepsilon_{k\sigma}^{(0)}$, and $\varepsilon_{a\sigma}^{(0)}$ indirectly and through an expansion of the core integral $< \chi_\lambda^{(0)} \mid \left(\boldsymbol{\Lambda}_{\lambda\varpi}\mathbf{F}_\sigma^{(0)}\right)^T \mid \chi_\varpi^{(0)} >$ directly. It is shown clearly by decomposition of the integral,

$$< \chi_\lambda^{(0)} | \left(\Lambda_{\lambda\varpi} \mathbf{F}_\sigma^{(0)}\right)^T | \chi_\sigma^{(0)} >$$
$$=< \chi_\lambda^{(0)} | \left(\Lambda_{\lambda\varpi} (\frac{\mathbf{p}^2}{2} + v_{eff}^\sigma) \right)^T | \chi_\varpi^{(0)} > + < \chi_\lambda^{(0)} | \left(\Lambda_{\lambda\varpi} (\sum_{C \in QCP} V_C^{QCP}(r_{kC}) - \sum_{J \in MM} \frac{q_J}{r_{kJ}}) \right)^T | \chi_\sigma^{(0)} > \tag{2.16}$$

Due to the last term of Eq. (2.16), the NMR codes with GIAO should be modified. This might be trivial if a DFT-NMR program can handle effective core potentials and point charges. However, since most MM (and QCPs) effects are transferred to the chemical shieldings of the QM subsystem through the atomic densities and orbital energies, the last integral, which denotes the coupling of gauge factors with MM charges (and QCPs), can be neglected in an approximation. Hence, if the MM effects are involved in the preliminary calculation of KS equations, the chemical shieldings of the QM region will be influenced by them implicitly in the UDFT-GIAO method.

In the IGLO approach

In the UDFT-IGLO scheme [19] combined with the present QM/MM approach, the diamagnetic shielding $\boldsymbol{\sigma}_N^d$ is defined as (see, Eqs. (1.107 and 1.108)):

$$\boldsymbol{\sigma}_N^d = \sum_{\mu\nu}^{basis} \widetilde{P}_{\mu\nu}^{(0)} < \chi_\mu^{(0)} | \widetilde{\mathbf{H}}_N^{(110)} | \chi_\nu^{(0)} > \tag{2.17}$$

where

$$\widetilde{P}_{\mu\nu}^{(0)} = \sum_{k\sigma}^{occ} \widetilde{C}_{\mu k\sigma}^{(0)} \widetilde{C}_{\nu k\sigma}^{(0)} = \sum_{k\sigma}^{occ} \left(\sum_{p}^{occ} U_{pk} C_{\mu p\sigma}^{(0)} C_{\nu p\sigma}^{(0)} U_{pk} \right) \tag{2.18}$$

The paramagnetic contribution is decomposed into the two terms (refer to Eqs. (1.109-1.110)). The first contribution $\boldsymbol{\sigma}_N^{p0}$ is given by:

$$\begin{aligned}\boldsymbol{\sigma}_N^{p0} &= \sum_{kj\sigma}^{occ} < \tilde{\phi}_{k\sigma}^{(0)} \mid \mathbf{H}_N^{(010)} \mid \tilde{\phi}_{j\sigma}^{(0)} > < \tilde{\phi}_{j\sigma}^{(0)} \mid \left(\boldsymbol{\Lambda}_{jk}\right)^T \mid \tilde{\phi}_{k\sigma}^{(0)} > \\ &= \sum_{\mu\nu\lambda\varpi}^{basis} \tilde{P}_{\mu\varpi}^{(0)} \tilde{P}_{\lambda\nu}^{(0)} < \chi_\mu^{(0)} \mid \mathbf{H}_N^{(010)} \mid \chi_\nu^{(0)} > < \chi_\lambda^{(0)} \mid \left(\boldsymbol{\Lambda}_{jk}\right)^T \mid \chi_\sigma^{(0)} >\end{aligned} \tag{2.19}$$

The second contribution $\boldsymbol{\sigma}_N^{p1}$ takes the form:

$$\begin{aligned}\boldsymbol{\sigma}_N^{p1} &= 2\sum_{k\sigma}^{occ}\sum_{a}^{vir} < \tilde{\phi}_{k\sigma}^{(0)} \mid \mathbf{H}_N^{(010)} \mid \tilde{\phi}_{a\sigma}^{(0)} > \tilde{\mathrm{d}}_{ak\sigma}^{(1)} \\ &= 2\sum_{k\sigma}^{occ}\sum_{a}^{vir}\sum_{\mu\nu}^{basis} A^{(0)} < \chi_\mu^{(0)} \mid \mathbf{H}_N^{(010)} \mid \chi_\nu^{(0)} > \tilde{\mathrm{d}}_{ak\sigma}^{(1)}\end{aligned} \tag{2.20}$$

where

$$\begin{aligned}\tilde{\mathrm{d}}_{ak\sigma}^{(1)} = &\sum_{m}^{occ}\left[\frac{\sum_{n\sigma}^{occ}\sum_{\lambda\varpi}^{basis} B^{(0)} < \chi_\lambda^{(0)} \mid \left(\mathbf{H}_N^{(100)}\right)^T \mid \chi_\varpi^{(0)} > U_{nm}}{\varepsilon_{m\sigma}^{(0)} - \varepsilon_{a\sigma}^{(0)}}\right] U_{km} \\ &+ \sum_{m}^{occ}\left[\frac{\sum_{nj\sigma}^{occ}\sum_{\lambda\varpi\tau\kappa}^{basis} D^{(0)} < \chi_\lambda^{(0)} \mid (\boldsymbol{\Lambda}_{jn})^T \mid \chi_\varpi^{(0)} > < \chi_\tau^{(0)} \mid \mathbf{F}_\sigma^{(0)} \mid \chi_\kappa^{(0)} > U_{nm}}{\varepsilon_{m\sigma}^{(0)} - \varepsilon_{a\sigma}^{(0)}}\right] U_{km}\end{aligned} \tag{2.21}$$

Here, $A^{(0)} = \tilde{C}_{\mu k}^{(0)} C_{\nu a}^{(0)}$, $B^{(0)} = C_{\lambda a\sigma}^{(0)} \tilde{C}_{\varpi n\sigma}^{(0)}$, and $D^{(0)} = C_{\lambda a\sigma}^{(0)} \tilde{C}_{\varpi j\sigma}^{(0)} \tilde{C}_{\tau j\sigma}^{(0)} \tilde{C}_{\kappa n\sigma}^{(0)}$.

From Eqs. (2.17, 2.19-2.21), we can see that the shieldings ($\boldsymbol{\sigma}_N^d$, $\boldsymbol{\sigma}_N^{p0}$, and $\boldsymbol{\sigma}_N^{p1}$) of the QM part is influenced by MM charges and QCPs just through $\tilde{P}_{\mu\nu}^{(0)}$, $A^{(0)}$, $B^{(0)}$, $D^{(0)}$, and KS orbital energies $\varepsilon_k^{(0)}$ and $\varepsilon_a^{(0)}$ which are all magnetic field-free terms and are decided from the self-consistent solution of Eq. (2.7). Unlike the UDFT-GIAO method, the KS operator $\mathbf{F}_\sigma^{(0)}$ is not coupled with the gauge factor $\boldsymbol{\Lambda}_{jn}$ directly in the integral and we do

not need to modify the NMR codes in the present QM/MM approach. The MM effects can be delivered to the chemical shieldings of the QM region only implicitly. This QM/MM approach can be applied to the sum-over-state density functinal theory (SOS-DFPT) method [22] in the same way as the UDFT-IGLO treatment, since the SOS-DFPT method is basically equivalent to the UDFT-IGLO approach but has an additional orbital energy correction term in Eq. (2.21).

2.2.3.2 Other Magnetic Resonance Parameters

Under the influence of QCPs and MM charges, the reduced nuclear spin-spin coupling tensors ($\mathbf{K}_{MN} = \mathbf{K}_{MN}^{PSO} + \mathbf{K}_{MN}^{DSO} + \mathbf{K}_{MN}^{FC}$) can be defined as (refer to Eqs. (1.112-1.120)):

$$\begin{aligned}\mathbf{K}_{MN}^{PSO} &= -2\sum_{k\sigma}^{occ}\sum_{a}^{vir}\frac{<\phi_{k\sigma}^{(0)}\,|\,\mathbf{H}_{M}^{(010)}\,|\,\phi_{a\sigma}^{(0)}><\phi_{a\sigma}^{(0)}\,|\,\left(\mathbf{H}_{N}^{(010)}\right)^{T}\,|\,\phi_{k\sigma}^{(0)}>}{\varepsilon_{k\sigma}^{(0)}-\varepsilon_{a\sigma}^{(0)}-\Delta E_{k\to a}^{XC}} \\ &= -2\sum_{k\sigma}^{occ}\sum_{a}^{vir}\sum_{\mu\nu\lambda\varpi}^{basis}C_{\mu k\sigma}^{(0)}C_{\nu a\sigma}^{(0)}C_{\lambda a\sigma}^{(0)}C_{\varpi k\sigma}^{(0)}\frac{<\chi_{\mu}^{(0)}\,|\,\mathbf{H}_{M}^{(010)}\,|\,\chi_{\nu}^{(0)}><\chi_{\lambda}^{(0)}\,|\,\left(\mathbf{H}_{N}^{(010)}\right)^{T}\,|\,\chi_{\varpi}^{(0)}>}{\varepsilon_{k\sigma}^{(0)}-\varepsilon_{a\sigma}^{(0)}-\Delta E_{k\to a}^{XC}}\end{aligned} \tag{2.22}$$

$$\begin{aligned}\mathbf{K}_{MN}^{DSO} &= 2\sum_{k\sigma}^{occ}<\phi_{k\sigma}^{(0)}\,|\,\mathbf{H}_{MN}^{(020)}\,|\,\phi_{k\sigma}^{(0)}> \\ &= 2\sum_{\mu\nu}^{basis}P_{\mu\nu}^{(0)}<\chi_{\mu}^{(0)}\,|\,\mathbf{H}_{MN}^{(020)}\,|\,\chi_{\nu}^{(0)}>\end{aligned} \tag{2.23}$$

$$\mathbf{K}_{MN}^{FC} = \left(\frac{8\pi}{3}\right)^{2}\left(\frac{\alpha}{2}\right)^{2}\left(\frac{g_e}{2}\right)^{2}(\lambda)^{-1}\sum_{\mu\nu}P_{\mu\nu}^{\alpha-\beta}(\lambda)<\chi_{\mu}^{(0)}\,|\,\delta(\mathbf{r}_N)\mathbf{1}\,|\,\chi_{\nu}^{(0)}> \tag{2.24}$$

The hyperfine coupling tensors ($\mathbf{A}_N = \mathbf{A}_N^{iso} + \mathbf{A}_N^{dip}$) are given by (see, Eqs. (1.121-1.123)):

$$\mathbf{A}_{N}^{iso} = \frac{4\pi}{3}g_e\beta g_N\beta_N\left\langle S_z\right\rangle^{-1}\sum_{\mu\nu}^{basis}P_{\mu\nu}^{\alpha-\beta}<\chi_{\mu}^{(0)}\,|\,\delta(\mathbf{r}_{iN})\mathbf{1}\,|\,\chi_{\nu}^{(0)}> \tag{2.25}$$

$$\mathbf{A}_N^{dip} = \frac{1}{2} g_e \beta g_N \beta_N \langle S_z \rangle^{-1} \sum_{\mu\nu}^{basis} P_{\mu\nu}^{\alpha-\beta} < \chi_\mu^{(0)} | \frac{|\mathbf{r}_{kN}|^2 \mathbf{1} - 3\mathbf{r}_{kN}\mathbf{r}_{kN}^T}{|\mathbf{r}_{kN}|^5} | \chi_\nu^{(0)} > \tag{2.26}$$

Finally, the electronic g-tensors ($\mathbf{g} = g_e \mathbf{1} + \Delta\mathbf{g}$, where $\Delta\mathbf{g} = \Delta\mathbf{g}_{SO.OZ}^{para} + \Delta\mathbf{g}_{GC}^{dia} + \Delta\mathbf{g}_{RMC}$), where we consider only one-electron operators, have the forms (see, Eqs. (1.125-1.128)):

$$\begin{aligned} \Delta\mathbf{g}_{SO/OZ}^{para}(1e) = g_e \sum_k^{occ(\alpha)} \sum_a^{vir(\alpha)} \sum_{\mu\nu\lambda\varpi}^{basis} X_\alpha^{(0)} \frac{< \chi_\mu^{(0)} | \mathbf{H}^{(100)} | \chi_\nu^{(0)} >< \chi_\lambda^{(0)} | \left(\mathbf{H}_k^{(001)}\right)^T | \chi_\varpi^{(0)} >}{\varepsilon_{k\alpha}^{(0)} - \varepsilon_{a\alpha}^{(0)}} \\ - g_e \sum_k^{occ(\beta)} \sum_a^{vir(\beta)} \sum_{\mu\nu\lambda\varpi}^{basis} X_\beta^{(0)} \frac{< \chi_\mu^{(0)} | \mathbf{H}^{(100)} | \chi_\nu^{(0)} >< \chi_\lambda^{(0)} | \left(\mathbf{H}_k^{(001)}\right)^T | \chi_\varpi^{(0)} >}{\varepsilon_{k\beta}^{(0)} - \varepsilon_{a\beta}^{(0)}} \end{aligned} \tag{2.27}$$

$$\Delta\mathbf{g}_{GC}^{dia}(1e) = g_e \sum_{\mu\nu}^{basis} P_{\mu\nu}^{\alpha-\beta} < \chi_\mu^{(0)} | \mathbf{H}_k^{(101)} | \chi_\nu^{(0)} > \tag{2.28}$$

$$\Delta\mathbf{g}_{RMC} = -\frac{1}{2}\alpha^2 g_e \sum_{\mu\nu}^{basis} P_{\mu\nu}^{\alpha-\beta} < \chi_\mu^{(0)} | p_k^2 \mathbf{1} | \chi_\nu^{(0)} > \tag{2.29}$$

From the final QM/MM formulas of magnetic resonance parameters based on uncoupled DFT method (current density is not considered), we can see that the MM partial charges and QCPs just polarize the magnetic field-free wave function of the QM region (KS molecular orbital coefficients and energies are changed) and all core integrals, with field-free basis functions $\chi_\mu^{(0)}$, of magnetic parameters are intact in this QM/MM procedure. In consequence, the MM (and QCPs) effects are only involved in the calculation of the magnetic field-free KS equations and they are transfered to the magnetic parameters through KS orbitals and corresponding orbital energies indirectly.

2.3. Implemenation and Computational Details

The current QM/MM approach applies to the calculations of chemical shielding tensors, nuclear spin-spin coupling constants, and hyperfine structures. This approach can be extended to g-tensor calculations but here we will not consider them since they are not a local property.

2.3.1 NMR Chemical Shielding Tensors and Spin-Spin Coupling Constants

In order to test the capping potential approach [1] and the present QM/MM method for NMR chemical shielding tensor calculations, several organic molecules including neutral histidine and cytosine monophosphate (CMP) were chosen. All molecules were fully optimized with B3LYP[23]/6-311G(d,p)[24] except histidine and CMP which are optimized with B3LYP/6-31G(d) using the GAUSSIAN 98 program [25]. The NMR shielding tensors and spin-spin coupling constants were calculated using the optmized structures in the deMon program [26]. In this case, the Perdew/Wang 91 (PW91) [27] and Perdew-86 (P86) [28] exchange-correlation functionals were used for chemical shift and spin-spin coupling constant calculations, respectively. The specific functionals were chosen based on the previous works, which give the best for some organic molecules [26(b)]. The IGLO-III basis sets [21] are used for orbital basis sets and the auxiliary basis sets (5,1;5,1) for H and (5,2;5,2) for the other atoms which fit charge density and exchange correlation potentials. In the deMon calculations, a random numerical integration grid with FINE angular quadrature and 64 radial points per atom was chosen. For the chemical shielding tensor calculations, the IGLO method was used and the localization of the occuppied MO's was done by the method of Boys [29]. For the NMR spin-spin coupling calculations using the finite perturbation theory (FPT) [30], the value of 0.001 was used as the perturbation parameter. For the QM/MM calculations, the MM subspace were described by either Mulliken or RESP (restrained electrostatic potential) charges [31] and the boundary carbons were replaced with quantum capping potentials

(QCPs). All QM/MM calculations were carried out with the deMon program. Both point charges and QCPs were read from the input stream. For this work, QCPs were added to the basis set library of the deMon program.

2.3.2. Hyperfine Coupling Tensors

In this work, hyperfine tensors were calculated in the QM/MM framework. The QM part was treated by DFT, using the deMon program. The MM part was treated with an empirical AMBER 1994 force field [32]. The capping carbon approach [1] was adopted for the boundary atoms. Spin-unresticted Kohn-Sham calculations were performed, with Becke exchange [33] and Perdew correlation functionals [28]. A double zeta plus polarization (DZVP2) basis set [34a], augmented by the most diffuse functions (a 1s1p set) from ECP valence basis of Dolg et al. [34b], (16s10p5d)/[9s6p4d] was used for copper. The IGLO-III basis set was used for the main group atoms. Molecular structures of azurin and stellacyanin were taken from X-ray diffraction results (4AZU and 1JER files from the Protein Data Bank). The remaining hydrogen atoms were generated using the AMBER Xleap program [35], without reoptimizing the geometry. For azurin, four aminoacids (His46, His117, Cys112, and Met121) were included in the QM calculation. The weakly bound Gly45 was not considered in the QM calculation, but was treated as part of the MM subsystem. For stellacyanin, four aminoacids (His46, His94, Cys89, and Gln99) were involved in the QM calculation. In both cases, the aminoacids of the QM region were truncated at the α-carbon. The only sidechains were treated at the QM level (see Figures 2.5 and 2.6). Two approaches were used for terminating the polypeptide chain. In the hydrogen link atom approach, hydrogen atoms were added to the MM side of the broken C-C covalent bond of the chain to satisfy the valency of the QM region (here, the C-H bond length is set to 1.09 Å). In the capping carbon approach, broken bonds were terminated by one-electron "carbon" atoms, carrying parameterized effective core potentials. All the remaining atoms of both proteins were treated as electronically

innocent bystanders, using MM partial charges. Solvent effects were treated by including the crystallographic water molecules in the MM subsystem.

2.4. Results and Discussion

2.4.1. NMR Chemical Shielding Tensors

Since quantum capping potentials (QCPs) were designed using the ethane molecule, they must be validated for their effects on chemical shielding in different chemical environments. Computed NMR chemical shielding constants of several organic molecules using QCPs are collected and compared with the full QM results in Table 2.1.

The shielding constants of the carbon nucleus directly bound to the capping carbon at the boundary are very sensitive to the types of hybrid orbitals. The isotropic shielding constants of the sp^3 carbon (absolute deviation error, $|\Delta| = 4.5$ ppm) and the sp^2 carbon ($|\Delta| = 5.8$ ppm) are close to the full QM result but those of the sp carbon ($|\Delta| = 38.3$ ppm) are deviated greatly. For anisotropic shielding, the result of the sp^3 carbon ($|\Delta| = 3.6$ ppm) with QCPs is in good agreement with the full QM result while the others (sp^2: $|\Delta| = 41.7$ ppm; sp^3: $|\Delta| = 38.2$ ppm) show large deviations, which is not unexpected because the explicit anisotropies from the hydrogen bond orbitals are removed by using spherical capping potentials. Overall the error of shielding constants with QCPs increases as hybridization decreases. This is due to the fact that the QCPs are produced based on the sp^3 model system.

Table 2.1 also shows that the anisotropic shieldings of the nitrogen and oxygen atoms directly attached to the capping carbon are less sensitive to QCPs. Their anisotropic values (N: $|\Delta| = 3.6$ ppm; O: $|\Delta| = 2.3$ ppm) are as good as that of carbon ($|\Delta| = 3.6$ ppm) in the same case, compared to the full QM results and the isotropic value of nitrogen shows ($|\Delta| = 1.2$ ppm) shows even better than that of carbon ($|\Delta| = 4.5$ ppm). However,

the isotropic value ($|\Delta| = 39.5$ ppm) of the oxygen is still sensitive to QCPs. The shielding error of nearest neighbours with QCPs has the order: O > N ≈ C. In consequence, QCPs can be used for NMR chemical shielding calculation even for carbon in heterogenous bonds such as C-N and C-O.

Finally, from Table 2.1, it is shown that the isotropic shielding constants with QCPs are in good agreement with the full QM results within the absolute deviation of 6.8 ppm irrespective of the number of covalent bonds between the magnetic nucleus and the capping carbon. On the other hand, anisotropic shieldings with capping potentials are sensitive to the number of covalent bonds. However, even for anisotropic shieldings, the values of third neighbor nuclei ($|\Delta| = 2.9$ ppm) are already reasonable and, from the fourth neighbor, the values ($|\Delta| = 0.4$ ppm) are almost the same as the full QM results. In the QM/MM appoach, the artificial effect of the capping potentials on the chemical shielding of the QM part disappears quickly as the number of bonds from the capping carbon increases. This is graphically seen in Fig 2.2.

In Table 2.2, we can see the effects of capping potentials on the chemical shieldings of propanoic acid and alanine. The two systems have relatively similar structures but the effect of capping potentials on the chemical shielding are much different. For alanine (amino acid), overall shielding values with QCPs are improved. Specifically, the anisotropic results of oxygen and carbon nuclei in alanine ($|\Delta|_{av} = 6.5$ ppm) is much better than that of propanoic acid ($|\Delta|_{av} = 21.2$ ppm), compared to the full QM result. This encourages us to use the capping potentials for the calculations of chemical shieldings in proteins. In addition, DiLabio et al. showed that there are no breakdowns or pathological defects associate with QCPs when used with point charges [1].

Table 2.1. Calculated NMR chemical shielding constants (in ppm) using quantum capping pontetials (QCPs) for small organic molecules in comparison with full QM results.[a]

		Cap QM		Full QM		$\|\Delta\|$[b]	
molecule	nucleus	iso	aniso	iso	aniso	iso	aniso
H_3C^{cap}-$C^{sp3}H_3$	C^{sp3}	180.2	20.1	175.7	16.5	4.5	3.6
H_3C^{cap}-$C^{sp2}HO$	C^{sp2}	-7.6	119.0	-13.4	160.7	5.8	41.7
H_3C^{cap}-$C^{sp}N$	C^{sp}	92.4	277.5	71.6	324.6	38.3	38.2
H_3C^{cap}-NH_2	N	237.6	42.3	238.9	38.8	1.2	3.6
H_3C^{cap}-OH	O	277.4	90.5	316.8	92.8	39.5	2.3
H_3C^{cap}-CH_2NH_2	N	228.2	36.1	218.6	42.0	9.6	5.9
H_3C^{cap}- $CH_2CH_2NH_2$	N	214.8	45.8	221.0	38.6	6.2	7.2
H_3C^{cap}- $CH_2CH_2CH_2NH_2$	N	221.2	38.0	221.4	38.8	0.2	0.8
H_3C^{cap}-CH_2OH	O	287.2	64.5	271.9	39.8	15.3	24.7
H_3C^{cap}-CH_2CH_2OH	O	280.2	112.4	288.9	104.3	8.7	8.1
H_3C^{cap}-$CH_2CH_2CH_2OH$	O	289.2	104.8	290.3	103.8	1.1	1.0
H_3C^{cap}-$C^{(1)}H_2C^{(2)}H_2C^{(3)}H_2C^{(4)}H_3$	$C^{(1)}$	150.0	38.6	154.1	23.2	4.1	15.4
	$C^{(2)}$	149.4	28.8	142.6	40.7	6.8	11.9
	$C^{(3)}$	152.1	26.1	154.1	23.2	2.0	2.9
	$C^{(4)}$	167.8	28.4	167.7	28.8	0.1	0.4
	$H^{(1)}$	29.5	7.4	30.0	7.0	0.5	0.4
	$H^{(2)}$	29.7	6.9	30.1	5.0	0.4	1.9
	$H^{(3)}$	29.9	7.2	30.0	7.0	0.1	0.2
	$H^{(4)}$	30.3	9.6	30.4	9.4	0.1	0.2

[a] Calculations were performed at the PW91/IGLO-III level. [b] Absolute deviation errors of the shielding constants with capping potentials from the full QM results.

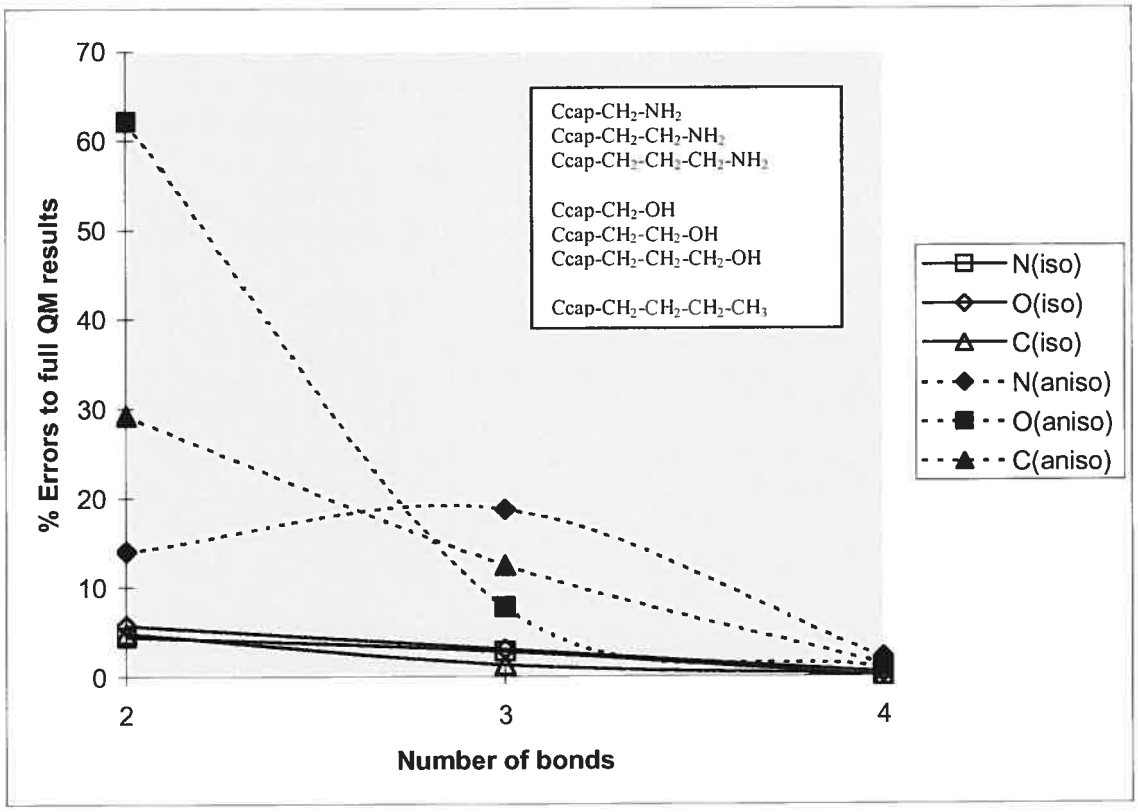

Figure 2.2. The % errors of shielding constants with capping potentials vs. the number of bonds from the capping carbon.

Table 2.2. Calculated NMR chemical shielding constants (in ppm) using QCPs for propanoic acid and alanine in comparison with full QM results.[a]

		Cap QM		Full QM		[b]|Δ|	
molecule	nucleus	iso	aniso	iso	aniso	iso	aniso
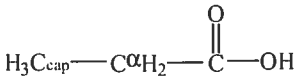	C^{α}	150.6	53.4	155.2	35.2	4.6	18.2
	H^{α}	28.5	5.7	28.8	7.3	0.3	1.6
	C	11.9	86.3	8.1	86.3	3.8	0.0
	(C=O) O	-90.3	458.6	-73.0	517.5	17.3	58.9
	(O-H) O	119.0	199.6	117.0	207.2	2.1	7.6
	H	25.1	12.3	25.2	12.1	0.2	0.2
					[c]$\|\Delta\|_{av}$(C,O)	7.0	21.2
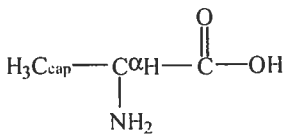	C^{α}	119.0	48.2	127.5	39.0	8.5	9.2
	H^{α}	26.9	5.6	27.7	6.3	0.8	0.7
	C	4.9	86.7	1.8	93.4	3.1	6.7
	(C=O) O	-66.7	523.8	-60.7	519.1	6.0	4.7
	(O-H) O	126.5	191.0	123.0	185.6	3.5	5.4
	(O-H) H	24.9	12.8	25.2	12.5	0.3	0.3
	N	220.0	29.2	214.0	39.4	6.0	10.2
	(N-H) H	30.1	13.1	30.2	13.5	0.1	0.4
					$\|\Delta\|_{av}$(C,O)	5.3	6.5

[a] Calculations were performed at the PW91/IGLO-III level.

[b] Absolute deviation errors of the shielding constants with capping potentials from the full QM results.

[c] Average absolute deviation of the shielding constants of oxygen and nitrogen nuclei with capping potentials.

In Table 2.3, calculated shieldings of some organic molecules are listed. Here, the results were obtained from the QM subsystem with capping potentials at the boundary (Cap QM), the QM/MM system which includes QCPs at the boundary and Mulliken charges in the MM subsystem, and the full QM system. In these calculations, the QM subsystems including the capping carbon are all same ($H_3C\text{-}C^{cap}$) and therefore it enables us to make a systematic investigation for the effects of the point charges of the MM subdomain on the chemical shielding tensors of the QM region. This QM/MM approach includes only electrostatic interactions and if the polarization of the QM part by the point charges of the MM subdomain is not too great, the QM/MM approach can not improve the shielding results over the pure QM results using only QCPs. For propane, ethyl amine, and propanoic acid, the QM/MM results are slightly worse rather than the pure QM results with QCPs. However, we can see the best improvement from the results of the amino acid (alanine) whose electric fields are relatively stronger than those of the other systems.

Table 2.3. Calculated NMR chemical shielding constants (in ppm) for some organic molecules.[a]

		Cap QM		QM/MM		Full QM		[b]|Δ|	
molecule	nucleus	iso	aniso	iso	aniso	iso	aniso	Cap	QM /MM
H_3C(QM)-	C	179.8	20.2	182.2	16.0	166.3	30.3	13.5/10.1	15.9/14.3
$C^{cap}H_2CH_3$	H	30.3	10.2	30.6	10.2	30.4	9.1	0.1/1.1	0.2/1.1
H_3C(QM)-	C	180.6	18.5	180.8	17.1	165.2	30.8	15.4/12.3	15.6/13.7
$C^{cap}H_2NH_2$	H	30.3	10.2	30.5	10.0	30.3	9.0	0.0/1.2	0.2/1.0
H_3C(QM)-	C	180.7	18.4	179.8	19.9	162.4	33.6	18.3/15.2	17.4/13.7
$C^{cap}H_2OH$	H	30.3	10.2	30.3	10.1	30.3	8.3	0.0/1.9	0.0/1.8
H_3C(QM)-	C	180.9	18.6	167.8	38.0	174.5	14.5	6.3/4.1	6.7/23.5
$C^{cap}H_2COOH$	H	30.4	10.3	29.5	9.7	30.3	9.5	0.1/0.8	0.8/0.2
H_3C(QM)-	C	179.5	19.8	170.7	33.0	161.0	38.0	18.6/18.2	9.7/5.0
$C^{cap}HCOOHNH_2$	H	30.3	10.1	29.8	9.6	30.1	8.4	0.2/1.7	0.3/1.2

[a] Calculations were performed at the PW91/IGLO-III level. [b] Absolute deviation errors from full QM results.

The NMR chemical shielding constants of neutral histidine were calculated for the various systems: the full QM system, the QM subsystems capped by hydrogen-link atoms and by capping potentials at the boundary, and the QM/MM system with capping potentials at the boundary and point charges in the MM region. The results are collected in Table 2.4. The molecular structure and capping scheme for neutral histidine are shown in Fig 2.3.

In this study, two types of point charges were used for comparison: Mulliken charges and RESP (restrained electrostatic potential) charges based on Hartree-Fock calculation. As seen in Table 2.4, the shielding results of the capping carbon approach are better than those of the hydrogen-link atom approach compared to full QM results for three different types of magnetic nuclei (C, N, and H) but the QM/MM results do not show any significant improvement over the pure QM (C-Cap) results. Different types of point charges mainly affect the nuclei close to the charges such as the β-carbon and the δ1-nitrogen. For carbon shielding constants, Mulliken charges ($|\Delta|$ = 0.6/3.8 ppm, absolute deviation errors of isotropic/anisotropic shieldings) give slightly better results than RESP charges ($|\Delta|$ = 3.7/8.2 ppm) but, for nitrogen shielding constants, the opposite trend is found (Mull: $|\Delta|$ = 2.8/14.5 ppm; RESP: $|\Delta|$ = 1.8/11.7 ppm). In this case, since the electric field is not so strong, there are no large differences between the QM/MM results (N, Mull: $|\Delta|$ = 2.7/22.0 ppm; RESP: $|\Delta|$ = 1.8/11.7 ppm) and the pure QM results with QCPs (N: $|\Delta|$ = 2.7/22.0 ppm).

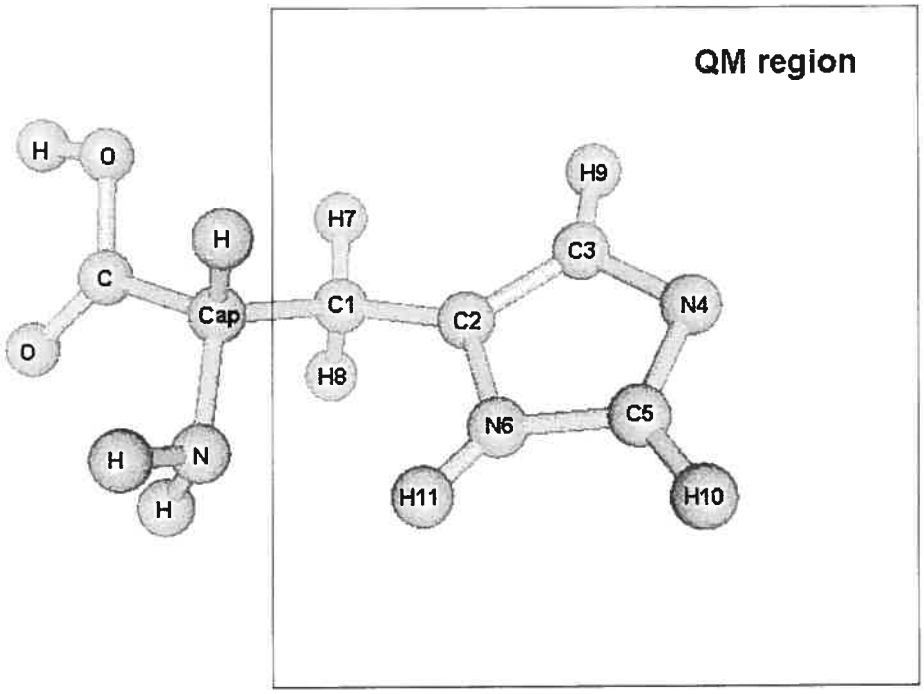

Figure 2.3. Optimized structure and numbering scheme of neutral histidine.

Table 2.4. Calculated NMR chemical shielding constants (in ppm) for neutral histidine.[a]

	QM/MM	QM			
	[b]Mull	[c]RESP/HF	H-link	C-Cap	Full
C_1	[d]148.0/[e]33.6	138.1/47.7	185.7/30.8	155.3/29.8	148.2/25.0
C_2	53.8/109.8	54.0/108.8	52.0/116.1	53.4/112.4	53.2/112.9
C_3	51.6/102.0	51.1/102.5	50.1/107.9	53.3/101.1	53.3/98.6
C_5	49.2/93.0	47.6/95.2	50.6/87.2	50.8/90.9	49.1/93.1
$\|\Delta\|$	0.6/3.8	3.7/8.2	10.8/6.0	2.2/2.5	
N_4	-31.8/389.8	-31.4/389.7	-38.2/398.3	-31.2/384.5	-28.1/397.3
N_6	76.3/115.7	74.8/121.5	77.1/95.6	76.8/106.0	74.5/137.2
$\|\Delta\|$	2.8/14.5	1.8/11.7	6.4/21.3	2.7/22.0	
H_7	27.8/8.3	27.0/7.8	32.3/9.4	28.0/8.7	28.7/6.2
H_8	27.8/6.7	27.3/5.8	31.8/10.6	28.0/7.1	28.1/7.2
H_{11}	22.0/6.3	21.7/6.5	23.0/5.9	22.6/5.8	19.9/11.9
H_9	24.2/3.6	24.2/3.5	24.3/4.1	24.3/3.6	24.3/4.6
H_{10}	23.7/5.1	23.7/4.9	24.0/5.3	23.8/5.1	23.7/5.4
$\|\Delta\|$	0.7/1.9	0.9/2.0	2.1/2.6	0.7/2.0	

[a] Calculations were performed at the PW91/IGLO-III level. [b] Mulliken charges were obtained at the B3LYP/6-311G** level using the G98 program. [c] RESP charges were obtained using the Amber program based on the Hartree-Fock electrostatic potential calculation. [d] Isotropic shielding constants. [e] Anisotropic shielding constants.

Finally, the NMR shielding constants of cystosine monophosphate (CMP) were calculated and are listed in Table 2.5. In the QM/MM calculation, the pyrimidine base atoms in CMP are only included in the QM region and the backbone atoms (the pentose and the phosphate) are treated as MM atoms. The QM/MM boundary is treated with QCPs. The QM/MM partition and numbering schemes are shown in Fig 2.4. The first partition of the QM and MM regions was made at the carbon (Ccap(PI)) and the second extended partition was made at the carbons (Ccap(PII)). In the hydrogen-link atom approach, the capping carbon in the first partition is replaced with a hydrogen atom. In this work, three kinds of point charges were used: Mulliken (Mull), RESP based on HF calculation (HF). Two types of QCPs are used: QCPs without Pauli repulsion (Cap1) and with Pauli repulstion (Cap2).

First, let us focus on the carbon shieldings. The isotropic shielding results of the QM/MM ($|\Delta|$ = 1.1~2.4 ppm) and pure QM ($|\Delta|$ = 1.6~3.3 ppm) approaches are not so different and even the different types of charges ($|\Delta|$ = 1.1~2.4 ppm) and the extension of the QM region ($|\Delta|$ = 2.0 ppm) do not give any large effect on the isotropic shieldings. However, the anisotropic shielding results are much more sensitive to the types of approaches (QM/MM(PI): $|\Delta|$ = 6.2~8.4 ppm; QM(PI): $|\Delta|$ = 7.4~11.4 ppm) and partition schemes (QM/MM(PII): $|\Delta|$ = 0.8 ppm). It reflects that the types of charges (Mulliken, RESP-HF) and potentials (Cap1 and Cap2) are not important for both isotropic and anisotropic shieldings. On the contrary, the extension of the QM region has a large effect on the anisotropy of carbon.

Nitrogen shielding results show a different trend from the carbon results. For the isotropic shielding, the capping carbon approaches (PI+Cap1: $|\Delta|$ = 4.5 ppm) give closer results to the full QM results than the H-link approach ($|\Delta|$ = 14.6 ppm) and the Pauli repulsion (PI+Cap2: $|\Delta|$ = 6.8 ppm) is not important in this case. The QM/MM results even including the extended partition results ($|\Delta|$ = 5.5~8.4 ppm) do not show any great improvement to the pure QM results ($|\Delta|$ = 4.5~14.6 ppm). For the anisotropic shielding, the inclusion of Pauli repulsion (PI+Cap2: $|\Delta|$ = 32.9 ppm) makes the results of the pure

QM approaches (PI+Cap1: $|\Delta|$ = 17.8 ppm) worse, and even in the QM/MM scheme the same trend is shown. For QM/MM, the results with RESP charges ($|\Delta|$ = 4.0~7.4 ppm) are better than the others including the extended partition results ($|\Delta|$ = 13.2~23.1 ppm).

As seen in Table 2.5, for the oxygen shieldings, the pure QM results with capping potentials (PI+Cap1: $|\Delta|$ = 30.3/115.0 ppm) are much worse than the results with H-link atoms ($|\Delta|$ = 20.6/20.2 ppm). The results (PI+Cap2: $|\Delta|$ = 22.0/66.6 ppm) can be improved by the QCPs with Pauli repulsion but they are still far from the full QM results. For isotropic shieldings, the first partition (PI) QM/MM results ($|\Delta|$ = 0.1~8.7 ppm) show great improvement over the pure QM results but still their anisotropies ($|\Delta|$ = 107.1~169.9 ppm) are seriously deviated from the full QM results. This problem is alleviated with the extended partition (PII) ($|\Delta|$ = 19.2 ppm). In this work, the electrostatic effects between the MM and QM subregions are only included in the QM/MM approach and, therefore, other short-range quantum interactions from the MM atoms (e.g. polarization, exchange repulsion, charge transfer) should be considered in order to obtain accurate anisotropic shielding constants of the oxygen. Here, this is achieved simply by the slight extension of the QM part.

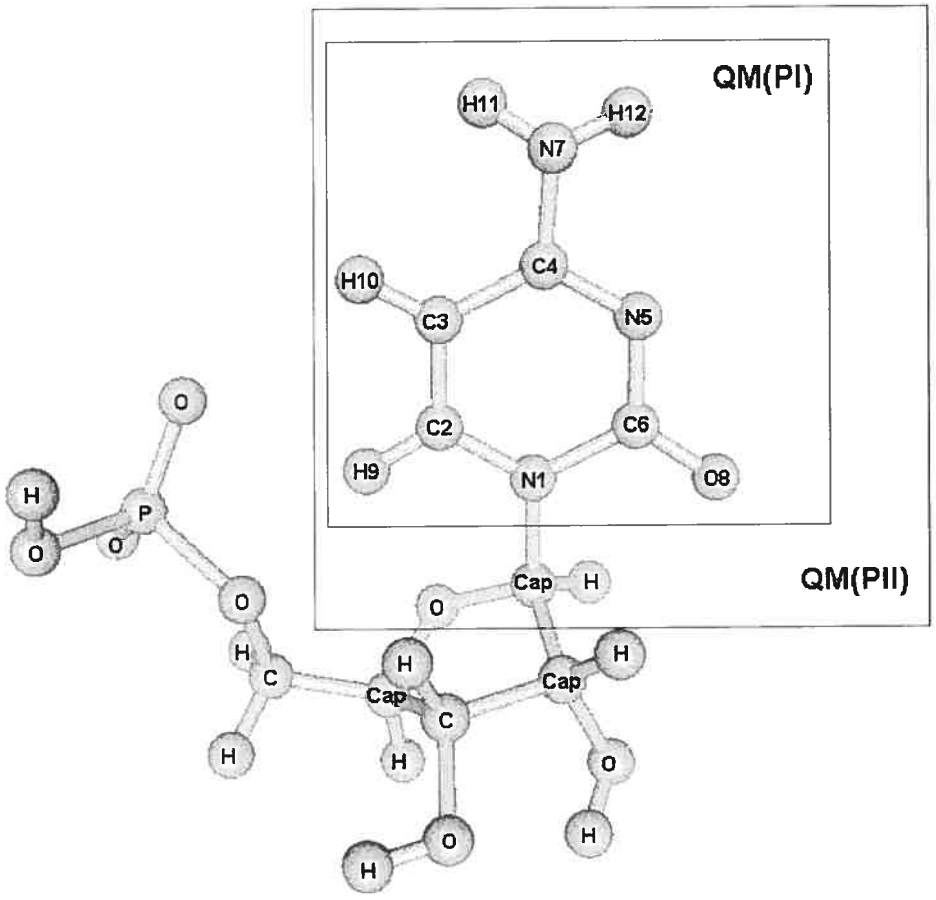

Figure 2.4. Optimized structure and numbering scheme of cytosine monophosphate (CMP).

Table 2.5. Calculated NMR chemical shielding constants (in ppm) for the base of cytosine monophosphate (CMP).[a]

	QM/MM					QM			
	PI+Cap1 Mull	PI+Cap1 HF	PI+Cap1 MP2	PI+Cap2 Mull	PII+Cap1 Mull	PI+Cap1	PI+Cap2	PI+H H-link	Full
C2	[b]16.4/	16.0/	16.1/	16.5/	16.7/	16.6/	16.9/	15.9/	15.6/
	[c]152.0	153.3	153.1	152.5	151.7	152.7	152.5	151.5	151.1
C3	87.4/	84.4/	85.3/	88.2/	88.9/	88.2/	89.2/	91.0/	87.7/
	114.0	115.2	114.5	114.6	114.6	106.0	108.9	110.2	114.3
C4	25.5/	24.9/	25.3/	28.3/	34.0/	32.6/	35.1/	36.8/	29.4/
	191.0	160.7	161.0	160.0	178.3	147.3	157.2	154.0	179.8
C8	23.0/	23.8/	23.8/	23.4/	26.4/	26.7/	26.1/	27.3/	25.1/
	78.5	77.5	77.3	76.1	65.3	69.1	65.9	73.0	66.1
[d]|Δ|	1.8/	2.4/	2.1/	1.1/	2.0/	1.6/	2.4/	3.3/	
	6.2	8.4	8.1	7.9	0.8	11.4	7.4	9.3	
N1	19.8/	21.3/	20.7/	17.0/	10.4/	11.3/	8.1/	5.9/	13.6/
	264.9	265.4	265.6	265.8	259.8	274.6	277.6	278.1	260.2
N5	52.4/	50.3/	51.4/	41.4/	44.0/	55.4/	51.4/	90.8/	61.8/
	88.6	134.1	124.0	74.7	175.4	104.5	61.5	107.3	136.7
N10	168.1/	167.1/	167.0/	168.5/	168.5/	162.3/	162.9/	160.2/	167.2/
	95.2	93.2	93.3	95.8	97.1	90.8	91.5	93.5	97.5
|Δ|	5.5/	6.4/	5.9/	8.4/	7.4/	4.5/	6.8/	14.6/	
	18.4	4.0	7.4	23.1	13.2	17.8	32.9	17.1	
O9	-14.5/	-23.1/	-21.8/	-8.2/	-28.0/	-44.6/	-36.3/	-34.9/	-14.3/
	312.3	286.8	294.2	349.6	475.9	341.7	390.1	436.7	456.7
|Δ|	0.1/	8.7/	7.5/	8.3/	13.7/	30.3/	22.0/	20.6/	
	144.4	169.9	162.5	107.1	19.2	115.0	66.6	20.2	

[a] Calculations were performed at the PW91/IGLO-III level. [b] Isotropic shielding constants. [c] Anisotropic shielding constants. [d] Absolute deviation errors from full QM results.

2.4.2 Nuclear Spin-Spin Coupling Constants

In this work, the QM/MM approach using the electrostatic embedding model of the QM part has been applied to the calculation of nuclear spin-spin coupling constant for the first time. In order to consider the strong electrostatic effect, CMP was used for the calculations. Calculated results at the various approaches are collected in Table 2.6. From Table 2.6, we can see that the QM/MM results are in good agreement with the full QM results and they are much better than the pure QM results with only QCPs. Mainly, the spin-spin coupling constants of $^{1}H_{9}{}^{13}C_{2}$ (see Fig 2.4 for structure and numbering scheme) are strongly affected by the MM partial charges and the others are not. Among contributions of the coupling constant, the Fermi contact and spin dipolar cross term (FC-SD) are most sensitive to the MM point charges. From the results, we can see that this QM/MM approach is valid for NMR spin-spin coupling calculations and especially if electrostatic interactions between the QM and MM subsystems are strong and short range quantum interactions are not important, the QM/MM results will be very close to the full QM results.

Table 2.6. Calculated NMR spin-spin coupling constants (in Hz) for the base of cystosine monophosphate (CMP).[a]

		QM/MM PI+Cap1 Mulliken	QM PI+Cap1	QM Full	|Δ| QM/MM	|Δ| QM
$^1H_9{}^{13}C_2$	[b]FC	179.71	167.02	181.00	1.29	13.98
	[c]PSO	-0.48	-0.17	-1.04	0.56	0.87
	[d]DSO	0.87	0.92	1.50	0.63	0.58
	SUM	180.10	167.77	181.47	1.37	13.70
$^1H_9{}^{15}N_1$	FC	2.61	2.95	2.00	0.61	0.95
	PSO	-0.33	-0.37	-0.44	0.11	0.07
	DSO	-0.09	-0.09	0.06	0.15	0.15
	SUM	2.18	2.49	1.62	0.56	0.87
$^1H_9{}^{13}C_3$	FC	4.75	5.13	3.84	0.91	1.29
	PSO	-0.68	-0.75	-1.05	0.37	0.30
	DSO	-0.35	-0.35	0.00	0.35	0.35
	SUM	3.72	4.04	2.79	0.93	1.25
$^1H_9{}^1H_{10}$	FC	7.03	6.79	6.87	0.16	0.08
	PSO	0.10	0.08	-1.09	1.19	1.17
	DSO	-0.31	-0.31	0.96	1.27	1.27
	SUM	6.82	6.55	6.74	0.08	0.19

[a] Calculations were performed at the P86/IGLO-III level. [b] The Femi contact term. [c] The paramagnetic spin-orbit term. [d] The diamagnetic spin-orbit term.

2.4.3. Hyperfine Coupling Tensors

We begin by examining the influence of MM partial charges on the hyperfine structure and Mulliken atomic spin population of the QM region. To this end, we employ two model systems, labeled as "C-Cap QM" and "QM/MM". The first model (C-Cap QM) consists of the pure QM subsystem, capped with "carbon" QCPs. It contains 42 atoms. The QM/MM model additionally incorporates MM partial charges (2140 and 1929 MM atoms for azurin and stellacyanin, respectively). Results, obtained with these two models, are compared to the experimental data [36-39], and to published QM results for an extended model, capped by hydrogen link atoms (H-Link L-QM) [2]. In the latter case, four aminoacids, directly coordinated to the copper center, were supplemented by the atoms of the neighboring aminoacids, for a total of 117 and 93 QM atoms in azurin and stellacyanin, respectively. DFT results for the extended model of stellacyanin, calculated in the present work, were obtained for a slightly smaller model, where the peptide chain of the axial aminoacid (Gln99) was not elongated. Tables 2.7 and 2.8 compare calculated hyperfine parameters of azurin and stellacyanin for these model systems. Mulliken spin populations of the two models, studied presently, are shown in Table 2.9.

From Tables 2.7 and 2.8, it can be seen that the capping pseudopotential technique gives similar results to the hydrogen link atom approach, but at a significantly lower computational cost (in terms of numbers of electrons that have to be explicitly treated in the QM subsystem). Potentially, the capping carbon approach also provides a better description of spin delocalization by retaining carbon atom character at the domain boundary.

The qualitative difference between the protein environment of the copper center in azurin and stellacyanin can be seen clearly from the simplified ribbon structures, shown in Figures 2.5 and 2.6. In azurin, the aminoacids directly coordinated to the copper center are well screened by the protein backbone. The only exception is the δ2 and ε2 positions of His117, which are exposed to the solvent. On the other hand, in stellacyanin, parts of

His46 and His94 opposite from the copper center are easily accessible for the solvent molecules. These characteristic structural features lead to quite different trends in the QM/MM results for the hyperfine structure and Mulliken spin population.

For the copper nucleus, the anisotropic hyperfine tensors of azurin are greatly affected by the MM partial charges (changes of 8 ~ 32 MHz), but the isotropic hyperfine constant is not (change of 1 MHz). On the other hand, both the dipolar and isotropic constants of stellacyanin copper are greatly affected by MM partial charges (changes of 5 ~ 18 MHz and 17 MHz for the dipolar and isotropic constants, respectively). As can be seen from Table 2.9, the unpaired electron spin populations (p- and d-types) on the copper atom in azurin and stellacyanin are increased by 0.038 and 0.017, respectively, under the influence of MM charges. This illustrates the stronger influence of the MM charges on the anisotropic tensors of the copper in azurin. (We note that dipolar tensors are mainly determined by the interaction between the nuclear spin and anisotropic spin-density distribution, provided by the valence p and d-orbitals on copper). At the same time, the isotropic results indicate that, in azurin, s-type populations on copper are not affected by MM charges, in contrast to stellacyanin.

In order to test the convergence of the QM/MM calculations with the QM subsystem size for the copper center in stellacyanin, we also examined an alternative QM region for the QM/MM calculation in this system (M-QM/MM). In this model (53 QM atoms), some atoms of neighboring residues attached to Cys89 were transferred from the MM part into the QM region. Because Cys89 sulfur interacts strongly with the copper (see Table 3), accurate handling of Cys89 may be expected to be more important, compared to His46 and His95. From the results (see M-QM/MM in Table 2), it is seen that the hyperfine structures of the copper are not affected much by the elongation of Cys89 chain. By inference, extension of the QM subsystem to the direct neighbours of the histidine ligands, is likely to be even less important.

For the histidine nitrogen, in azurin, our QM/MM results for the hyperfine structure are in good agreement with the previously published results for larger, pure QM models, and

the experimental data. Nitrogen atoms, coordinated directly to the copper center (in δ1 position), carry larger spin populations compared to the remote ε2 nitrogen atoms. As a result, calculated isotropic hyperfine parameters of δ-nitrogen atoms (His46: 15.6 MHz; His117: 18.5 MHz in C-Cap QM; 18.7 and 22.0 MHz in QM/MM; vs. 18.1 and 25.1 MHz in experiment) are somewhat more sensitive to MM charges, than those of ε-nitrogen atoms (His 46: 0.56 MHz; His117: 0.93 MHz in C-Cap QM; 0.62 and 1.21 MHz in QM/MM; vs. 0.87 and 1.30 MHz in experiment). The absolute difference (3.1 and 3.5 MHz in δ1 position; 0.06 and 0.28 MHz in ε2 position) of A_{iso} values between the pure QM (C-Cap QM) and QM/MM models indicates relatively strong effects from the MM subsystem.

In stellacyanin, the QM/MM calculations give nitrogen hyperfine parameters similar to the QM results (L-QM, this work) for larger models. As can be seen from Table 2.7 and Figure 2.6, the effects from the protein backbone and solvent molecules are small, compared to azurin. At the same time, the results from the extended QM/MM model (M-QM/MM) are closer to the results from the large QM region (L-QM), and to the experiment. This indicates that additional short-range interactions from neighbors of Cys89 (e.g. induction, exchange repulsion, charge transfer), completely neglected in standard QM/MM models, should be treated explicitly.

For the cysteine β-hydrogen, in azurin, the QM/MM A_{iso} values (β1: 30 MHz; β2: 54 MHz) represent a significant improvement relative to the pure QM (C-Cap QM) results (34 and 64 MHz). The values are close to the previously published QM results [40, 41] for larger models (28 and 46 MHz in L-QM1; 28 and 32 MHz in L-QM2), and to the experiment (27 and 28 MHz). On the contrary, in stellacyanin, there is no significant difference between the pure QM (C-Cap) (β1: 33 MHz; β2: 40 MHz) and QM/MM (36 and 38 MHz) results and the QM/MM results are far from the QM values for a larger model (β1: 22 MHz; β2: 27 MHz), and from experiment (13 and 16 MHz). In both cases, there are still significant discrepancies between the QM/MM and experimental values for β-hydrogens. Again, these discrepancies arise from the omission of short-range

interactions of the cystein residue with the protein backbone. Treating these interactions explicitly within the DFT region improves the results considerably (M-QM/MM - β1: 28 MHz; β2: 28 MHz in stellacyanin).

For the histidine hydrogen, the QM/MM results are in better agreement with experiment than the pure QM (C-Cap) treatment of the radical center. In azurin, QM/MM A_{iso} values represent a significant change (0.11 ~ 0.34 MHz) relative to the pure QM (C-Cap) results, except ε2 hydrogen of His46. Following the trend seen for other hyperfine parameters, in stellacyanin, the QM/MM results deviate much less from the pure QM results (by 0.02 ~ 0.13 MHz). In azurin, the hyperfine parameters of histidine hydrogens should be affected mainly by the protein backbone (δ2: 0.24 MHz; ε1: 0.34 MHz in His46, ε1: 0.34 MHz in His117), while those of the δ2 and ε2 hydrogens in His117 should be affected mainly by solvent molecules (δ2: 0.21 MHz; ε2: 0.11 MHz). In stellacyanin, an influence of the solvent may be expected for most hydrogens, but the effect (0.02 ~ 0.13 MHz) is less pronounced than in azurin.

Table 2.7. Calculated hyperfine parameters of azurin in MHz.[a]

			H-Link QM	C-Cap QM	QM/MM	H-Link L-QM1[b]	H-Link L-QM2[c]	EXP[d]
	Cu	A_{iso}	-109	-106	-105	-207	-158	~ -100
		T_1	147	144	152	193		
		T_2	117	114	138	154		
		T_3	-263	-258	-290	-347		
His46	$N_{\delta 1}$	A_{iso}	15.6	15.6	18.7	20.3	16.1	18.1
		T_1	-1.7	-1.7	-2.2	-2.0		-1.3
		T_2	-1.4	-1.4	-1.9	-1.6		-0.8
		T_3	3.1	3.1	4.1	3.6		1.2
	$N_{\varepsilon 2}$	A_{iso}	0.60	0.56	0.62	0.7	0.9	0.87
		T_1	-0.14	-0.14	-0.18	-0.2		-0.17
		T_2	-0.04	-0.04	-0.05	0.0		-0.07
		T_3	0.18	0.17	0.23	0.2		0.23
	$H_{\delta 2}$	A_{iso}	0.68	0.63	0.87	0.9	0.79	1.49
	$H_{\varepsilon 1}$	A_{iso}	0.89	0.96	1.30	0.4	1.32	1.06/1.48
	$H_{\varepsilon 2}$	A_{iso}	0.41	0.33	0.34	0.3	0.60	0.56
His117	$N_{\delta 1}$	A_{iso}	19.1	18.5	22.0	22.6	22.4	25.1
		T_1	-2.1	-2.0	-2.4	-2.2		-1.5
		T_2	-1.7	-1.6	-1.9	-1.7		-1.1
		T_3	3.8	3.7	4.3	3.9		2.7
	$N_{\varepsilon 2}$	A_{iso}	1.01	0.93	1.21	1.0	1.5	1.30
		T_1	-0.19	-0.18	-0.19	-0.2		-0.32
		T_2	-0.05	-0.05	-0.07	-0.1		-0.04
		T_3	0.24	0.23	0.25	0.3		0.35
	$H_{\delta 2}$	A_{iso}	0.68	0.62	0.83	1.5	2.00	1.61
	$H_{\varepsilon 1}$	A_{iso}	1.48	1.43	1.77	0.4	0.79	1.45/1.02
	$H_{\varepsilon 2}$	A_{iso}	0.70	0.66	0.77	0.4	1.06	
Cys112	$H_{\beta 1}$	A_{iso}	34	34	30	28	28	27
	$H_{\beta 2}$	A_{iso}	60	64	54	46	32	28

[a] Calculations were performed at the BP level. [d] UB1LYP results of the large model taken from Ref [38].

[b] BP results of the large model taken from Ref [40]. [c] ENDOR, ESEEM and NMR results taken from Ref [36-39, 42].

Table 2.8. Calculated hyperfine parameters of stellacyanin in MHz.[a]

			H-Link QM	C-Cap QM	QM /MM	M-QM /MM[b]	H-Link L-QM[c]	EXP[d]
	Cu	A_{iso}	-73	-70	-53	-53	-59	
		T_1	176	172	190	198	175	
		T_2	113	112	100	106	93	
		T_3	-289	-284	-289	-304	-263	
His46	$N_{\delta 1}$	A_{iso}	16.93	16.63	16.49	17.75	18.30	
		T_1	-2.15	-2.12	-2.06	-2.24	-2.45	
		T_2	-1.75	-1.73	-1.66	-1.82	-1.97	
		T_3	3.90	3.85	3.72	4.05	4.42	
	$N_{\varepsilon 2}$	A_{iso}	1.04	1.02	0.96	1.04	1.04	
		T_1	-0.18	-0.18	-0.17	-0.18	-0.21	
		T_2	-0.03	-0.03	-0.04	-0.04	-0.03	
		T_3	0.22	0.21	0.21	0.22	0.24	
	$H_{\delta 2}$	A_{iso}	1.56	1.51	1.48	1.65	1.46	1.53/1.78
	$H_{\varepsilon 1}$	A_{iso}	1.26	1.28	1.25	1.32	1.12	0.70/1.09
	$H_{\varepsilon 2}$	A_{iso}	0.95	0.89	0.76	0.81	0.77	0.62
His94	$N_{\delta 1}$	A_{iso}	23.92	23.54	25.33	26.43	26.79	
		T_1	-3.10	-3.04	-3.28	-3.50	-3.39	
		T_2	-2.49	-2.45	-2.63	-2.82	-2.71	
		T_3	5.59	5.49	5.91	6.32	6.10	
	$N_{\varepsilon 2}$	A_{iso}	1.71	1.64	1.68	1.75	1.61	
		T_1	-0.23	-0.22	-0.25	-0.26	-0.26	
		T_2	-0.06	-0.06	-0.08	-0.08	-0.06	
		T_3	0.29	0.29	0.32	0.34	0.32	
	$H_{\delta 2}$	A_{iso}	1.82	1.74	1.79	1.98	1.56	1.77/1.51
	$H_{\varepsilon 1}$	A_{iso}	1.53	1.50	1.61	1.72	1.36	1.40/1.01
	$H_{\varepsilon 2}$	A_{iso}	1.69	1.67	1.75	1.81	1.38	
Cys89	$H_{\beta 1}$	A_{iso}	32	33	36	28	22	13
	$H_{\beta 2}$	A_{iso}	38	40	38	28	27	16

[a] Calculations were performed at the BP level. [b] The peptide chain of Cys89 is elongated by the atoms of neighboring aminoacids. [c] This work. [d] NMR results taken from Ref [39].

Table 2.9. Comparison of Mulliken spin populations for azurin and stellacyanin models, with different approaches for the dangling bond capping.

	Azurin		Cys112			His46	His117
	Stellacyanin		Cys89			His46	His94
		Cu	S	$H_{\beta 1}$	$H_{\beta 2}$	$N_{\delta 1}$	$N_{\delta 1}$
Azurin	H-Link QM	0.236[a]	0.661	0.014	0.026	0.031	0.037
		-0.016[b]	0.020	0.013	0.024	0.008	0.009
	C-Cap QM	0.230	0.666	0.018	0.029	0.033	0.037
		-0.014	0.021	0.017	0.027	0.008	0.009
	QM/MM	0.267	0.608	0.016	0.024	0.047	0.044
		-0.013	0.019	0.016	0.023	0.009	0.011
Stellacyanin	H-Link QM	0.270	0.602	0.012	0.017	0.042	0.057
		-0.008	0.015	0.011	0.016	0.011	0.012
	C-Cap QM	0.264	0.611	0.012	0.019	0.044	0.057
		-0.009	0.016	0.012	0.018	0.011	0.013
	QM/MM	0.278	0.583	0.012	0.017	0.044	0.062
		-0.006	0.013	0.012	0.017	0.009	0.015

[a] Total spin populations (s- , p- and d-type orbitals). [b] Spin populations of s-type orbitals.

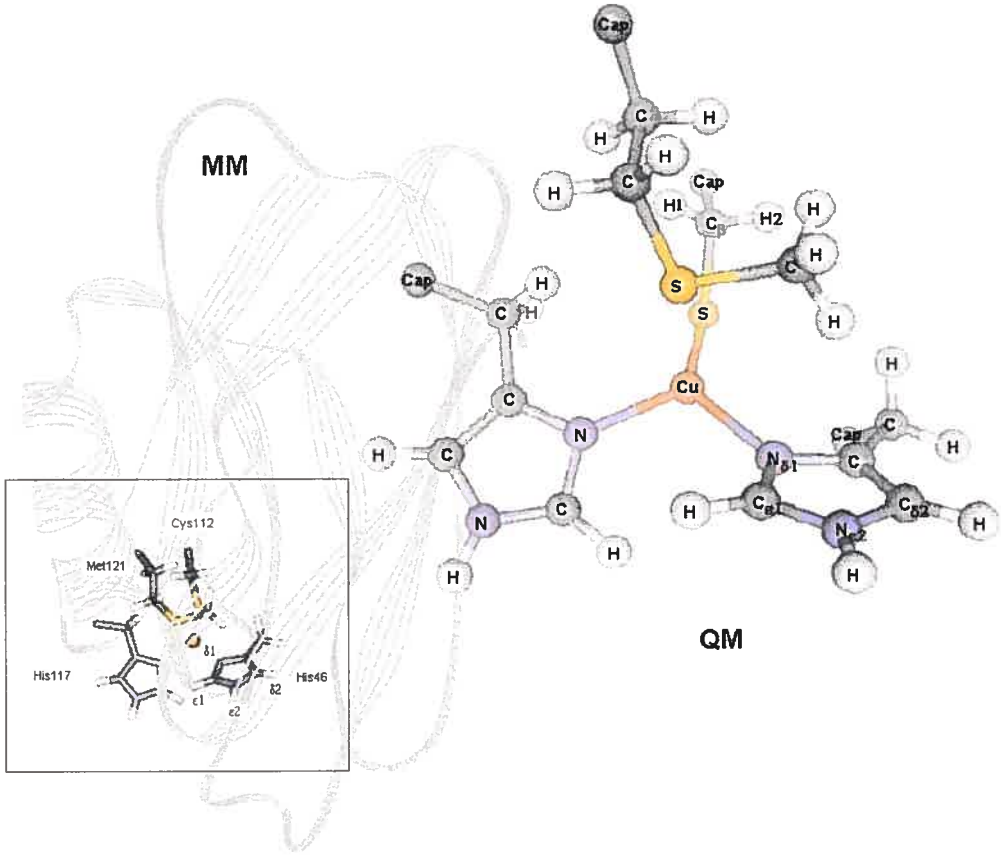

Figure 2.5. The QM part in wild type azurin from *Pseudomonas aeruginosa*; terminal carbon atoms were replaced by capping carbon atoms in the QM/MM calculations.

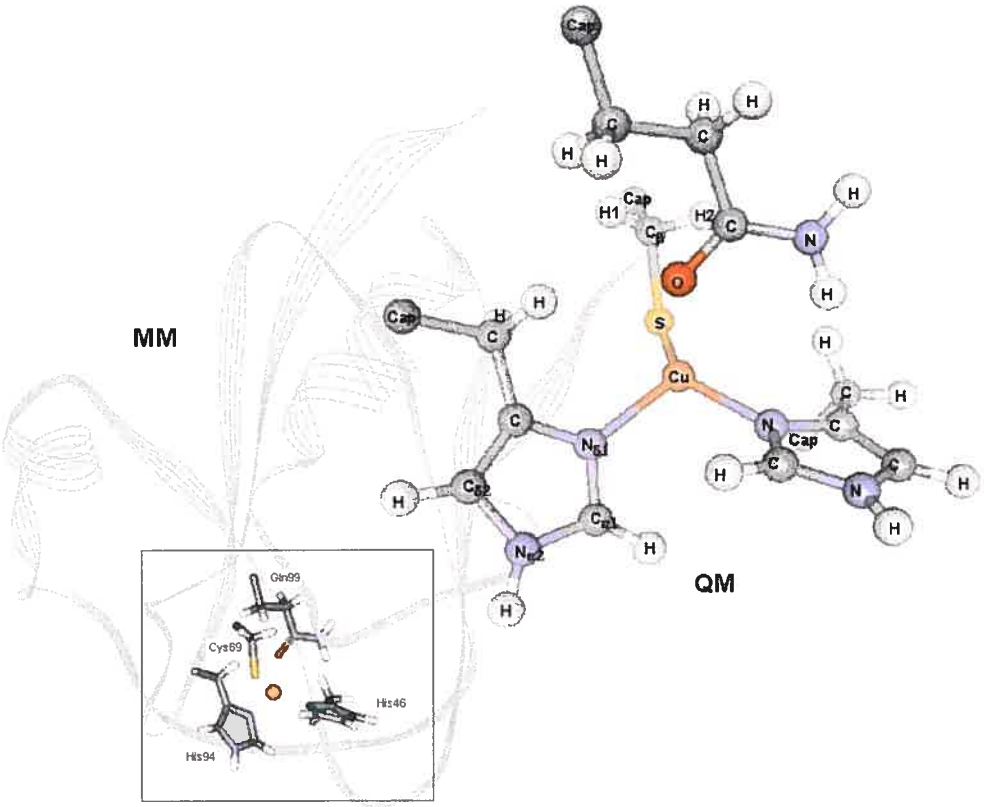

Figure 2.6. The QM part in stellacyanin from *Cucumis sativus*; terminal carbon atoms were replaced by capping carbon atoms in the QM/MM calculations.

2.5. Conclusion

We proposed a QM/MM approach for the calculations of various magnetic properties such as NMR shielding tensors, nuclear spin-spin coupling constants, and hyperfine tensors. The technique employs one-electron carbon pseudopotentials, parameterized, for capping bonds at the domain boundary. Long-range interactions between the QM and MM subsystems are treated by adding an electrostatic term, due to the MM charges, to the one-electron part of the QM Hamiltonian. In this study, it is demonstrated that the effects from the MM partial charges on the QM part mainly transfer through field-free KS orbitals and corresponding energies implicitly. Hence, we do not need to modify the codes of the core integrals for magnetic properties which are not changed in this QM/MM approach. This QM/MM approach was applied to calculations of various magnetic properties: (1) NMR chemical shielding tensors for several organic molecules, some aminoacids (alanine and histidine), and a nucleic acid model (CMP) (2) NMR spin-spin coupling constants for CMP (3) hyperfine structures for paramagnetic blue copper proteins (Azurin and Stellacyanin).

This QM/MM approach shows two significant advantages: Firstly, it can be implemented easily without code modification. Capping potentials can be treated as conventional effective core potentials, and point charges can be handled for energy calculations by most DFT programs. Secondly, the magnetic parameters of biological systems are well described by a small QM model surrounded by MM partial charges. This is in part due to the use of the capping potentials, which reduce disturbances of the electronic structure of the QM subsystem, arising from broken bonds at the domain boundary. At the same time, care should be taken not to place the domain boundary too close to the nuclei of interest which are strongly affected by quantum effects. In the present study, the oxygen of CMP in NMR chemical shielding calculation and β-hydrogens of the cysteine residue (directly coordinated to the copper center) in hyperfine structure calculation were placed too close to the domain boundary used in our initial QM/MM model. Adequate treatment of such centers requires that additional short-range interactions at the boundary (induction,

exchange repulsion, and charge transfer) should be included. In this work, the desired effects were achieved by a small increase in the size of the QM subsystem.

In summary, our hybrid QM/MM method provides computationally efficient access to most magnetic parameters of the interesting local (QM) part in biological systems such as proteins and nucleic acids, while at the same time including the essential effects from the surroundings.

2.6. References

1. DiLabio, G. A.; Hurley, M. M.; Christiansen, P. A. *J. Chem. Phys.* **2002**, 116, 9578.
2. DiLabio, G. A.; Moon, S.; Christiansen, P. A. "Quantum capping potentials: Application to the calculation of NMR chemical shifts" Fourth European Computational Chemistry Conference, Assisi, Italy, 2002.
3. Moon, S.; Christiansen, P. A; DiLabio, G. A. "Quantum capping potentials with point charges: Density functional theory calculation of large molecule NMR chemical shielding tensors using QM/MM" *manuscript in preparation.*
4. Moon, S.; Patchkovskii, S.; Salahub, D. R. "QM/MM calculations of EPR hyperfine coupling constants in blue copper proteins" *J. Mol. Struct. (THEOCHEM)* in print (2003).
5. (a) Warshel, A., *Computer Modeling of Reactions in Enzymes*, Wiley, New York, 1991.

   (b) Gao, J., in *Reviews in Computational Chemistry*, edited by Lipkowitz, K. B. and Boyd, D. B., VCH, New York, 1996, Vol. 7., p. 119.
6. Singh, U.C.; Kollman, P.A. *J. Comput. Chem.* **1986**, 7, 718.
7. Eurenius, K. P.; Chatfield, D. C. ; Brooks, B. R.; Hodoscek, M. *Int. J. Quantum. Chem.* 1996, 60, 1189.
8. Antes, I,; Thiel, W. *J. Phys. Chem. A* **1999**, 103, 9290.
9. Assfeld, X.; Rivail, J.-L. *Chem. Phys. Lett.* **1996**, 263, 100.
10. Gao, J.; Amara, P.; Alhambra, C.; Field, M. J. *J. Phys. Chem. A* **1998**, 102, 4714.
11. Reuter, N., Dejaegere, A.; Maigret, B. ; Karplus, M. *J. Phys. Chem. A* **2000**, 104, 1720.
12. Zhang, Y.; Lee, T.-S.; Yang, W. *J. Chem. Phys.* **1998**, 110, 46.
13. (a) Christiansen, P. A.; Lee, Y. S.; Pitzer, K. S. *J. Chem. Phys.* **1979**, 71, 4445.

    (b) Christiansen, P. A.; Ermler, W. C.; Pitzer, K. S. *Ann. Rev. Phys. Chem.* **1985**, 36, 407.

    (c) Berger, A.; Dolg, M.; Küchle, W.; Stoll, H.; Preuss, H. *Mol. Phys.* **1993**, 80, 1431.

14. Gordon, M. S.; Freitag, M. A.; Banyopadhyay, P. B.; Jensen, J. H.; Kairys, V.; Stevens, W. J. *J. Phys. Chem. A* **2001**, 105, 293.
15. Cui, Q.; Karplus, M. *J. Phys. Chem. B* **2000**, 104, 3721.
16. Schreckenbach, G., Ph. D. Thesis, The University of Calgary, Canada, 1996.
17. Helgaker, T.; Jaszuński, M.; Ruud, K. *Chem. Rev.*, **1999**, 99, 293.
18. Malkina, O. L.; Vaara, J.; Schimmelpfennig, B.; Munzarova, M.; Malkin, V. G.; Kaupp, M. *J. Am. Chem. Soc.* **2000**, 122, 9206.
19. Malkin, V. G.; Malkina, O. L.; Salahub, D. R. *Chem. Phys. Lett.* **1993**, 204, 80.
20. Ditchfield, R. *Mol. Phys.* **1974**, 27, 789.
21. Kutzelnigg, W.; Flesicher, U.; Schindler, M. In *NMR-Basic Principles and Progress*, Springer, Heidelberg, 1990, Vol. 28.
22. Malkin, V. G.; Malkina, O. L.; Casida, M. E.; Salahub, D. R. *J. Am. Chem. Soc.* **1994**, 116, 5898.
23. Becke, A. D. *J. Chem. Phys.* **1993**, 98, 5648.
24. Krishnan, R.; Binkley, J. S.; Seeger, R.; Pople, J. A. *J. Chem. Phys.* **1980**, 72, 650.
25. Frisch, M. J.; Trucks, G. W.; Schelegel, H. B. et al. GAUSSIAN 98, A.7, Gaussian, Inc., Pittsburgh, PA, 1998.
26. (a) St-Amant, A.; Salahub, D. R. *Chem. Phys. Lett.* **1990**, 169, 387. (b) Malkin, V. G., Malkina, O. L., Erisson, L. A., Salahub, D. R., In *Modern Density Functional Theory: A Tool for Chemistry; Theoretical and Computational Chemistry*; Seminario, J. M., Politzer, P., Eds.; Elsevier, Amsterdam, 1995. Vol. 2.
27. Perdew, J. P.; Wang, Y. *Phys. Rev. B* **1992**, 45, 13244.
28. Perdew, J. P. *Phys. Rev. B* **1986**, 33, 8822.
29. Boys, S. F. *In Quantum theory of Atoms, Molecules and the Solid State*; Löwdin, P.-O., Ed., Academic Press, New York, 1966, p253.
30. Pople, J. A., McIver Jr., J. W., Ostlund, N. S. *J. Chem. Phys.* **1968**, 49, 2965.
31. Bayly, C. I.; Cieplak, P.; Cornell, W. D.; Kollman, P. A. *J. Phys. Chem.* **1993**, 97, 10269.

32. Cornell, W. D.; Cieplak, P.; Bayly, C. I.; Gould, I. R.; Merz, K. M.; Ferguson, D. M.; Spellmeyer, D. C.; Fox, T.; Caldwell, J. W.; Kollman, P. *J. Am. Chem. Soc.* **1995**, 117, 5179.

33. Becke, A. D. *Phys. Rev. A* **1998**, 38, 3098.

34. (a) Godbout, N; Salahub, D. R.; Andzelm, J.; Wimmer, E. *Can. J. Chem.* **1992**, 70, 560.

(b) Dolg, M.; Wedig. U.; Stoll, H.; Preuss, H. *J. Chem. Phys.* **1987**, 86, 866.

35. The X-leap program is distributed with the AMBER (version 6.0) program. (http://www.amber.ucsf.edu/amber/amber.html)

36. Coreman, J. W. A.; Poluektov, O. G.; Groenen, E. J. J.; Canters, G. W.; Nar, H., Messerschmidt, A. *J. Am. Chem. Soc.* **1996**, 118, 12141.

37. Coreman, J. W. A.; Poluektov, O. G.; Groenen, E. J. J.; Canters, G. W.; Nar, H., Messerschmidt, A. *J. Am. Chem. Soc.* **1997**, 119, 4726.

38. Bertini, I.; Ciurli, S.; Dikiy, A.; Gasanov, R.; Luchinat, C.; Martini, G.; Safarov, N. *J. Am. Chem. Soc.* **1999**, 121, 2037.

39. Bertini, I.; Fernandez, C. O.; Karlsson, B. G.; Leckner, J., Luchinat, C.; Malmstrom, C.; Nersissian, A. M.; Pierattelli, R.; Shipp, E.; Valentine, J. J.; Vila, A. J. *J. Am. Chem. Soc.* **2000**, 122, 3701.

40. Jaszewski, A. R.; Jezierska, J. *Chem. Phys. Lett.* **2001**, 343, 571.

41. Swart, M., Ph. D. Thesis, Materials Science Center, Rijksuniversiteit Groningen (RuG), Nijenborgh 4 (2002).

42. Werst, M. M.; Davoust, C. E.; Hoffman, B. M. *J. Am. Chem. Soc.* **1991**, 113, 1533.

Chapter 3. Paramagnetic NMR Shifts

The goal of this chapter is to present and validate a new theoretical approach for NMR chemical shifts in paramagnetic species within the framework of quantum mechanics. [1,2]. Through this chapter we mainly focused on theoretical works rather than computational applications. The detail applications will be shown in the following paper [2] and the near future works. This chapter is organized as follows: In section 1, a general introduction about paramagnetic NMR chemical shifts including their unique character is provided. In section 2, the previous theoretical approaches are reviewed. In section 3, we introduce a general expression for the paramagnetic NMR shielding based on the work of Moon and Patchkovskii [1]. In section 4, for a special case (spatially non-degenerate Kramers doublet), working equations are provided. In section 5, a new method is applied to the NMR chemical shift calculation of organic radicals (nitroxides) and metalloproteins (hemes and blue copper proteins) and the results are validated. In section 5, the conclusions of this chapter are presented.

3.1. Introduction

The existence of unpaired electrons in a molecule has a great effect on the NMR signals of magnetic nuclei through both line broadening and a large shift from the position of resonance [3-6]. This has been a huge obstacle to the study of paramagnetic systems by NMR. However, under the conditions that the electron spin-lattice relaxation rate, $1/T_1$, and/or the electron spin exchange rate, $1/T_e$, is much greater than the nuclear-electron hyperfine interaction, the NMR signals can be detected [3-6]. In this case, magnetic nuclei sense only the time-averaged spin density of unpaired electrons which is determined by the Boltzmann statistics at a certain temperature [6]. In the presence of a magnetic field, the electron spin states will be populated differently and the paramagnetic shifts arise from a small population difference of the spin states.

The NMR spectra of organic radicals can be detected in concentrated solutions since electron exchange may be rapid enough [7-11]. The electron spin relaxation or ligand exchange of many transition metal ion complexes in solution are also fast enough to allow observation of the NMR spectra of the ligand nuclei [4]. From the observed NMR shifts, the sign and magnitude of the electron spin density can be determined in a straightforward manner. This is the advantage of NMR spectroscopy over electron spin resonance (ESR) spectroscpy in which the sign of the electron spin density can not be measured directly from the spectra [11].

For the interpretation of the paramagnetic NMR signals theoretical studies are indispensible. Therefore, up to now, intensive theoretical studies for the NMR chemical shift in paramagnetic systems have been performed, based on the electronic structure from ligand field theory, magnetic susceptibility, and optical properties of paramagnetic compounds together with a background in NMR theory and statistics [12-22]. Due to the lack of generality of the equations and temperature dependence of the electron spin density, it is hard to use first-principles electronic structure methods for paramagnetic NMR shift calculations. However, completely non-empirical prediction of the paramagnetic NMR chemical shifts is finally becoming possible, since the recent rapid development of first-principles methods enables us to calculate most magnetic resonance parameters such as NMR chemical shifts, hyperfine coupling constants, and electronic g-tensors [25-28]. In fact, very recently, Mao et al. reported the detail investigation of the chemical shifts in some paramagnetic metalloprotein systems and showed a good correlation between DFT results and experiment [29]. Despite their successful computational results, still we can not see any theoretical work for the paramagnetic shift itself because they just focused on the Fermi contact contribution which mainly depends on the spin density of unpaired electrons. Later, Rinkevicius el al. reported the orbital contribution to the shifts in some organic radicals for the first time [23]. In the work, they emphasized the importance of the orbital contribution which is smaller than the Fermi contact contribution but not negligible. However, they also ignored the pseudocontact contribution and did not compare the orbital contribution with the shielding contribution of corresponding diamagnetic compound which is usually used for experimental works

(see section 3.4 for the detail description of the contributions). Hence, in this thesis, we provide a complete, general expression for the paramagnetic shift [1] and a working formalism for the special case (isolated Kramers doublet state), which is derived by using an effective spin Hamiltonian and Boltzmann statistics using some assumptions: the ground states are only thermally populated and there are no second-order Zeeman mixings between thermally populated ground and excited states.

For implementation and validation of this new approach, two types of systems are chosen due to the abundant experimental data for them and their relatively simple electronic structures. One is a series of nitroxides which are stable in solution [7-11] and the other is the metal active sites of metalloproteins such as copper complexes of blue copper proteins [30-33] and ferric cyanide-imidazole complexes of heme proteins [34]. The NMR chemical shifts of the nitroxides and metal complexes are calculated within density functional theory and the results are compared with the experimental data. They are also correlated to other physical properties.

3.2. Short Theoretical Reviews of Paramagnetic Systems

Unpaired electrons may be delocalized over the whole system through the molecular orbitals. In general, there are two types of delocalization: one is the direct delocalization through the molecular orbitals with unpaired electrons and the other is the delocalization by spin polarization [6]. The magnetic nuclei of the system will interact with the delocalized unpaired electrons. The interactions are often divided into two kinds of interactions: the Fermi contact and dipolar interactions [12-22]. The Fermi contact interaction arises from the spin density at a magnetic nucleus. This is the case where the spin density exists in the s-type atomic orbital of the magnetic nucleus. The dipolar interaction results from through-space interactions between the electron and nuclear spins. In this case, one should evaluate an integral over all space. In common, the isotropic NMR shifts of paramagnetic molecules in solution are explained by two contact

terms, the Fermi contact and pseudocontact terms, which arise from the Fermi contact and dipolar interactions, respectively.

Due to the rapid electron spin relaxation, the magnetic nuclei in a paramagnetic system may experience a time-averaged electron spin density [3-6]. In this case, the NMR spectra depend on the temperature of the system due to the Boltzmann distribution of the electron spin density. If the thermal energy kT is much greater than the transition energy, the time average of the spin projection is defined as [6]:

$$\langle S_Z \rangle = \frac{\sum_{M_S=-S}^{S} S \exp(-E_{Ms}/kT)}{\sum_{M_S=-S}^{S} \exp(-E_{Ms}/kT)} = -\frac{\bar{g}\beta B_0 S(S+1)}{3kT} \qquad (3.1)$$

Here, E_{Ms} is the energy of the electron spin state M_S and $\bar{g}$ denotes the rotationally averaged g-value which is different from the free-electron g-value (2.0023) due to spin-orbit couplings in the system. β is the Bohr magneton, k is Boltzmann's constant and T is the temperature of the system. The external magnetic field $\mathbf{B}_0$ is aligned with the z direction. In this approach, the abovementioned two assumptions are imposed.

The commonly used expressions for the isotropic paramagnetic NMR shifts were derived by McConnell et al. [12,15] using the above spin density fomula. The Fermi contact term [12] takes the form:

$$\delta_{iso}^{FC} = A_N^{iso} \frac{\bar{g}\beta S(S+1)}{g_N \beta_N 3kT} \qquad (3.2)$$

where A_N^{iso} is the Fermi coupling constant, g_N is the nuclear g-value, and β_N is the nuclear magneton. The pseudocontact term [15,16] is given by:

$$\delta_{iso}^{PC} = \frac{\beta^2 S(S+1)}{3kT} \frac{(3\cos^2 \Omega - 1)}{R^3} F(g) \tag{3.3}$$

Here, Ω is the angle between the principal symmetry axis and the vector made by the metal ion and the magnetic nucleus of interest, R is the distance between the metal ion and the nucleus, and $F(g)$ is an algebraic function of the g-tensors which depends on the relative magnitudes of electron relaxation times and rotational correlation times. In this case, it is assumed that the unpaired electrons reside only in the centered metal and R is large enough that the metal ion may be treated as a point dipole.

In the derivation of McConnell's equations, two main assumptions, mentioned above, were imposed, which restrict their application. In 1970, McGarvey et al. suggested more general equations which can handle both zero field splittings and thermal Zeeman mixing of the ground and excited states [13]. Their theory is as follows. The hyperfine interaction can be expressed by three operators: the Fermi contact (FC), the dipolar (DIP), and the nuclear-electron orbital (ORB) operators. The operators have the forms:

$$\mathbf{H}_{FC} = \frac{8\pi}{3} g_e \beta g_N \beta_N \sum_j \delta(\mathbf{r}_{jN}) \mathbf{s}_j \cdot \mathbf{I}_N \tag{3.4}$$

and

$$\mathbf{H}_{DIP} = g_e \beta g_N \beta_N \sum_j \mathbf{s}_j \cdot \frac{3\mathbf{r}_{jN}\mathbf{r}_{jN}^T - |\mathbf{r}_{jN}|^2 \mathbf{1}}{|\mathbf{r}_{jN}|^5} \cdot \mathbf{I}_N \tag{3.5}$$

and

$$\mathbf{H}_{ORB} = g_e \beta g_N \beta_N \sum_j \frac{\mathbf{l}_{jN}}{|\mathbf{r}_{jN}|^3} \cdot \mathbf{I}_N \tag{3.6}$$

where $\delta(\mathbf{r}_{jN})$ is the Dirac delta function, $\mathbf{r}_{jN}$ is the vector between the locus of the jth electron and the nucleus N, $\mathbf{s}_j$ is the electron spin angular momentum operator, $\mathbf{I}_N$ is the nuclear spin angular momentum operator, $\mathbf{l}_{jN}$ is the orbital angular momentum operator of the ith electron from the nucleus N. If the nuclear spin transition energy is much larger than the hyperfine interaction, the nuclear spin can be quantized along the external magnetic field (here, we assume that the magnetic field is aligned with the z direction, $\mathbf{I} = \mathrm{I}_Z \cdot \mathbf{z}$). The local magnetic field arising from the electron spin density at the nucleus is obtained from an average over thermally populated states,

$$\Delta B = \left\langle \mathbf{H}_{FC} + \mathbf{H}_{DIP} + \mathbf{H}_{ORB} \right\rangle \cdot \mathbf{z} \tag{3.7}$$

where $\mathbf{z}$ is the unit vector along the external magnetic field $\mathbf{B}$. In McGarvey's approach, the thermal equilibrium values of the operators $\mathbf{H}_{FC}$, $\mathbf{H}_{DIP}$, and $\mathbf{H}_{ORB}$ were obtained from a density matrix expression,

$$\left\langle \mathbf{H}_{FC} + \mathbf{H}_{DIP} + \mathbf{H}_{ORB} \right\rangle = tr\left(\boldsymbol{\rho}\left(\mathbf{H}_{FC} + \mathbf{H}_{DIP} + \mathbf{H}_{ORB}\right)\right) / tr(\boldsymbol{\rho}) \tag{3.8}$$

and

$$\boldsymbol{\rho} = \exp[-\mathbf{H} / kT] \tag{3.9}$$

where $\boldsymbol{\rho}$ are the density matrix operator, *tr* denotes the trace and $\mathbf{H}$ indicates the time-independent nonrelativistic Hamiltonian for the system. Since the electronic transition energy is much greater than the electron spin transition energy, the system can be treated by the perturbation method.

$$\mathbf{H} = \mathbf{H}_0 + \mathbf{H}_Z \tag{3.10}$$

and

$$\mathbf{H}_Z = -\mathbf{m}\cdot\mathbf{B}_0 = \beta(\mathbf{L} + g_e\mathbf{S})\cdot\mathbf{B}_0 \tag{3.11}$$

where $\mathbf{H}_0$ is the field-free Hamiltonian, $\mathbf{H}_Z$ is the electronic Zeeman Hamiltonian, **m** represents the electron magnetic moment, **L** is the total orbital angular momentum operator, and **S** is the total electron spin angular momentum operator. If the Hamiltonian $\mathbf{H}_0$ has the eigenstates $|\Gamma>$ for the Kramers multiplet and the corresponding eigenvalues E_Γ, the density matrix elements for the case $\Gamma = \Gamma'$ are given by,

$$\rho_{\Gamma_n,\Gamma_m} = \frac{e^{-E_\Gamma/kT}}{kT}\left[\delta_{nm} - \frac{<\Gamma_n|\mathbf{H}_Z|\Gamma_m>}{kT}\right] \tag{3.12}$$

and when $\Gamma \neq \Gamma'$

$$\rho_{\Gamma_n,\Gamma'_m} = \frac{e^{-E_\Gamma/kT} - e^{-E_{\Gamma'}/kT}}{E_\Gamma - E_{\Gamma'}} <\Gamma_n|\mathbf{H}_Z|\Gamma'_m> \tag{3.13}$$

Finally, McGarvey's formula for the paramagnetic NMR shifts in solution takes the form:

$$\delta^{para} = \frac{1}{3kT\sum_{\Gamma_n} e^{-E_\Gamma/kT}} \sum_{i\sim x,y,z}\left\{\sum_{\Gamma_n,\Gamma_m} e^{-E_\Gamma/kT} <\Gamma_n|\mathbf{m}_i|\Gamma_m><\Gamma_m|\mathbf{H}_{FC}+\mathbf{H}_{DIP}+\mathbf{H}_{ORB}|\Gamma_n> \right.$$
$$\left. -kT\sum_{\Gamma_n,\Gamma'_m(\Gamma\neq\Gamma')} \frac{e^{-E_\Gamma/kT} - e^{-E_{\Gamma'}/kT}}{E_\Gamma - E_{\Gamma'}} <\Gamma_n|\mathbf{m}_i|\Gamma'_m><\Gamma'_m|\mathbf{H}_{FC}+\mathbf{H}_{DIP}+\mathbf{H}_{ORB}|\Gamma_n>\right\} \tag{3.14}$$

where *i* (~*x*, *y*, *z*) represents the components of the principal axes in the system. Although the limit of McConnell's formulas can be overcome by this approach, still this requires many other theoretical and empirical factors (e.g. magnetic susceptibility tensor and zero field sppilting parameter) in order to have the final formulas of the Fermi contact and pseudocontact shifts [13,14]. If the transition energies between the different electronic states are much greater than the thermal energy *kT* and zero field splittings do not exist, McGarvey's equation may be readily reduced to McConnell's equations which are shown in Eqs (3.2) and (3.3).

3.3. Paramagnetic Shifts for the General Case

In the presence of the external magnetic field **B**, the nuclear magnetic moment **M**, and the electronic magnetic moment **m**, the total electronic energy of the *i*th electronic state, only including the terms linear and bilinear in **B** and **M**, is given by:

$$\begin{aligned} E_i(\mathbf{B},\mathbf{M},\mathbf{m}) &= <\Psi_i(\mathbf{B},\mathbf{M},\mathbf{m})\,|\,\mathbf{H}(\mathbf{B},\mathbf{M},\mathbf{m})\,|\,\Psi_i(\mathbf{B},\mathbf{M},\mathbf{m})> \\ &= E_i^{(0,0)} + \mathbf{E}_i^{(\mathbf{B},0)}\cdot\mathbf{B} + \mathbf{E}_i^{(0,\mathbf{M})}\cdot\mathbf{M} + \mathbf{B}^T\cdot\mathbf{E}_i^{(\mathbf{B},\mathbf{M})}\cdot\mathbf{M} \end{aligned} \tag{3.15}$$

where the Hamiltonian **H(B,M,m)** is shown in Eq. (1.63). The **B** and **M** field-free energy and the derivatives of the electronic energy with respect to **B** and **M** are defined as:

$$E_i^{(0,0)} = <\Psi_i(0,0,\mathbf{m})\,|\,\mathrm{H}^{(0)} + \sum_k \mathbf{m}_k^T\cdot\mathbf{H}_k^{(001)}\,|\,\Psi_i(0,0,\mathbf{m})> \tag{3.16}$$

$$\begin{aligned} \mathbf{E}_i^{(\mathbf{B},0)} &= \left(\frac{\partial E_i}{\partial \mathbf{B}}\right)_{\mathbf{B}=\mathbf{M}=0} \\ &= <\Psi_i(0,0,\mathbf{m})\,|\,\mathbf{H}^{(100)} + \sum_k (\mathbf{1}+\mathbf{H}_k^{(101)})\cdot\mathbf{m}_k\,|\,\Psi_i(0,0,\mathbf{m})> \end{aligned} \tag{3.17}$$

$$\begin{aligned} \mathbf{E}_i^{(0,\mathbf{M})} &= \left(\frac{\partial E_i}{\partial \mathbf{M}}\right)_{\mathbf{B}=\mathbf{M}=0} \\ &= <\Psi_i(0,0,\mathbf{m})\,|\,\mathbf{H}^{(010)} + \sum_k \mathbf{m}_k^T\cdot\mathbf{H}_k^{(011)}\,|\,\Psi_i(0,0,\mathbf{m})> \end{aligned} \tag{3.18}$$

$$\begin{aligned} \mathbf{E}_i^{(\mathbf{B},\mathbf{M})} &= \left(\frac{\partial^2 E_i}{\partial \mathbf{B}\partial \mathbf{M}}\right)_{\mathbf{B}=\mathbf{M}=0} \\ &= <\Psi_i(0,0,\mathbf{m})\,|\,\mathbf{H}^{(110)}\,|\,\Psi_i(0,0,\mathbf{m})> \\ &+ \left(\frac{\partial}{\partial \mathbf{B}} <\Psi_i(\mathbf{B},0,\mathbf{m})\,|\,\mathbf{H}^{(010)}\,|\,\Psi_i(\mathbf{B},0,\mathbf{m})>\right)_{\mathbf{B}=0} \end{aligned} \tag{3.19}$$

where the operators are defined in Eqs. (1.66-1.73). The energy levels, arising from the interactions with the fields **B**, **M**, and **m**, can be populated by the thermal energy kT in general. There is an important point related to the choice of the wavefunctions used for the evaluation of the derivatives (Eqs. 3.17-3.19). The energy derivative $\mathbf{E}_i^{(0,\mathbf{M})}$ can be taken for the eigenstates of the Hamiltonian adapted to the perturbation **B** due to its large magnitude compared to the perturbation **M**. For example, the total energy E must include the electronic Zeeman and spin-orbit operators (Eq. 3.17) variationally, but the hyperfine terms (Eq. 3.18) only through the first order [12]. The derivatives $\mathbf{E}_i^{(0,\mathbf{M})}$ are then implicitly dependent on the direction of the magnetic field **B**.

If the electronic energy levels in the fields are in a thermal equilibrium, the average energy in a temperature can be defined as:

$$\langle E(\mathbf{B},\mathbf{M},\mathbf{m})\rangle = \frac{\sum_i E_i(\mathbf{B},\mathbf{M},\mathbf{m}) e^{-W_i(\mathbf{B},\mathbf{M},\mathbf{m})/kT}}{\sum_i e^{-W_i(\mathbf{B},\mathbf{M},\mathbf{m})/kT}} \tag{3.20}$$

Because of the different time scales of the nuclear and electron spin relaxation, the Boltzmann energy factor W_i in Eq. (3.20) are not necessarily identical to E_i. In general, the electron spin relaxation is much faster than the nuclear spin relaxation and the nuclear spins feel an average local magnetic field arising from the electron spins in a thermal equilibrium state. In this case, equilibrium state populations can be determined by the electron spin relaxation process. For the moment, it is sufficient to assume that $W_i(\mathbf{B},\mathbf{M},\mathbf{m})$ can be expanded similarly to Eqs. (3.16-3.19).

Assuming that the equilibrium implied by Eq. (3.20) is fast on the NMR time scale, the average components of the absolute NMR shielding tensor $\boldsymbol{\sigma}$ are given by:

$$\boldsymbol{\sigma} = \left(\frac{\partial^2 \langle E(\mathbf{B},\mathbf{M})\rangle}{\partial \mathbf{B} \partial \mathbf{M}} \right)_{\mathbf{B}=\mathbf{M}=0} \tag{3.21}$$

$$= \left\langle \mathbf{E}^{(\mathrm{B,M})} \right\rangle_0 \tag{3.22a}$$

$$-\frac{1}{kT}\left\langle \mathbf{E}^{(0,\mathrm{M})}\mathbf{W}^{(\mathrm{B},0)} \right\rangle_0 \tag{3.22b}$$

$$-\frac{1}{kT}\left\langle \mathbf{E}^{(\mathrm{B},0)}\mathbf{W}^{(0,\mathrm{M})} \right\rangle_0 \tag{3.22c}$$

$$-\frac{1}{kT}\left[\left\langle \mathbf{E}^{(0,0)}\mathbf{W}^{(\mathrm{B,M})} \right\rangle_0 - \left\langle \mathbf{E}^{(0,0)} \right\rangle_0 \left\langle \mathbf{W}^{(\mathrm{B,M})} \right\rangle_0\right] \tag{3.22d}$$

$$+\frac{1}{(kT)^2}\left[\left\langle \mathbf{E}^{(0,0)}\mathbf{W}^{(\mathrm{B},0)}\mathbf{W}^{(0,\mathrm{M})} \right\rangle_0 - \left\langle \mathbf{E}^{(0,0)} \right\rangle_0 \left\langle \mathbf{W}^{(\mathrm{B},0)}\mathbf{W}^{(0,\mathrm{M})} \right\rangle_0\right] \tag{3.22e}$$

In Eq. (3.22), the averages are taken in the absence of magnetic fields:

$$\left\langle X \right\rangle_0 = \frac{\sum_i X_i e^{-W_i^{(0,0)}/kT}}{\sum_i e^{-W_i^{(0,0)}/kT}} \tag{3.23}$$

Note that a number of other terms containing $\left\langle \mathbf{E}^{(\mathrm{B},0)} \right\rangle_0$, $\left\langle \mathbf{W}^{(\mathrm{B},0)} \right\rangle_0$, $\left\langle \mathbf{E}^{(0,0)}\mathbf{W}^{(\mathrm{B},0)} \right\rangle_0$ of Eq. (3.21) vanish since the field-free Hamiltonian and spin-orbit operator are invariant through time reversal and the operators with respect to $\mathbf{E}^{(\mathrm{B},0)}$ are time-odd operators (Eq. 3.17) which have opposite expectation values in two Kramers conjugate states.

The first term (3.22a) is simply the Boltzmann average of the familiar, orbital NMR shielding tensor. The second term (3.22b) describes the interaction of the nuclear magnetic moment with the average spin-density, induced by the orbital- and electron spin-Zeeman interactions. The remaining three terms (3.22c,d,e) arise from the changes in the electronic state populations, induced by flipping of the nuclear spin. Under the conditions where the nuclear relaxation time is sufficiently long to allow observation of the NMR transition, thermal populations of the electronic states are determined solely by the orbital and electron spin-Zeeman interactions [12,13,15], so that:

$$\mathbf{W}^{(0,M)} = \mathbf{W}^{(B,M)} = 0 \tag{3.24}$$

Finally, if the electron spin relaxation is faster than any spatial reorientation process (the so-called "solid state case" [12,15]), derivatives of the Boltzmann energy factors and the electronic energy, with respect to the external field strength, coincide:

$$\mathbf{W}^{(B,0)} = \mathbf{E}^{(B,0)} \tag{3.25}$$

Substituting Eqs. (3.24 and 3.25) into Eq. (3.22), we obtain the working equation for the paramagnetic shielding tensor:

$$\boldsymbol{\sigma} = \left\langle \mathbf{E}^{(B,M)} \right\rangle_0 - \frac{1}{kT} \left\langle \mathbf{E}^{(0,M)} \mathbf{E}^{(B,0)} \right\rangle_0 \tag{3.26}$$

In Eq. (3.26), the second term is equivalent to the general-case expression of Kurland and McGarvey [13]. The first term is the generalization of the orbital contribution of Rinkevicius et al. [23].

Practical calculations of the paramagnetic shielding tensor can proceed as follows: First, energies and wavefunctions for all thermally accessible electronic states must be determined, in the absence of magnetic fields. For each of the states [35], the orbital NMR shielding tensor defines $\mathbf{E}_i^{(B,M)}$. The EPR g-tensor determines $\mathbf{E}_i^{(B,0)}$, while the hyperfine A-tensor leads to $\mathbf{E}_i^{(0,M)}$. The Boltzmann averages in Eq. (3.26) then fully determine the paramagnetic NMR shielding tensor. Obviously, each of the ingredients in Eq. (3.26) can be treated independently, using the most suitable theoretical technique. A similar approach was developed by Lohr, Miller, and Sharp [36], within the ligand field theory.

3.4. Paramagnetic Shifts for an Isolated Kramers Doublet State

Once magnetic parameters are obtained by quantum mechanical calculations, the energy levels of the nuclear spin states in the presence of the external magnetic field and the unpaired electrons can be described by an effective spin Hamiltonian [24]. In fact, the observed energies and intensities of the spin transitions can be reproduced by the effective spin Hamiltonian to a good approximation. At a certain temperature, the electron spin states might not be equally populated and the thermal average of the spin density can be obtained from the Boltzmann distribution if the electron spin relaxation time is much shorter than the correlation time. For a doubly degenerate electronic ground state (S = 1/2), the expression of an effective spin Hamiltonian with an effective electron spin $\widetilde{\mathbf{S}}$ and a nuclear spin $\mathbf{I}$ is given by:

$$\mathbf{H}_{spin} = \beta\widetilde{\mathbf{S}}^{T} \cdot \mathbf{g} \cdot \mathbf{B} - g_N \beta_N \mathbf{I}_N^{T} \cdot (\mathbf{1} - \boldsymbol{\sigma}^{orb}) \cdot \mathbf{B} + \widetilde{\mathbf{S}}^{T} \cdot \mathbf{A} \cdot \mathbf{I}_N \qquad (3.27)$$

Here, the electronic g-tensor $\mathbf{g}$ is defined as the sum of the free electron g-value g_e and the g-shift $\Delta\mathbf{g}$ ($\mathbf{g} = g_e\mathbf{1} + \Delta\mathbf{g}$). The hyperfine tensor $\mathbf{A}$ is composed of the Fermi (isotropic) contact coupling constant A^{iso} and the anisotropic dipolar tensor $\mathbf{A}^{dip}$ ($\mathbf{A} = A^{iso}\mathbf{1} + \mathbf{A}^{dip}$). $\boldsymbol{\sigma}^{orb}$ represents the orbital nuclear shielding tensor. The total effective spin is chosen to reproduce the experimental $(2\widetilde{S}+1)$-level multiplet structure. If the external magnetic field is aligned to the z-direction, the effective spin Hamiltonian is redefined as,

$$\mathbf{H}_{spin} = \beta B_Z \widetilde{\mathbf{S}}^{T} \cdot (g_e\mathbf{1} + \Delta\mathbf{g}) \cdot \mathbf{z} - g_N \beta_N B_Z \mathbf{I}_N^{T} \cdot (\mathbf{1} - \boldsymbol{\sigma}^{orb}) \cdot \mathbf{z} + \widetilde{\mathbf{S}}^{T} \cdot (A^{iso}\mathbf{1} + \mathbf{A}^{dip}) \cdot \mathbf{I}_N \qquad (3.28)$$

where B_Z is the z-direction component of the magnetic field and $\mathbf{z}$ is a unit vector.

For two contact coupled S=1/2, I=1/2 spins, the corresponding energy matrix using the spin Hamiltonian can be defined as:

	$\|1/2, 1/2\rangle$	$\|1/2,-1/2\rangle$	$\|-1/2, 1/2\rangle$	$\|-1/2,-1/2\rangle$
$<1/2, 1/2\|$	$\mathbf{1/2\beta B_Z (g_e+\Delta g_{zz})}$ $-1/2 g_N\beta_N B_Z (1-\sigma_{zz})$ $+1/4\, A_{zz}^{dip} +1/4\, A^{iso}$	$1/2 g_N\beta_N B_Z (\sigma_{xz}-i\sigma_{yz})$ $+1/4\,(A_{xz}^{dip} - i\, A_{yz}^{dip})$	$\mathbf{1/2\beta B_Z (\Delta g_{xz}-i\Delta g_{yz})}$ $+1/4\,(A_{xz}^{dip} - i\, A_{yz}^{dip})$	$1/4(A_{xx}^{dip} - A_{yy}^{dip}$ $- 2i\, A_{xy}^{dip})$
$<1/2,-1/2\|$	$1/2 g_N\beta_N B_Z (\sigma_{xz}+ i\sigma_{yz})$ $+1/4\,(A_{xz}^{dip} + i\, A_{yz}^{dip})$	$\mathbf{1/2\beta B_Z (g_e+\Delta g_{zz})}$ $+1/2 g_N\beta_N B_Z (1-\sigma_{zz})$ $-1/4\, A_{zz}^{dip} -1/4\, A^{iso}$	$1/4\,(A_{xx}^{dip} + A_{yy}^{dip})$ $+1/2\, A^{iso}$	$\mathbf{1/2\beta B_Z (\Delta g_{xz}-i\Delta g_{yz})}$ $-1/4\,(A_{xz}^{dip} - i\, A_{yz}^{dip})$
$<-1/2,1/2\|$	$\mathbf{1/2\beta B_Z (\Delta g_{xz}+ i\Delta g_{yz})}$ $+1/4\,(A_{xz}^{dip} + i\, A_{yz}^{dip})$	$1/4\,(A_{xx}^{dip} + A_{yy}^{dip})$ $+1/2\, A^{iso}$	$\mathbf{-1/2\beta B_Z (g_e+\Delta g_{zz})}$ $-1/2 g_N\beta_N B_Z (1-\sigma_{zz})$ $-1/4\, A_{zz}^{dip} -1/4\, A^{iso}$	$1/2 g_N\beta_N B_Z (\sigma_{xz}-i\sigma_{yz})$ $-1/4\,(A_{xz}^{dip} - i\, A_{yz}^{dip})$
$<-1/2,-1/2\|$	$1/4\,(A_{xx}^{dip} - A_{yy}^{dip}$ $+ 2i\, A_{xy}^{dip})$	$\mathbf{1/2\beta B_Z (\Delta g_{xz}+ i\Delta g_{yz})}$ $- 1/4\,(A_{xz}^{dip} + i\, A_{yz}^{dip})$	$1/2 g_N\beta_N B_Z (\sigma_{xz}+ i\sigma_{yz})$ $-1/4\,(A_{xz}^{dip} + i\, A_{yz}^{dip})$	$\mathbf{-1/2\beta B_Z (g_e+\Delta g_{zz})}$ $+1/2 g_N\beta_N B_Z (1-\sigma_{zz})$ $+1/4\, A_{zz}^{dip} +1/4\, A^{iso}$

In order to obtain the eigenstates, this energy matrix should be diagonalized. However, since the g-tensor and the hyperfine tensor have different principal axes, the above energy matrix can not be diagonalized at the same time. This problem can be solved approximately by the perturbation method. In the high field limit ($g_e\beta B >> A$), the Hamiltonian can be divided into a zero-order part and a perturbation ($\mathbf{H} = \mathbf{H}_0 + \mathbf{H}'$):

$$\mathbf{H}_0 = \beta B_Z \tilde{\mathbf{S}}^T \cdot (g_e \mathbf{1} + \Delta\mathbf{g}) \cdot \mathbf{z} \tag{3.29}$$

$$\mathbf{H}' = -g_N \beta_N B_Z \mathbf{I}_N^T \cdot (\mathbf{1} - \boldsymbol{\sigma}^{orb}) \cdot \mathbf{z} + \tilde{\mathbf{S}}^T \cdot (A^{iso}\mathbf{1} + \mathbf{A}^{dip}) \cdot \mathbf{I}_N \tag{3.30}$$

Here, we can expect the contribution from $\mathbf{H}'$ to be small compared with those from $\mathbf{H}_0$. The energy matrix elements are readily separable into contributions from $\mathbf{H}_0$ and $\mathbf{H}'$.

The eigenfunctions in the zero-order approximation can be obtained by the diagonalization of the matrix elements purely related to the electron spin states for a nuclear spin state K,

	| 1/2, K>	| -1/2, K>
< 1/2, K|	$\mathbf{1/2\beta B_Z (g_e+\Delta g_{zz})}$	$\mathbf{1/2\beta B_Z (\Delta g_{xz} -i\Delta g_{yz})}$
< -1/2, K|	$\mathbf{1/2\beta B_Z (\Delta g_{xz} +i\Delta g_{yz})}$	$\mathbf{-1/2\beta B_Z (g_e+\Delta g_{zz})}$

↓ diagonalization

	| 1, K>	| 2, K>
< 1, K|	$\mathbf{1/2\beta B_Z \Delta G_{zz}}$	0
< 2, K|	0	$\mathbf{-1/2\beta B_Z \Delta G_{zz}}$

where the diagonalized g-tensor is defined as,

$$\Delta G_{zz} = [(\Delta g_{xz})^2+(\Delta g_{yz})^2+ (g_e+\Delta g_{zz})^2]^{1/2} \tag{3.31}$$

The corresponding zero-order eigenfunctions by the diagonalization are given by,

$$| 1, K> = cos\theta | 1/2, K> + sin\theta e^{-ix} |-1/2, K>,$$

$$| 2, K> = cos\theta |-1/2, K> - sin\theta e^{-ix} | 1/2, K> \tag{3.32}$$

Here, the angles θ and x are defined by the relations,

$$tan2\theta = [(\Delta g_{xz})^2+(\Delta g_{yz})^2]^{1/2} / (g_e+\Delta g_{zz}) , \qquad tanx = \Delta g_{yz} / \Delta g_{xz} \tag{3.33}$$

The energy matrix elements of $\mathbf{H}'$ can be redefined by the basis sets {|1,K>, |2,K>} and, finally, the effective hyperfine tensors T in the basis sets {|1,K>, |2,K>} are given by,

$$T_{zz} = cos2\theta\ A_{zz}^{dip} + sin2\theta(cosx\ A_{xz}^{dip} - sinx\ A_{yz}^{dip})$$

$$T_{xz} = cos2\theta\ A_{xz}^{dip} + sin2\theta(cosx\ A_{xy}^{dip} - sinx\ A_{xy}^{dip}) \qquad (3.34)$$

$$T_{yz} = cos2\theta\ A_{yz}^{dip} + sin2\theta(cosx\ A_{xy}^{dip} - sinx\ A_{yy}^{dip})$$

The reorganized energy matrix by the diagonalization are given, up to first order where the off-diagonal terms between the different electron spin states are not considered by,

	|1, 1/2>	|1,-1/2>	|2, 1/2>	|2,-1/2>
<1, 1/2|	**$1/2\beta B_Z \Delta G_{ZZ}$** $-1/2g_N\beta_N B_Z(1-\sigma_{zz})$ $+1/4\ T_{zz}+1/4\ A^{iso}$	$1/2g_N\beta_N B_Z(\sigma_{xz}-i\sigma_{yz})$ $+1/4\ (T_{xz}-i\ T_{yz})$		
<1,-1/2|	$1/2g_N\beta_N B_Z(\sigma_{xz}+i\sigma_{yz})$ $+1/4\ (T_{xz}+i\ T_{yz})$	**$1/2\beta B_Z \Delta G_{ZZ}$** $+1/2g_N\beta_N B_Z(1-\sigma_{zz})$ $-1/4\ T_{zz}-1/4\ A^{iso}$		
<2,1/2|			**$-1/2\beta B_Z \Delta G_{ZZ}$** $-1/2g_N\beta_N B_Z(1-\sigma_{zz})$ $-1/4\ T_{zz}-1/4\ A^{iso}$	$1/2g_N\beta_N B_Z(\sigma_{xz}-i\sigma_{yz})$ $-1/4\ (T_{xz}-i\ T_{yz})$
<2,-1/2|			$1/2g_N\beta_N B_Z(\sigma_{xz}+i\sigma_{yz})$ $-1/4\ (T_{xz}+i\ T_{yz})$	**$-1/2\beta B_Z \Delta G_{ZZ}$** $+1/2g_N\beta_N B_Z(1-\sigma_{zz})$ $+1/4\ T_{zz}+1/4\ A^{iso}$

In the high field limit ($g\beta\Delta G >> T$), all off-diagonal terms can be reasonably neglected due to their small magnitude compared to the diagonal terms. In this zero-order approximation, the energy levels are

$$\begin{aligned}
E_{1,zz} &= +1/2B_Z\Delta G_{zz} - 1/2g_N\beta_N B_Z(1-\sigma_{zz}^{orb}) + 1/4T_{zz} + 1/4A^{iso} \\
E_{2,zz} &= +1/2B_Z\Delta G_{zz} + 1/2g_N\beta_N B_Z(1-\sigma_{zz}^{orb}) - 1/4T_{zz} - 1/4A^{iso} \\
E_{3,zz} &= -1/2B_Z\Delta G_{zz} - 1/2g_N\beta_N B_Z(1-\sigma_{zz}^{orb}) - 1/4T_{zz} - 1/4A^{iso} \\
E_{4,zz} &= -1/2B_Z\Delta G_{zz} + 1/2g_N\beta_N B_Z(1-\sigma_{zz}^{orb}) + 1/4T_{zz} + 1/4A^{iso}
\end{aligned} \tag{3.35}$$

The nuclear spin transition energies are given by,

$$\begin{aligned}
\Delta E_{zz}^{+} &= E_{2,zz} - E_{1,zz} = g_N\beta_N B_Z(1-\sigma_{zz}^{orb}) - 1/2T_{zz} - 1/2A^{iso} \\
\Delta E_{zz}^{-} &= E_{4,zz} - E_{3,zz} = g_N\beta_N B_Z(1-\sigma_{zz}^{orb}) + 1/2T_{zz} + 1/2A^{iso}
\end{aligned} \tag{3.36}$$

The first nuclear spin transition arises in the presence of an unpaired electron with positive spin (S = +1/2), the second nuclear spin transition happens with a negative electron spin (S = −1/2). Magnetic nuclei in a paramagnetic system might experience an average additional field from the electron spin magnetic moment due to its fast relaxation. If the electron spin relaxation is faster than any correlation, the thermal average of the nuclear spin transition energies can be defined by the Boltzmann distribution of the electron spin states as,

$$\Delta E_{zz}^{av} = \frac{e^{-E_S/kT}}{e^{-E_S/kT}+e^{E_S/kT}}\Delta E_{zz}^{+} + \frac{e^{-E_S/kT}}{e^{-E_S/kT}+e^{E_S/kT}}\Delta E_{zz}^{-} \tag{3.37}$$

where E_S denotes the energy of the electron spin state ($1/2\beta G_{zz}$) and, in the limit ($E_S << kT$):

$$\begin{aligned}\Delta E_{zz}^{av} &\approx \frac{1}{2}(1\text{-}E_S/kT)\ \Delta E_{zz}^{+} + \frac{1}{2}(1+E_S/kT)\ \Delta E_{zz}^{-} \\ &= g_N\beta_N B_Z(1-\sigma_{zz}^{orb}) + \frac{1}{4kT}\beta B G_{zz}(T_{zz}+A^{iso}) \\ &= g_N\beta_N B_Z(1-\Sigma_{zz}^{para})\end{aligned} \tag{3.38}$$

where Σ represents the paramagnetic NMR shielding tensor.

The same process can be applied for the case that the external magnetic field is aligned to the x- or y- direction. In general, the paramagnetic NMR shielding tensors for the principal axes ($i \sim x, y, z$) take the form:

$$\Sigma_{ii} = \sigma_{ii}^{orb} - \frac{1}{4kTg_N\beta_N}\beta G_{ii}(T_{ii}+A^{iso}) \tag{3.39}$$

In solution, rapid molecular rotation produces an average value of the shift anisotropy and results in the isotropic shift,

$$\begin{aligned}\Sigma_{iso} &= \frac{1}{3}Tr(\boldsymbol{\Sigma}) \\ &= \sigma_{iso}^{orb} - \frac{1}{4kTg_N\beta_N}\beta G_{iso}A^{iso} - \frac{1}{12kTg_N\beta_N}\beta[G_{xx}T_{xx}+G_{yy}T_{yy}+G_{zz}T_{zz}]\end{aligned} \tag{3.40}$$

where $\sigma_{iso}^{orb} = \frac{1}{3}Tr(\boldsymbol{\sigma}^{orb})$ and $G_{iso} = \frac{1}{3}Tr(\mathbf{G})$.

In the above equation, the second term denotes the Fermi contact shift and the third term presents the pseudocontact shift. In this approach, unlike McConnell's formula (see, Eq.

3.3), the pseudocontact term is independent of geometrical factors because the hyperfine tensors can be calculated quantum mechanically. Therefore, a system with significant delocalization of unpaired electrons can be treated without any further modifications of the equations. In addition, the spin-orbit couplings between the populated ground states and unpopulated excited states can be taken into account through the electronic g-tensors which can be also calculated quantum mechanically. It should be noted that the shielding constants σ_{iso}^{orb} of paramagnetic molecules are different from that of diamagnetic molecules because of the different orbital contribution to the shielding [23].

Finally, for the general case of more than one electron spin, the calculated isotropic NMR chemical shift of a paramagnetic molecule relative to a reference molecule is,

$$\delta_{iso} = \sigma_{iso}^{ref} - \Sigma_{iso} = \delta_{iso}^{orb} + \delta_{iso}^{FC} + \delta_{iso}^{PC} \tag{3.41}$$

where the shift due to the orbital shielding in a paramagnetic molecule, which is analogous to the chemical shift of a diamagnetic molecule, is given by,

$$\delta_{iso}^{orb} = \sigma_{iso}^{ref} - \sigma_{iso}^{orb} \tag{3.42}$$

and the Fermi contact shift is defined as,

$$\delta_{iso}^{FC} = A^{iso} \frac{G_{iso}\beta S(S+1)}{g_N \beta_N 3kT} \tag{3.43}$$

and the pseudocontact shift is expressed by the form,

$$\delta_{iso}^{PC} = \frac{\beta S(S+1)}{g_N \beta_N 9kT} [G_{xx}T_{xx} + G_{yy}T_{yy} + G_{zz}T_{zz}] \tag{3.44}$$

In most experimental works, the hyperfine contact shift ($\delta_{iso}^{con} = \delta_{iso}^{FC} + \delta_{iso}^{PC}$) is obtained from the shift difference between a paramagnetic molecule and a similar diamagnetic molecule:

$$\begin{aligned} \delta_{iso}^{\text{con}} &= \delta_{iso} - \delta_{iso}^{dia} \\ &= (\sigma_{iso}^{ref} - \sigma_{iso}^{orb}) + (\delta^{FC} + \delta^{PC}) - (\sigma_{iso}^{ref} - \sigma_{iso}^{dia}) \\ &\approx (\delta^{FC} + \delta^{PC}) \end{aligned} \tag{3.45}$$

and

$$\delta_{iso} \approx \delta_{iso}^{dia} + \delta_{iso}^{FC} + \delta_{iso}^{PC} \tag{3.46}$$

This approach neglects the errors from the orbital shielding and structual differences between the paramagnetic and diamagnetic molecules ($\delta_{iso}^{orb} \approx \delta_{iso}^{dia}$). However, the Fermi contact shift δ^{FC} often dominates the whole shift and the errors can be neglected reasonably. In fact, the contact shifts by this approximate approach are in good agreement with those determined by the temperature dependence of the NMR spectra.

In this work, we will compare two approaches (in Eqs. 3.41 and 3.46) and provide numerical differences between them for some test systems. The individual contributions of the paramagnetic shift will be calculated and investigated using the new equations.

3.5. Implementation and Computational Details

The procedure to obtain the chemical shifts in paramagnetic systems are composed of two major steps. The first step is to calculate the orbital shift δ_{iso}^{orb}, which requires a modification of the existing methods which are only available for shielding calculations of closed-shell systems. For this purpose, the deMon-NMR code [25,39] was modified based on the deMon-EPR code [28] in this work. The second step is to calculate the contact shifts which consist the Fermi (Eq. 3.43) and pseudo (Eq. 3.44) contact shifts. For this purpose, we calculated the hyperfine tensors whose explicit expressions are seen in Eqs (1.122, 1.123) and the electronic g-tensors where we considered only the one-electron integrals of the paramagnetic second-order spin-orbit/orbital Zeeman cross term and of the diamagnetic spin-Zeeman gauge correction.

For the comparison of the orbital shifts in paramagnetic systems with the chemical shifts in corresponding diamagnetic systems, we calculated the chemical shifts δ_{iso}^{dia} of the diamagnetic compounds which were designed by modifying the charge and spin multiplicity of paramagnetic compounds without any structural change. The NMR calculations were performed using the sum-over-states density functional perturbation theory (SOS-DFPT) shown in Eqs (1.107-1.111).

Finally, we calculated the paramagnetic shifts using the equations with orbital shifts (Eq. 3.41) and without orbital shifts (Eq. 3.46). The code for the paramagnetic shift was combined with the deMon program [25,28,39] for an automatic procedure.

3.5.1. Nitroxides

For proton NMR shift calculations, a series of aromatic *t*-butyl nitroxide radicals were chosen (Fig. 3.1). For ^{13}C NMR shift calculations, a series of aliphatic nitroxide radicals were selected (Fig. 3.2). To investigate the sensitivity of the paramagnetic shifts to structural changes, we calculated the ^{1}H chemical shifts in the aromatic compound (1) on the orientation of the t-BuN(O)- subsituent to the aromatic ring and the ^{13}C chemical shift in the aliphatic compound **I** (in Fig 3.2) on the two conformers: chair and twisted forms.

All structures were optimized at the B3LYP [37]/6-311G** level using GAUSSIAN 98 [38] and from these calculations the hyperfine coupling constants at the same level of theory were also obtained. The optimized structures were used for magnetic property calculations in the deMon program [25,39]. The PW91 exchange-correlation functional [40] was used for NMR chemical shielding tensor calculation for the diamagnetic case (closed shell) since it has given a slightly better results than other pure GGA functionals in a broad range of diamagnetic organic molecules [25]. The orbital shielding tensor, the hyperfine tensor and the electronic g-tensor calculations were carried out using the deMon program with the P86 [41], BP [41(b),42] and PW91 functionals. For the NMR shielding and orbital shielding tensor calculations which are very sensitive to the gauge origin, the IGLO method [43] was used, where the occupied MO's were localized by the methods of Boys [44(a)] and Pipek-Mezey [44(b)], respectively. On the contrary, the g-tensor is usually not sensitive to the gauge origin and therefore the common origin method was used [28]. The Loc 1. approximation was used for the NMR shielding calculations and the uncoupled SOS method was used for the orbital shielding calculations [25]. All deMon calculations were performed using a random numerical integration grid with FINE angular quadrature and 64 radial points per atom. For the fitting of charge density and exchange correlation potentials using Gaussian functions, the auxiliary basis set (5,1:5,1) for H and (5,2:5,2) for the others were used. IGLO-III was chosen as the orbital basis sets [43].

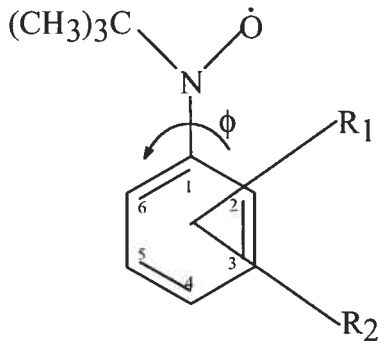

1. R_1=2-CH_3
2. R_1=2-CH_3; R_2=3-CH_3
3. R_1=2-CH_3; R_2=4-CH_3
4. R_1=2-CH_3; R_2=5-CH_3
5. R_1=2-CH_3; R_2=6-CH_3

Figure 3.1. Molecular structures and numbering schemes for a series of aromatic *t*-butyl nitroxides. The angle ϕ denotes the ONC_1C_2 dihedral angle.

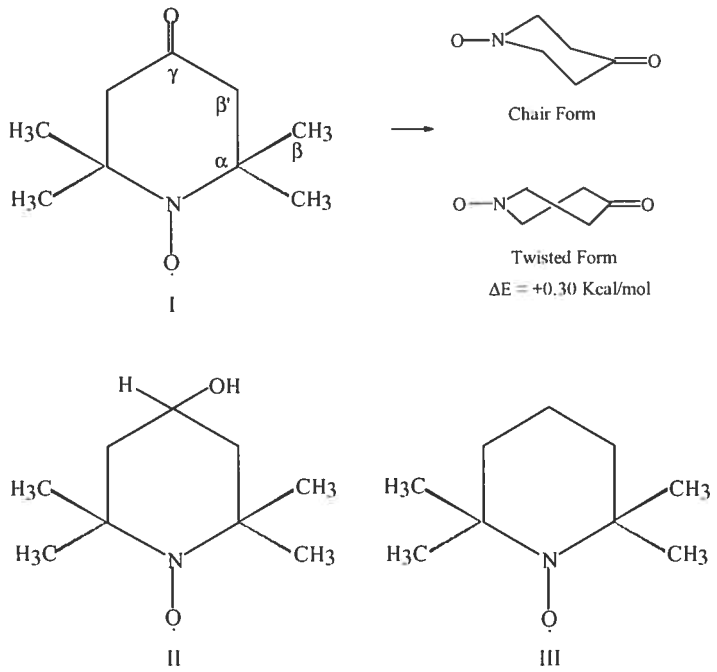

Figure 3.2. Molecular structures of a series of aliphatic nitroxide radicals.

3.5.2. Blue Copper Proteins

Blue copper proteins have been intensively studied due to their unique spectroscopic characteristics [47]. Their physical and spectral features can be summarized as follows: (1) The blue copper is involved in the long-range electron transfer process and therefore magnetic spectroscopy studies have been widely performed, since one of the redox states is paramagnetic. (2) the blue copper has a d_{x2-y2} ground state which is indicated by the EPR spectrum result $g_{\|} > g_{\perp} > 2.0023$. (3) the blue copper exhibits an intense band ($\varepsilon \approx$ 5000 $M^{-1}cm^{-1}$) around 600 nm which is indicated by UV spectroscopy. The results suggested the blue copper site is tetrahedrally distorted, producing a ligand-to-metal charge transfer (from the thiolate sulfur of the copper-bound cysteine to the copper) which was confirmed by X-ray results [47]. The paramagnetic blue copper part has an unpaired electron and its electronic stucture is less complicated due to removal of the orbital degeneracy by structural distortion. In this work, four blue coppers were chosen for study: azurin, stellacyanin, plastocyanin, and amicyanin. Their model stuctures are shown in Fig. 3.3.

All calculations about NMR shielding tensors, hyperfine tensors, and g-tensors were implemented using the deMon program [25,28,39]. Spin-unresticted Kohn-Sham calculations were performed with the BP functionals [41(b),42] since it has previously shown to enable the accurate prediction of the hyperfine tensors [48] and g-tensors [28] of copper compounds. A double zeta plus polarization (DZVP2) basis set [50(a)], augmented by the most diffuse functions (a 1s1p set) from ECP valence basis of Dolg et al. [50(b)], (16s10p5d)/[9s6p4d] was used for copper and the IGLO-III basis set [43] for the main group atoms in all cases. Molecular structures of the models of azurin, stellacyanin, plastocyanin, and amicyanin were taken from X-ray diffraction results (4AZU, 1JER, 1AG6, and 1ID2 files from the Protein Data Bank). The remaining hydrogen atoms were generated using the AMBER Xleap program [49], without reoptimizing the geometry. For azurin, four aminoacids (His46, His117, Cys112, and Met121) were included in calculations. Weakly bound Gly45 was not included. For stellacyanin, four aminoacids (His46, His94, Cys89, and Gln99) were involved in

calculations. For placystocyanin, four aminoacids (His37, His87, Cys84, and Met92) were considered in the calculations. In all cases, the aminoacids of the models were truncated at the α-carbon and the only side-chains were treated. Two approaches were used for terminating the polypeptide chain. Hydrogen atoms and carbon quantum capping potentials (QCPs) were added to the broken C-C covalent bond of the chain to satisfy the valency (here, the C-H bond length is set to 1.09 Å).

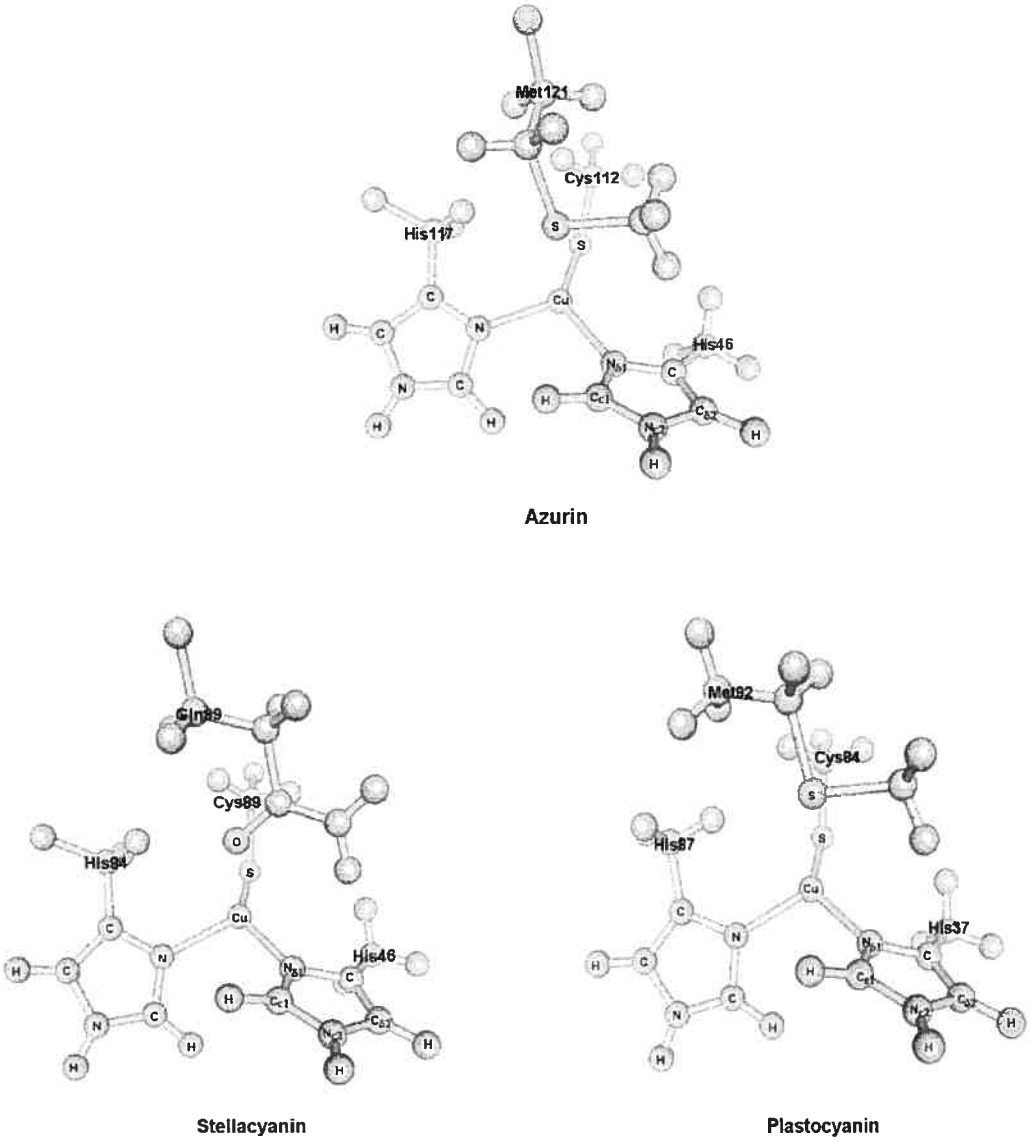

Figure 3.3 X-ray structures of the oxidized blue copper protein models.

3.5.3. Ferric Cyanide-Imidazole Complexes of Heme Proteins

Four different cyanide-imidazole models of low-spin iron(III) porphyrins were chosen in order to validate the importance of the contact shifts to the total paramagnetic NMR shift because this complexes show fairly large contact contributions and in order to show some useful applications for the determination of the nature of the proximal ligand in the ferric systems through ^{13}C NMR shift calculations of the iron-bound cyanide. These complexes are quite helpful for the study of the paramagnetic NMR since the iron-bound cyanide carbon has a strong interaction with the unpaired electron and its chemical shift is fairly sensitive to the environment. The structures of the models are seen in Fig 3.4 where the complex **I** is the model of cyanide-imidazol complexes of iron (III) protoporphyrinIX dimethyl ester (PPDME) and the complex **II** is the model of sperm whale myoglobin (Mb) and the complex **III** is the model of human hemoglobin (Hb) or horse heart cytochrome (Cyt-c) and the complex **IV** is the model of horseradish peroxidase (HRP).

All calculations in this section are based on DFT and were carried out with the Amsterdam Density Functional (ADF) program [46]. This program was chosen due to some advantages for the calculations of transitoin metal systems. For example, it provides good and fast SCF energy convergence for the systems and various levels of relativistic effects. The revPBE exchange-correlation functional [51] and the double-ξ valence Slater-type orbital (STO) basis set plus two polarization functions (DZP) [52] were used for the optimization. The BP functional and the triple-ξ valence Slater-type orbital (STO) basis set plus two polarization functions (TZ2P) [52] were used for the magnetic property calculations. In detail, the hyperfine tensors (all-electron) and orbital shifts (frozen-core) were calculated using the scalar Pauli Hamiltonian [26]. The g-tensor calculations were performed using the ZORA spin restricted method [53] which often provides accurate g-tensors (especially g-tensor anisotropy) due to its good performance for the spin-orbit couplings.

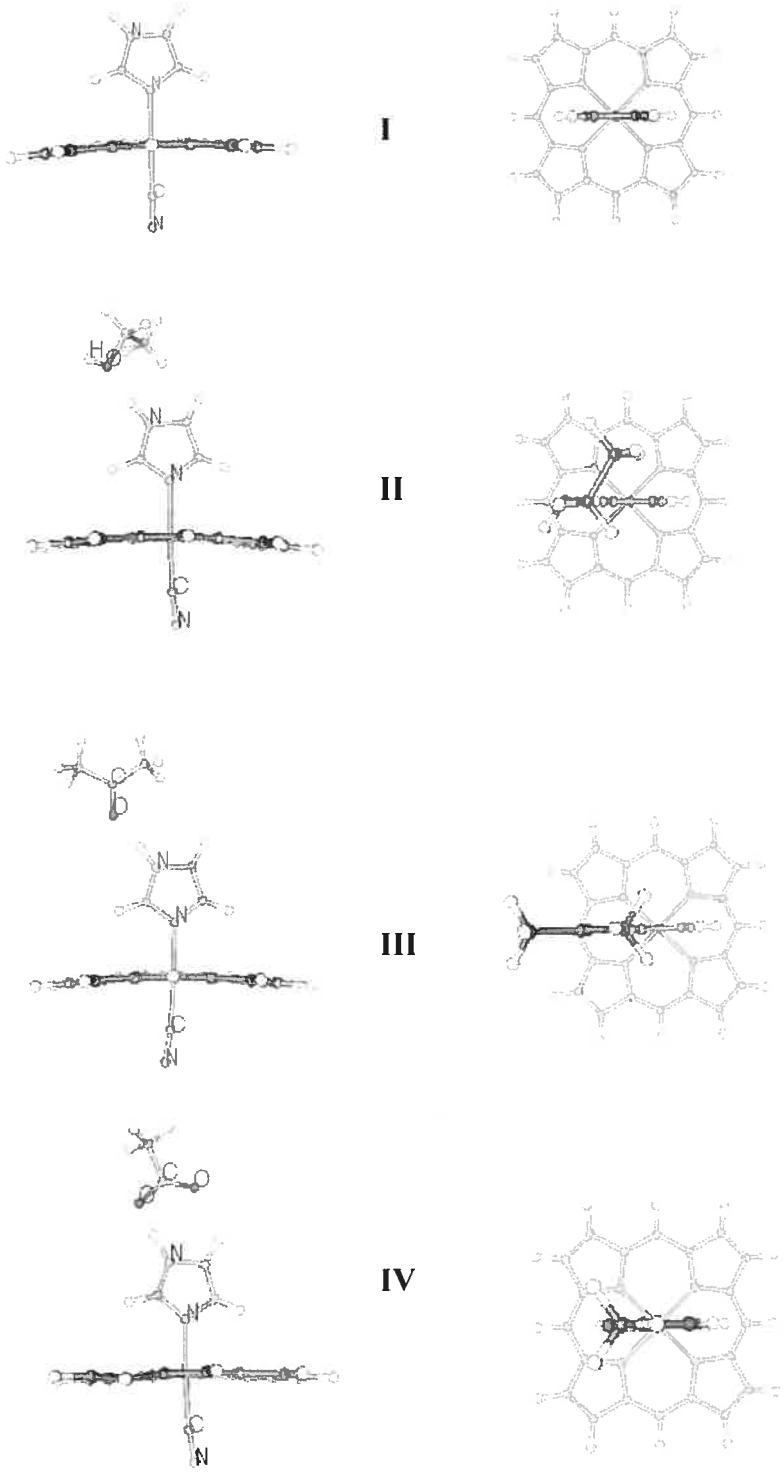

Figure 3.4 Schematic view of the calculated cyanide-imidazole complex models of the low-spin iron porphyrin. Here, **II** comes from sperm whale myglobin (Mb), **III** from human myoglobin (Hb) or horse heart cytochrome c(Cyt-c), **IV** from horseradish peroxidase (HRP).

3.6. Results and Discussion

3.6.1 Nitroxides

Table 3.1 compares the experimental ^{1}H NMR chemical shifts in a series of aromatic *t*-butyl nitroxide radicals to the present DFT calculations with pure GGA functionals (BP, P86 and PW91). For the DFT results, the root mean square errors (RMSE) are 14.39, 15.72 and 13.01 ppm over the experimental range of 115.47 ppm for the BP (R=0.959, slope=1.229, intercept=-1.5), P86 (R=0.946, slope=1.167, intercept=1.5) and PW91 (R=0.966, Slope=1.230, intercept=-2.6) functionals, respectively. Here, the total number of the protons for this statistics is 27. The discrepancies are reduced by about a factor of 2 if the proton shifts at the para-position are excluded from the statistics (RMSE, BP=7.94, P86=7.80, PW91=8.02 ppm). The DFT results show good correlations with the experiment even without the solvent and thermal motional effects. The results of three pure GGA functionals (BP, P86 and PW91) have a similar level of accuracy compared to the experiment. Table 3.1 also shows the individual contributions of the BP chemical shifts. In this work, the Fermi contact and pseudocontact shifts are calculated using the newly derived equations (Eqs. 3.43 and 3.44). The Fermi contact shifts dominate ^{1}H chemical shifts and determine all qualitative trends. On the other hand, the pseudocontact shifts are negligible and just contribute less than 0.2 ppm to any of the ^{1}H shifts in the radicals. This is due to their small g-tensor anisotropies (shown in Table 3.2) and the small magnitude of their anisotropic hyperfine tensors. In most cases, the orbital shifts are smaller than the Fermi contact shifts but not negligible ($|\delta_{iso}^{orb} / \delta_{iso}^{FC}| \leq 32$ % for all ^{1}H shifts except the 4-H of 2,6-dimethyl radical where the orbital contribution is even larger than the Fermi contact term). Therefore, the orbital contribution should be included to the shift calculations to have a better numerical agreement with experiment. Finally, Table 3.1 compares the orbital shifts to the chemical shifts in corresponding diamagnetic systems. The differnces of two contributions are rather small (the mean absolute deviation is 2.30 ppm) and it confirms the orbital shifts can be approximated by the diamagnetic shifts without a big loss of accuracy for ^{1}H chemical shifts.

Table 3.1 Calculated isotropic ^{1}H NMR chemical shifts (in ppm) of a series of aromatic *t*-butyl nitroxide radicals at 295K.[a]

			δ_{iso}			BP contributions		
		[b]EXP	BP	P86	PW91	δ_{iso}^{FC}	δ_{iso}^{PC}	δ_{iso}^{orb} / δ_{iso}^{dia}
2-methyl	*t*-bu-H	-16.70	-12.04	-7.07	-17.14	-14.26	-0.02	2.24/1.53
	2-CH_3	19.14	25.08	32.57	32.35	22.72	0.08	2.28/1.42
	3-H	52.44	54.94	61.23	53.60	51.14	0.01	3.79/6.06
	4-H	-23.44	-60.80	-61.21	-52.92	-64.83	-0.01	4.04/5.45
	5-H	60.02	59.42	61.82	60.38	53.19	0.00	6.23/6.21
	6-H	-55.45	-74.45	-63.05	-78.02	-79.88	-0.04	5.47/5.92
2,3-dimethyl	*t*-bu-H	-16.90	-13.27	-8.23	-14.49	-14.78	0.02	1.49/1.52
	2-CH_3	15.84	18.30	18.22	14.52	15.23	-0.05	3.11/1.46
	3-CH_3	-5.05	-9.82	-9.95	-14.09	-15.50	0.00	5.68/1.66
	4-H		-43.50	-39.74	-41.47	-53.43	0.01	9.92/5.29
	5-H	61.43	61.32	65.19	63.64	53.70	-0.02	7.64/6.06
	6-H	-50.14	-62.17	-61.99	-65.03	-74.83	-0.01	12.68/5.69
2,4-dimethyl	*t*-bu-H	-15.50	-11.56	-6.15	-14.69	-13.86	-0.03	2.33/1.53
	2-CH_3	20.15	27.95	30.71	28.91	24.21	0.08	3.66/1.56
	3-H	60.00	59.88	55.71	57.54	52.65	0.03	7.21/5.79
	4-CH_3	33.40	81.23	82.97	79.97	79.02	0.01	2.20/1.86
	5-H	54.15	67.76	62.33	56.58	55.48	0.02	12.27/5.99
	6-H	-54.60	-80.29	-66.69	-78.41	-84.71	-0.02	4.44/5.89
2,5-dimethyl	*t*-bu-H	-17.27	-11.94	-6.68	-14.94	-13.59	-0.04	1.69/1.55
	2-CH_3	18.47	29.72	32.70	29.25	25.61	0.07	4.04/1.52
	3-H	49.58	59.66	52.83	53.29	48.34	0.02	11.30/6.19
	4-H	-22.82	-57.56	-61.24	-46.35	-70.27	0.01	12.69/5.29
	5-CH_3	-7.07	-18.65	-14.70	-13.53	-19.53	0.00	0.88/1.82
	6-H	-53.60	-63.61	-59.38	-78.30	-73.25	-0.06	9.70/5.79
2,6-dimethyl	*t*-bu-H	-24.47	-16.25	-11.07	-19.57	-18.88	0.03	2.60/1.37
	2-CH_3	15.12	16.06	18.90	15.06	12.25	-0.12	3.93/1.99
	3-H	59.66	69.83	67.00	68.43	59.78	-0.02	10.06/6.39
	4-H	-4.61	7.02	12.56	9.67	-0.32	0.00	7.34/6.69
[d]RMSE			14.39	15.72	13.01			
			7.94	7.80	8.02			

[a] TMS was used as reference molecule (BP=31.46, P86=31.47, PW91=31.49 ppm). [b] in Ref [8]. [c] The chemical shifts of diamagnetic compounds were calculated at the PW91 level. [d] Root mean square (rms) error. The rms errors in the second line were obtained without the para-position shifts.

Table 3.2 Calculated electronic g-values of a series of aromatic *t*-butyl nitroxide radicals.

		g_1	g_2	g_3	g_{iso}	$^a g_{aniso}$
2-methyl	BP	2.002	2.008	2.013	2.008	0.008
	P86	2.002	2.008	2.014	2.008	0.009
	PW91	2.002	2.008	2.014	2.008	0.009
2,3-dimethyl	BP	2.002	2.008	2.014	2.008	0.009
	P86	2.002	2.008	2.014	2.008	0.009
	PW91	2.002	2.008	2.014	2.008	0.009
2,4-dimethyl	BP	2.002	2.008	2.013	2.008	0.008
	P86	2.002	2.008	2.014	2.008	0.009
	PW91	2.002	2.008	2.014	2.008	0.009
2,5-dimethyl	BP	2.002	2.008	2.013	2.008	0.008
	P86	2.002	2.008	2.014	2.008	0.009
	PW91	2.002	2.008	2.014	2.008	0.009
2,6-dimethyl	BP	2.002	2.008	2.014	2.008	0.009
	P86	2.002	2.008	2.014	2.008	0.009
	PW91	2.002	2.008	2.014	2.008	0.009

[a] Here, $g_{aniso}=g_3-1/2(g_1+g_2)$.

In Table 3.3, the calculated Fermi contact (isotropic) coupling constants are collected for the four different functionals (BP, P86, PW91 and B3LYP). All results are exactly in the same trend as the ^{1}H chemical shift results because the shifts are dominated by the Fermi contact shifts which depend mainly on the Fermi contact coupling constants. In this case, the pure GGA results show slightly better correlations with the experiment than the hybrid B3LYP functional results. The deviations of the calculated constants from the experiment are systematic according to the proton position as well as the calculated ^{1}H shifts in Table 3.1. In both results, the absolute errors between the calculations and experiment have the trend for the proton position (meta < ortho < para). Hence, we can infer that the errors may be related to the orientation of the t-BuN(O)-substituent which strongly influence the spin density of the aromatic ring through the conjugation.

Table 3.3 Calculated Fermi contact (isotropic hyperfine) coupling constants (in MHz) of a series of aromatic *t*-butyl nitroxide radicals.

		BP	P86	PW91	B3LYP	[a]EXP
2-methyl	*t*-bu-H	-0.531	-0.370	-0.633	-0.705	-0.658
	2-CH_3	0.846	1.127	1.049	1.045	0.680
	3-H	1.905	1.859	1.683	1.911	1.722
	4-H	-2.415	-2.458	-2.438	-2.340	-1.112
	5-H	1.981	2.013	1.868	2.005	2.005
	6-H	-2.975	-2.694	-3.051	-2.781	-2.307
2,3-dimethyl	*t*-bu-H	-0.551	-0.391	-0.607	-0.738	-0.675
	2-CH_3	0.567	0.598	0.518	1.044	0.549
	3-CH_3	-0.577	-0.586	-0.511	-0.790	-0.230
	4-H	-1.990	-1.891	-1.820	-1.784	
	5-H	2.000	1.992	1.892	1.898	2.030
	6-H	-2.787	-2.522	-2.645	-2.259	-2.131
2,4-dimethyl	*t*-bu-H	-0.516	-0.339	-0.622	-0.707	-0.647
	2-CH_3	0.902	0.997	0.975	0.979	0.686
	3-H	1.961	1.926	1.806	1.985	1.753
	4-CH_3	2.943	3.016	2.898	2.463	1.179
	5-H	2.066	2.040	1.931	2.058	1.974
	6-H	-3.155	-2.798	-3.148	-0.707	-2.302
2,5-dimethyl	*t*-bu-H	-0.506	-0.345	-0.591	-0.686	-0.669
	2-CH_3	0.954	1.010	0.973	1.079	0.666
	3-H	1.801	1.799	1.604	1.862	1.635
	4-H	-2.617	-2.504	-2.437	-2.366	-1.064
	5-CH_3	-0.728	-0.732	-0.646	-0.949	-0.288
	6-H	-2.729	-2.380	-2.756	-2.652	-2.215
2,6-dimethyl	*t*-bu-H	-0.703	-0.503	-0.831	-0.957	-0.986
	2-CH_3	0.457	0.634	0.400	0.416	0.498
	3-H	2.227	2.205	2.261	1.712	1.968
	4-H	-0.012	-0.030	-0.045	-0.054	-0.431
[b]RMSE		0.527	0.560	0.514	0.607	
		0.238	0.278	0.261	0.466	

[a] in Ref [8]. [b] The root mean square errors. The rms errors in the second line were obtained without the para-position shifts.

Table 3.4 Calculated Fermi contact (isotropic hyperfine) coupling constants (in MHz) of 2-methylphenyl-*t*-butylnitroxide radical according to the angle ϕ.[a]

	0	15	30	45	60	75	90	105	[b]EXP
t-Bu-H	0.14	0.01	-0.27	-0.57	-0.70	-0.75	-0.78	-0.80	-0.66
2-CH_3	9.53	8.02	5.55	2.86	1.05	-0.10	0.44	1.06	0.68
3-H	2.92	2.86	2.64	2.25	1.91	1.32	1.03	0.96	1.72
4-H	-7.68	-6.87	-5.48	-3.73	-2.35	-0.67	-0.04	-0.29	-1.11
5-H	3.00	2.83	2.62	2.29	2.01	1.88	2.06	2.55	2.01
6-H	-7.24	-6.50	-5.35	-3.89	-2.79	-1.56	-1.27	-1.68	-2.31
Relative Energies (kcal/mol)	3.93	2.93	1.35	0.28	0.00	0.47	0.93	1.19	

[a] Calculations were performed at the B3LYP/6-311G(d,p) level. [b] in Ref [8].

Table 3.4 shows the Fermi constant results of 2-methyl radical according to the angle ϕ (see, Fig 3.1). All structures were fully optimized except the angle ϕ at the B3LYP/6-311G(d,p) level and the Fermi constants were also calculated at the same level. The structural dependence is seen graphically with the energy potential curve in Fig 3.5. From the results, it is possible to understand the discrepancies of the ^{1}H chemical shifts between the calculation and experiment. The global minimum structure has the value of 56.8° for the angle ϕ. In the angle range of 45° ~ 75°, the relative energies to the global minimum are less than 0.5 kcal/mol (thermal energy kT is around 0.6 kcal/mol at the room temperature) and this refects the fact that the radical structure is so flexible at room temperature. In that angle range, it is also shown that para- and ortho-position proton shifts are very sensitive to the rotation but the other (meso-position and *t*-butyl protons) shifts are less sensitive. In consequence, thermal motion effects will be significant for the ^{1}H chemical shifts in these aromatic radicals and may lead a deviation from the T^{-1} Cuie law dependence of the paramagnetic chemical shifts. In this case, the solvent effect will also affect greatly the DFT results because of the soft potential energy surface for the angle ϕ. In fact, in the optimized structure of 2-methyl radical at the B3LYP/6-311G(d,p) using the isodensity surface polarized continuum model (IPCM) [54], the angle ϕ is about

65° . Note that this calculation was done in the present work and the dielectric constant (ε=2.2379) of carbon tetrachloride was used for the direct comparison with the experiment [8]. The DFT results revised by this solvent effect show a good agreement with the experiment especially for the Fermi coupling constant at the para-position (calc. 1.754 MHz vs. exp. 1.722 MHz).

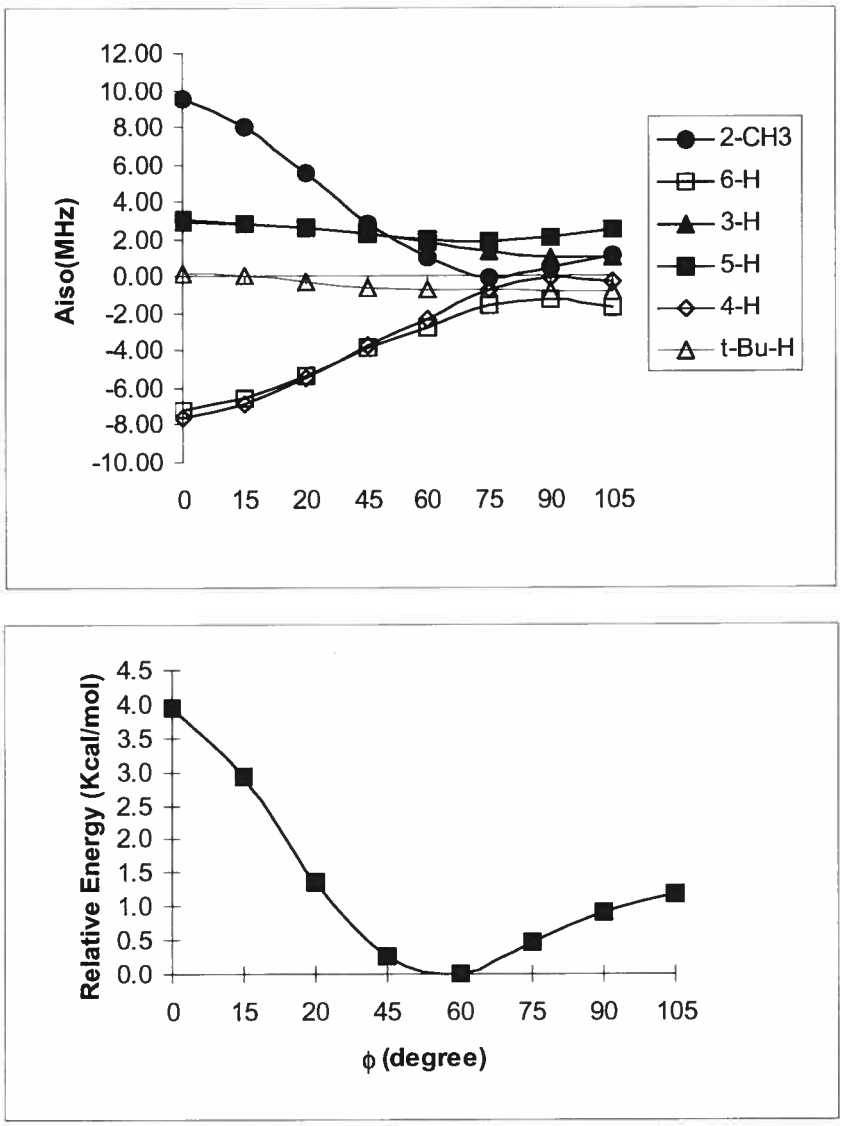

Figure 3.5. Structural dependence of the Fermi contact (isotropic hyperfine) coupling constants in 2-methylphenyl-*t*-butylnitroxide radical by change of the angle ϕ.

The calculated ^{13}C chemical shifts of a series of aliphatic nitroxides are collected in Table 3.5. The stuctures used in this study are shown in Fig 3.2. All the minimum structures of the gas-phase calculations have the chair form. The DFT results of the chair forms show a similar trend in sign and magnitude, while the experimental results in the radical **I** show a quite different trend from those in the radicals **II** and **III**. In fact, the radical **I** is thought to exist in a twisted form in solution and, on the contaray, the radicals **II** and **III** are in a chair form in solution based on the previous experimental work [9]. This can be confirmed by the comparison between the DFT shifts and the experiment. For the ^{13}C chemical shifts of the three radicals (**I**:twisted, **II**:chair, **III**:chair), the RMSE of the BP results is 203 ppm over the experimental range of 3112 ppm (N=12, R=0.980, slope=0.941, intercept=58.5 ppm). The results including the twisted form show a much better correlation with the experiment than all chair form results at the same level of theory (N=12, R=0.961, slope=0.722, intercept=67 ppm, RMSE=219 ppm). Furthermore, since the energy difference between the two conformers of the radical **I** is very small (~ 0.3 Kcal/mol at the B3LYP/6-311G(d,p) level), the relative stability of the comformations in solution might be easily changed by the solvent effect. As a result, The DFT results give a good prediction of ^{13}C chemical shifts in the aliphatic radicals and, at the same time, enable us to investigate the relationship between the shifts and molecular structures. The remaining errors can be reduced by considering the solvent effect and the motional effect arising from the rapid ring inversion.

Table 3.5 shows the individual contributions of the DFT shifts. The Fermi contact shifts dominate the shifts and determine the trend following the experiment both in sign and magnitude. In most cases the orbital contribution is small but not negligible. For the ^{13}C chemical shifts at the γ-position, the orbital shifts are even comparable to the Fermi contact shifts ($|\delta_{iso}^{orb}/\delta_{iso}^{FC}|_{max}$=44.7%). Therefore, the orbital contribution should be included for an accurate prediction of the shifts. The calculated shifts of the diamagnetic compounds δ_{iso}^{dia}, which have the same structure of the corresponding radical, have the mean absolute deviation of 12 ppm from the orbital shifts δ_{iso}^{orb}. It implies that the diamagnetic shifts can readily replace the orbital shifts in most cases, but for the shifts at

the γ-position the orbital contributions are important. The pseudocontact shifts are small and negligible (the absolute value of the shifts are less than 1 ppm). This is due to the small anisotropy of the g-tensors which is seen in Table 3.6. The contact shift contributions of some heavy atoms in the aliphatic radicals are also shown in Table 3.6. In these heavy atoms, we can see relatively large pseudocontact shifts but they are still quite smaller than the Fermi contact shifts ($|\delta_{iso}^{PC}/\delta_{iso}^{FC}| < 1\%$).

Finally, Table 3.7 lists the DFT results (BP, P86, and B3LYP) for the Fermi contact coupling contant in the aliphatic radicals and compares them to the experiment. The B3LYP hybrid functional, on average, show a slightly better agreement with the experiment for the Fermi constant than the pure BP and P86 functionals. It implies that the ^{13}C chemical shift results can be improved by using the hybrid functional, which was already shown in the previous work [23]. However, in order to have some confidence in the quality of the calculations, the solvent and motional effects should be included.

Table 3.5 Calculated isotropic ^{13}C NMR chemical shifts (in ppm) of a series of aliphatic nitroxide radicals at 298 K.[a]

			δ_{iso}		BP contributions			P86 contributions		
		[b]EXP	BP	P86	δ_{iso}^{FC}	δ_{iso}^{PC}	δ_{iso}^{orb}	δ_{iso}^{FC}	δ_{iso}^{PC}	δ_{iso}^{orb}
I (twisted)	C_α	-1460	-1569	-1474	-1588	0.01	18.7	-1484	0.03	10.4
	C_β	1652	1786	1854	1786	-0.24	0.0	1848	-0.24	6.4
	$C_{\beta'}$	660	717	749	668	0.23	48.9	707	0.20	41.5
	C_γ	-112	-72	-77	-61	0.13	-10.6	-61	0.14	-16.0
I (chair)	C_α		-751	-626	-804	0.12	52.7	-643	0.12	16.7
	C_β		1237	1278	1221	-0.28	16.3	1268	-0.30	10.2
	$C_{\beta'}$		190	260	194	0.15	-3.7	232	0.17	27.6
	C_γ		-66	-42	-46	0.13	-19.7	-33	0.13	-9.4
II (chair)	C_α	-1125	-780	-639	-787	0.05	6.8	-643	0.05	3.7
	C_β	1100	1316	1358	1300	-0.24	15.9	1349	-0.24	9.3
	$C_{\beta'}$	355	136	182	125	0.14	10.4	160	0.16	21.9
	C_γ	-8	-51	-54	-56	0.14	4.6	-47	0.14	-7.2
III (chair)	C_α	-1061	-639	-514	-688	0.07	49.4	-541	0.05	26.3
	C_β	1462	1273	1325	1279	-0.27	-5.3	1322	-0.28	3.4
	$C_{\beta'}$	249	137	147	121	0.17	16.0	155	0.18	-7.6
	C_γ	-95	-31	-87	-58	0.15	25.9	-57	0.15	-30.6
	[c]$\lvert\Delta\rvert_{av}$		163	175						

[a] The shifts are from 2,2,6,6-tetramethylpiperidine precursor of **III**. The calculated shielding constants are C_α (BP:122.6, P86:119.6 ppm), C_β (BP:145.4, P86:142.4 ppm), $C_{\beta'}$ (BP:137.4, P86: 133.6 ppm), and the C_β signal is used for C_γ of **I**. These values are taken from Ref [23]. The γ carbon of **I** which is referenced to the carbonyl carbon of cyclohexanone (BP:-30.2, P86:-33.7 ppm) and the γ carbon of **II** which is referenced to the hydroxyl carbon of isopropyl alcohol (BP:108.5, P86:105.3 ppm) from this work. [b] in Ref [9]. [c] Mean absolute errors from experiment.

Table 3.6 Calculated ^{15}N and ^{17}O contact shifts (in ppm) and g-values of a series of aliphatic nitroxide radicals at 298 K.[a]

		P86						
		g_1	g_2	g_3	g_{iso}	[b]A_{iso}	δ_{iso}^{FC}	δ_{iso}^{PC}
I	N	2.002	2.008	2.014	2.008	33.3	12233	-24
	O					-33.4	6542	-40
	O(C=O)					-0.24	47	-0.1
II	N	2.002	2.008	2.014	2.008	32.4	11914	-26
	O					-33.3	6528	-44
	O(HO)					-0.20	39	0.1
III	N	2.002	2.008	2.014	2.008	32.8	12061	-26
	O					-33.2	6506	-43

[a] Calculations were performed at the P86/IGLO-III level. [b] in MHz.

Table 3.7 Calculated Fermi contact coupling (isotropic hyperfine) coupling constants (in MHz) of a series of aliphatic nitroxide radicals.[a]

		BP	P86	B3LYP	[b]EXP
I (twisted)	C_α	-15.0	-14.1	-16.9	-14.3
	C_β	16.9	17.5	15.4	16.0
	$C_{\beta'}$	6.3	6.7	6.1	6.4
	C_γ	-0.6	-0.6	-0.6	-1.1
I (chair)	C_α	-7.6	-6.1	-9.2	
	C_β	11.6	12.0	10.6	
	$C_{\beta'}$	1.8	2.2	1.8	
	C_γ	-0.4	-0.3	-0.7	
II (chair)	C_α	-7.6	-6.1	-9.4	-10.6
	C_β	11.6	12.0	11.2	10.4
	$C_{\beta'}$	1.8	2.2	1.1	3.4
	C_γ	-0.44	-0.31	-0.56	-0.06
III (chair)	C_α	-6.5	-5.1	-8.7	-10.1
	C_β	12.1	12.5	11.1	13.7
	$C_{\beta'}$	1.1	1.5	1.2	2.3
	C_γ	-0.55	-0.54	-0.62	-0.90
	[c]$\lvert\Delta\rvert_{av}$	1.26	1.45	1.18	

a Calculations were carried out at the BP/IGLO-III, P86/IGLO-III, and B3LYP/6-311G(d,p) levels. [b] in Ref [9]. [c] Mean absolute errors from experiment.

3.6.2. Blue Copper Proteins

Here, we calculated the ^{1}H NMR chemical shifts of the active sites in three blue copper proteins (see, Fig. 3.3) and investigated the Fermi contact and pseudocontact contributions to the total paramagnetic shifts. Computed ^{1}H chemical shifts and their individual contributions for the copper-bound histidines are collected and compared with the experiment in Table 3.8. In most cases, the BP results are in good agreement with the experiment and provide the trend following the experiment both in sign and relative magnitude. However, for the shifts of δ_2 protons of His46 and His117 in azurin and ε_1 protons of His46 in stellacyanin and of His37 in plastocyanin, the BP results are in poor values. This discrepancies might arise from the fact that the NMR experiment has performed in solution [31] while the calculations have carried out in gas phase using the solid-phase X-ray structures.

The detail discussion for the relationship between the molecular and electronic structures gives a useful guide for the problem. Fig. 3.6 shows the structural differences of three blue copper proteins in an illustrative way. The histidine rings of azurin are not linear to the Cu-$N_{\delta 1}$ σ-bond. On the other hand, the histidine rings of stellacyanin and plastocyanin are almost linear to the Cu-$N_{\delta 1}$ σ-bonds. This structural difference may strongly affect the unpaired electron spin density distribution of the proteins. For example, the Mulliken atomic spin populations of the s- and p- type orbitals in $N_{\delta 1}$ of three blue coppers are as follows: 0.008e-0.024e, 0.011e-0.034e, and 0.011e-0.037e for azurin, stellacyanin, and plastocyanin, respectively. The bent structure of azurin may attenuate the direct spin delocalization through σ-bonds and the spin-polarization through π-bonds in histidine. In Table 3.9, we can see that the calculated hyperfine structures of azurin are systematically smaller than those of the other two proteins. This trend is also shown in Table 3.10 where the calculated hyperfine structures of some heavy atoms of the proteins are provided. It implies that the histidine rings of azurin may exist linearly to the Cu-$N_{\delta 1}$ σ-bond in solution. In consequence, for an accurate prediction of the ^{1}H

chemical shifts in the proteins, the structure optimization including the solvent effect should be performed.

Table3.8. Calculated ^{1}H NMR chemical shifts (in ppm) of the histidines in blue copper protein models.

			BP contributions			BP		
			$^b\delta_{iso}^{dia}$	δ_{iso}^{FC}	δ_{iso}^{PC}	δ_{iso}	[a]Exp	[d]|Δ|
Azurin	His46	$H_{\delta 2}$	7.23	20.03	-0.32([c]-1.3)	26.9	49.1	22.2
278 K		$H_{\varepsilon 1}$	7.87	26.09	-0.11(-4.5)	33.9	34.1	0.2
		$H_{\varepsilon 2}$	8.33	11.97	-0.14(-1.3)	20.2	26.9	6.7
	His117	$H_{\delta 2}$	7.21	19.84	-0.42(-1.1)	26.6	54.0	27.4
		$H_{\varepsilon 1}$	7.87	43.45	0.71(-3.4)	52.0	46.7	5.3
		$H_{\varepsilon 2}$	8.18	20.45	-0.10	28.5		
Stellacyanin	His46	$H_{\delta 2}$	7.19	42.26	-0.42(-1.3)	49.0	48.0	1.0
301 K		$H_{\varepsilon 1}$	7.84	34.14	0.41(3.1)	42.4	29.8	12.6
		$H_{\varepsilon 2}$	8.01	25.64	-0.21(-1.4)	33.4	26	7.4
	His94	$H_{\delta 2}$	7.16	49.14	0.20(-1.0)	56.5	55.0	1.5
		$H_{\varepsilon 1}$	8.16	41.39	0.38(-5.4)	49.9	41.2	8.7
		$H_{\varepsilon 2}$	7.72	45.76	0.31	53.8		
Plastocyanin	His37	$H_{\delta 2}$	7.10	39.68	-0.10(-1.0)	46.7	47.1	0.4
298 K		$H_{\varepsilon 1}$	8.05	45.73	-0.20(-3.5)	53.6	35.6	18.0
		$H_{\varepsilon 2}$	7.97	28.20	-0.18(-1.0)	36.0	31.4	4.6
	His87	$H_{\delta 2}$	7.09	48.21	0.08(-0.9)	55.4	51.6	3.8
		$H_{\varepsilon 1}$	7.45	34.60	-0.11(-0.3)	41.9	35.6	6.3
		$H_{\varepsilon 2}$	8.36	33.62	-0.03(-0.5)	42.0		

[a] in Ref [31]. [b] The reference molecule is TMS (σ = 31.46 ppm at the same level). [c] Results from McConnell's formula in Ref [31]. [d] Absolute deviations from the experiment.

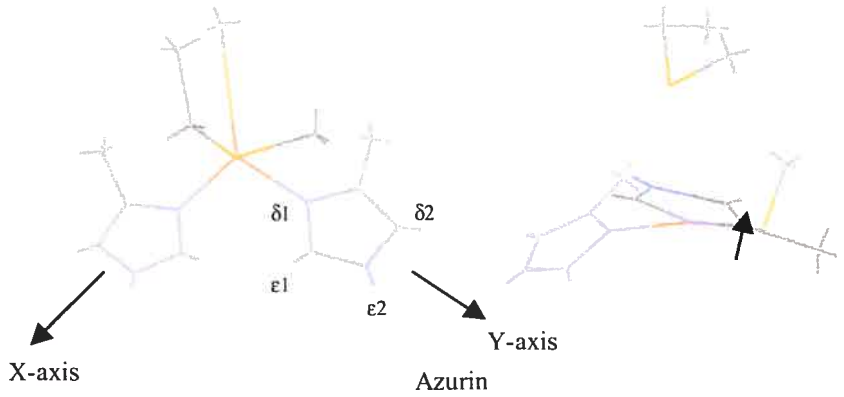

Cu-S(Met121) = 3.047 Å
Cu-S(Cys112) = 2.173 Å
Cu-N(His46) = 2.117 Å
Cu-N(His117) = 1.999 Å

His46
Cu-$H_{\delta 2}$ = 5.335 Å
Cu-$N_{\delta 1}$-C- $H_{\delta 2}$ = 16.51°

His117
Cu-$H_{\delta 2}$ = 5.216Å
Cu-$N_{\delta 1}$-C- $H_{\delta 2}$ = 12.71°

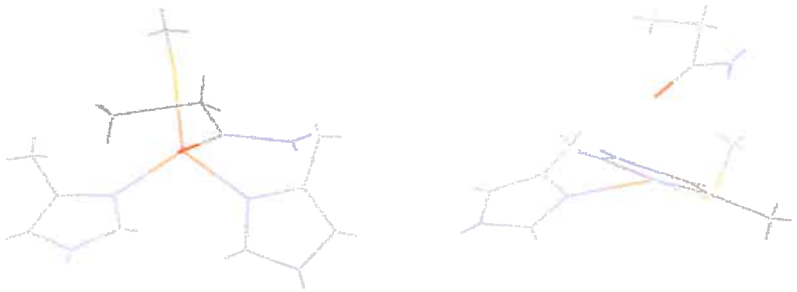

Stellacyanin

Cu-O(Gln99) = 2.210 Å
Cu-S(Cys89) = 2.178 Å
Cu-N(His46) = 1.960 Å
Cu-N(His94) = 2.043 Å

His46
Cu-$H_{\delta 2}$ = 5.176 Å
Cu-$N_{\delta 1}$-C- $H_{\delta 2}$ = 3.52°

His117
Cu-$H_{\delta 2}$ = 5.198Å
Cu-$N_{\delta 1}$-C- $H_{\delta 2}$ = 4.57°

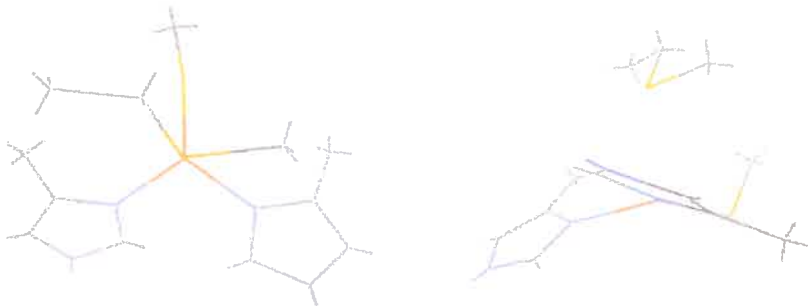

Plastocyanin

Cu-O(Gln99) = 2.883 Å
Cu-S(Cys89) = 2.149 Å
Cu-N(His46) = 1.963 Å
Cu-N(His94) = 2.010 Å

His46
Cu-$H_{\delta 2}$ = 5.177 Å
Cu-$N_{\delta 1}$-C- $H_{\delta 2}$ = 4.98°

His117
Cu-$H_{\delta 2}$ = 5.203Å
Cu-$N_{\delta 1}$-C- $H_{\delta 2}$ = 8.62°

Figure 3.6. Top and side view of the active sites of the blue copper proteins and the selected geometrical parameters.

Table 3.9. Calculated hyperfine structures (in MHz) of histidine hydrogens in blue copper protein models.

			BP				[a]Exp	
			T_{11}	T_{22}	T_{33}	A_{iso}	A_{iso}	[b]|Δ|
Azurin	His46	$H_{\delta 2}$	-0.49	-0.39	0.88	0.68	1.49	0.81
Hcap42		$H_{\varepsilon 1}$	-1.55	-1.17	2.71	0.89	1.06	0.17
		$H_{\varepsilon 2}$	-0.49	-0.36	0.85	0.41	0.56	0.15
	His117	$H_{\delta 2}$	-0.53	-0.45	0.98	0.68	1.61	0.93
		$H_{\varepsilon 1}$	-1.61	-1.31	2.92	1.48	1.45	0.03
		$H_{\varepsilon 2}$	-0.56	-0.40	0.95	0.70		
Stellacyanin	His46	$H_{\delta 2}$	-0.56	-0.44	1.00	1.56	1.53	0.03
Hcap42		$H_{\varepsilon 1}$	-1.78	-1.46	3.24	1.26	1.09	0.17
		$H_{\varepsilon 2}$	-0.54	-0.39	0.92	0.95	0.62	0.33
	His94	$H_{\delta 2}$	-0.60	-0.49	1.09	1.82	1.77	0.05
		$H_{\varepsilon 1}$	-1.73	-1.41	3.14	1.53	1.40	0.13
		$H_{\varepsilon 2}$	-0.60	-0.43	1.02	1.69		
Plastocyanin	His37	$H_{\delta 2}$	-0.56	-0.44	1.00	1.44	1.45	0.01
Hcap42		$H_{\varepsilon 1}$	-1.83	-1.50	3.33	1.66	1.14	0.52
		$H_{\varepsilon 2}$	-0.55	-0.39	0.94	1.02	0.74	0.28
	His87	$H_{\delta 2}$	-0.56	-0.46	1.02	1.75	1.63	0.12
		$H_{\varepsilon 1}$	-1.73	-1.44	3.18	1.25	1.01	0.24
		$H_{\varepsilon 2}$	-0.55	-0.40	0.95	1.22		

[a] in Ref [31]. [b] Asolute deviations from the experiment.

Table 3.10. Calculated hyperfine structures (in MHz) of selected heavy atoms in blue copper protein models.

[a]BP			T_1	T_2	T_3	A_{iso}
Azurin		Cu	147	117	-263	-109/[b]-100
Hcap42	His46	$N_{\delta 1}$	-1.7/-1.3	-1.4/-0.8	3.1/1.2	15.6/18.1
		$N_{\varepsilon 2}$	-0.14/-0.17	-0.04/-0.07	0.18/0.23	0.60/0.87
	His117	$N_{\delta 1}$	-2.1/-1.5	-1.7/-1.1	3.8/2.7	19.1/25.1
		$N_{\varepsilon 2}$	-0.19/-0.32	-0.05/-0.04	0.24/0.35	1.01/1.30
Stellacyanin		Cu	176	113	-289	-73
Hcap42	His46	$N_{\delta 1}$	-2.2	-1.8	3.9	16.9
		$N_{\varepsilon 2}$	-0.18	-0.03	0.22	1.04
	His94	$N_{\delta 1}$	-3.1	-2.5	5.6	23.9
		$N_{\varepsilon 2}$	-0.23	-0.06	0.29	1.71
Plastocyanin		Cu	145	131	-277	-94
Hcap42	His37	$N_{\delta 1}$	-2.3	-1.9	4.2	17.1
		$N_{\varepsilon 2}$	-0.19	-0.04	0.24	1.19
	His87	$N_{\delta 1}$	-2.6	-2.0	4.6	21.6
		$N_{\varepsilon 2}$	-0.20	-0.05	0.25	1.40

[a] All calculations were performed with the BP functional. [b] The experimental results in Ref [32].

As seen in Table 3.8, in most case, the Fermi contact shifts dominate the ^{1}H chemical shifts and determine the qualitative and quantitative trend of the ^{1}H chemical shifts. The orbital shifts are comparable to the Fermi contact shifts in magnitude and they are, therefore, important to predict the chemical shifts accurately. Note that in the calculations the orbital shifts were approximated by the chemical shifts of the diamagnetic systems and the ground of the approximation is provided by the study for ^{1}H chemical shifts in the organic radicals discussed above. In most case, the pseudocontact shifts are small and negligible.

Table 3.8 also compares two kinds of the pseudocontact shifts of the histidine protons: one was calculated by using Eq. (3.44) newly derived in this work and the other by using McConnell's formula in Eq. (3.3) combined with the experimental factors. The former are systematically smaller than the latter. This discrepancy can be attributed to the two factors: (1) the limits of McConnell's formula which arise from the assumptions used (2) the calculation errors of the magnetic resonance parameters which are involved in the new equation. McConnell's formula in Eq. (3.3) was derived based on the assumptions that the unpaired electron resides only on the center metal ion and the electron spin can be treated as point dipole. However, the blue copper active site exhibits a strong ligand (thiolate sulfur of cysteine) to metal (copper) charge transfer (LTMCT) and the unpaired electron delocalizes through the Cu-S bond. It may be proved by the analysis of the atomic Mulliken spin density. For the copper and sulfur of azurin, stellacyanin, and plastocyanin, the atomic spin densities are 0.236e-0.661e, 0.270e-0.602e, and 0.258e-0.623e at the BP/IGLO-III level. The copper bound histidine nitrogens also make a small contribution to LTMCT. From the results, we can deduce that McConnell's formula may overestimate the pseudocontact shifts by the imposed assumptions. Therefore, the calculated shifts using the new equation seem to be reasonable. However, we need further validation of the calculated values because the new equation depends on the accuracy of the g-tensor anisotropy. The electronic g-tensors are calculated in the different conditions (size and capping method) and collected in Table 3.9. Overall, the g_1 and g_2 values are in good agreement with the experimental results but the g_3 values are systematically smaller than the experimental ones. As a result, the present pseudocontact shift results may be

underestimated due to the small g-tensor anisotropy. In this work, we only considered the one electron integrals of the paramagnetic spin-orbit/orbital Zeeman cross term $\Delta\mathbf{g}^{para}_{SO/OZ}(1e)$ and of the diamagnetic spin-Zeeman gauge correction $\Delta\mathbf{g}^{dia}_{GC}(1e)$ for g-tensor calculations. From a theoretical point of view, the inclusion of two electon integral terms and other terms arising from relativistic effects is important. However, the inclusion of the two-electron terms rather deteriorates the g-tensor results calculated with pure GGA functionals [28]. In this case, the simple g-tensor calculations with the only one-electron terms give closer results to the experimental data due to the cancellation of the errors coming from the absence of the two-electron terms and the intrinsic limits of pure GGA functionals.

Table 3.11. Calculated g-values of blue copper protein models.

		g_1	g_2	g_3	g_{iso}
Azurin	[a]Hcap42	2.021	2.094	2.169	2.095
	[b]Ccap42	2.024	2.092	2.161	2.093
	[c]Hcap59	2.058	2.094	2.168	2.106
	[d]Exp	2.052	2.052	2.260	2.121
Stellacyanin	Hcap42	2.026	2.098	2.147	2.090
	Ccap42	2.026	2.096	2.144	2.089
	[c]Ccap53	2.028	2.101	2.145	2.092
	[e]Hcap93	2.052	2.082	2.149	2.095
	Exp	2.025	2.077	2.287	2.130
Plastocyanin	Hcap42	2.030	2.076	2.153	2.086
	Ccap42	2.030	2.075	2.149	2.085
	Exp	2.042	2.059	2.226	2.109

[a] For the Hcap42 models, the α-carbons of the four ligands directly bound with copper are terminated by hydrogen atoms and the number of atoms in the models are 42 (see, Fig. 3.3). [b] For the Ccap42 models, the α-carbons of the four ligands directly bound with copper are terminated by capping carbons and the number of atoms in the models are 42 (see, Fig. 3.3). [c] In the Hcap59 and Ccap53 models, the peptide chains of Cys112 (azurin) and Cys89 (stellacyanin) are elongated. [d] in Ref [47]. [e] In this model, the peptide chains of His46, His94 and Cys89 are elongated.

3.6.3. Ferric Cyanide-Imidazole Complexes of Heme Proteins

Table 3.12 compares calculated ^{13}CN chemical shifts in cyanide-bound porphyrin complexes (S=1/2) to the experiment which is shown in Ref [34]. The DFT results predict the shifts well both in sign and magnitude compared to the experiment. Although there are many contributors to the errors in the predictions such as structural uncertainty, methodological deficiencies, solven and motional effects, a reasonable level of accuracy seems to be achieved from the present calculations.

Table 3.12 also shows the relative importance of the different contributions to the ^{13}CN chemical shifts. In the porphyrins, the Fermi contact term dominate the shifts and determine all qualitative trends, as already seen in the previous studies, while the pseudocontact (PC) term is not negligible any more. In this case, the pseudocontact term (239~258 ppm) is even much larger than the orbital shift (-13~4 ppm). Often the PC term is estimated by McConnell's formula (Eq. 3.3) with experimental factors and has a value of about 400 ppm for the cyanide-imidazole complex (g_1~0.74, g_2~1.89, g_3~3.4) [34]. This value exhibits large difference (142~161 ppm) from the present values which were obtained by the accruate ZORA spin-orbit calculations for g-tensors and scalar relativistic all-electron calculations using the Pauli Hamiltonian for hyperfine tensors (the results are collected in Table 3.13 and 3.14). This discrepancy seems to arise from the point dipole approximation used in McConnell's where the induced paramagnetic moment is concentrated on the centered metal ion. In most practical cases, the spin density is often delocalized through the π-conjugated systems such as the porphyrin and imidazole or through the spin-polarization process. The spin delocalization may attenuate the PC contribution. This can be confirmed by the ZORA spin-orbit calculations for hyperfine tensors where the terms due to the spin-polarization density at the nucleus are absent (it seems to be a good approximation for the classical point dipole-dipole interaction). In this approach, the PC terms of the porphyrins show similar values (434~483 ppm) to the emprical value and it implies that the PC shifts from McConnell's might be overestimated. The orbital shift have the smallest contribution to the total shift, which

was not seen in the previous studies. In this case, the orbital contribution is completely negligible.

Table 3.12. Calculated ^{13}CN NMR chemical shifts (in ppm) in cyanide-bound prophyrin complexes (S=1/2) at 296 K.

	BP contributions			BP	
complex	$^{a}\delta_{iso}^{orb}$	$^{b}\delta_{iso}^{FC}$	$^{c}\delta_{iso}^{PC}$	δ_{iso}	Exp
I	-13	-4500	154/257	-4359/-4230	-3926
II(Mb)	-7	-4480	148/239	-4339/-4248	-4145
III(Hb/Cyt-c)	-4	-4380	157/258	-4227/-4126	-4074/-3761
IV(HRP)	4	-4023	156/257	-3863/-3762	-3543

[a] The orbital shifts were calculated at the BP/TZ2P(frozen core) level using the ADF program. Scalar relativistic effects were included using the Pauli Hamiltonian (Pauli-scalar). [b] For the Fermi contact shifts, the isotropic hyperfine constants were calculated at the BP/TZ2P(all-electron) level using the ADF program (Pauli-scalar) and the experimental isotropic g-value was used (~2.01 in [34]). [c] For the pseudocontact shifts, the results before the slash were calculated using the experimental g-values ($g_1 \sim 0.74$, $g_2 \sim 1.89$, $g_3 \sim 3.4$ in [34]) and the results after the slash were obtained from the g-tensors calculated using the ZORA spin-orbit method [53]. In both case, the used anisotropic hyperfine tensors were calculated at the same level as the isotropic hyperfine constants.

The g-tensors and hyperfine structures of the porphyrins are collected in Table 3.13 and calculated Fermi contact coupling constants of selected nuclei in the porphyrins are shown in Table 3.14. The ZORA spin-orbit results for the g-tensors are in good agreement with the experiment which can not be achieved by the Pauli approach. It implies that for the accurate g-tensors (or g-tensor anisotropies) the two-component methods like ZORA are essential in the porphyrins where the spin-orbit coupling is important. For the hyperfine constants, the ADF results are consistent and follow the

trend seen in the NMR experiment while the Gaussian results are not. It seems to arise from the disadvantage of the Gaussian-type basis sets for the Fermi contact interaction.

Table 3.13. Calculated g-values of cyanide-bound prophyrin complexes (S=1/2) and calculated hyperfine structures of their cyanide carbons.[a]

complex	sign of $g_1g_2g_3$	g_1	g_2	g_3	A_{iso}	T_1	T_2	T_3
I	-	0.657	0.861	3.498	-42.40	-1.44	-3.25	4.70
II(Mb)	-	0.690	0.917	3.451	-42.21	-1.36	-3.11	4.49
III(Hb/Cyt-c)	-	0.618	0.900	3.498	-41.27	-1.49	-3.27	4.76
IV(HRP)	+	0.002	1.178	3.493	-37.91	-1.46	-3.30	4.76
[b]EXP		0.74	1.89	3.4				

[a] The g-values were calculated at the BP/TZ2P level using ZORA spin unrestricted frozen core method. The hyperfine structures were calculated at the BP/TZ2P(all-electron) level using scalar Pauli Hamiltonian. [b] in Ref [34].

Table 3.14. Calculated Fermi contact coupling constants (in MHz) of selected nuclei in cyanide-bound prophyrin complexes (S=1/2).[a]

	Complex			
	I	**II**	**III**	**IV**
C	-52.63/-42.40	-40.12/-42.21	-51.97/-41.27	-34.05/-37.91
N	1.57/1.72	1.04/1.62	1.26/1.59	1.10/1.24
Fe	-16.00/-8.74	-17.79/-8.73	-17.48/-9.15	-17.34/-8.90
N_1	-1.39/-3.33	-2.35/-3.47	-3.05/-3.59	-4.24/-3.35
N_2	-0.09/-0.24	-0.30/-0.20	-0.08/-0.22	-1.24/-0.33

[a] For the Fermi constants, the results before the slash were calculated at the B3LYP/EPR-III[55] level using the G98 program. Here, the 6-311G(d,p) basis set was used for iron. The results after the slash were calculated at the BP/TZ2P(all-electron) level using the ADF program. Scalar relativistic effects were included with the Pauli Hamiltonian.

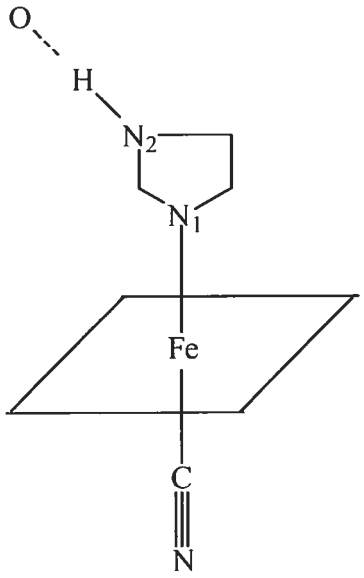

Figure 3.7. Numbering scheme of cyanide-imidazole complexes of iron (III).

3.7. Conclusion

Unlike the closed-shell NMR shielding tensor, and many other NMR and EPR parameters, paramagnetic NMR shielding is an intrinsically statistical property, defined only as an ensemble average. Calculations of the paramagnetic NMR shifts therefore require knowledge of magnetic parameters for thermally accessible excited states. In this study, we derive the first complete, general expression for the shielding tensor in open-shell species. The treatment considers all relevant contributions linear and bilinear in the external magnetic field and nuclear spin. Calculated values can therefore be compared directly to experiment. In diamagnetic compounds, our expression reduces to the "standard" closed-shell NMR shielding tensor. For paramagnetic species, knowledge of the state energies in the absence of the field, together with the per-state orbital shieldings, hyperfine tensors, and EPR g-tensors, is sufficient to determine the paramagnetic shifts.

The theory takes a particularly simple form for an isolated Kramers doublet state, with no thermally accessible excited states.

The newly derived equations for the paramagnetic NMR shift only depend on the magnetic resonance parameters (such as orbital shielding tensors, hyperfine tensors and g-tensors) which can be calculated by first-principles methods. The importance of this new theoretical approach can be summarized by the two factors: (1) The new theory validates McConnell's formula for the Fermi contact shift in Eq. (3.2) quantum mechanically within the same assumptions. The new formula is identified with McConnell's. (2) The new formula for the pseudocontact shift in Eq. (3.32) can overcome the restrictions of McConell's formula in Eq. (3.3). Precisely speaking, the new formula depends on the pure quantum mechanical parameters and can consider the delocalization of the upaired electron spin density without any further approximation, but McConnell's depends on the geometrical factors arising from the classical point dipole approximation and can not consider any quantum effect for the spin density distribution.

From the DFT calculations for the NMR chemical shifts in paramagnetic species (nitroxides, blue copper proteins, and ferric cyanide-imidazole complexes), we can summarize as follows: (1) The DFT results are in good agreement with the experiment. However, for the confidence of calculations, the solvent effect and thermal motion should be included. (2) The Fermi contact shift dominates the total shift and determines all qualitative trend following the experiment. (3) The orbital shift is small, compared to the Fermi contact term, but not negligible and can be readily replaced by the chemical shifts of similar diamagnetic systems. However, for better numerical accuracy, this term should be included correctly. (4) In most cases, the pseudocontact term is negligible but is comparable to the orbital shift in magnitude for ^{13}CN in iron porphyrin complexes which exhibit large g-tensor anisotropies. In consequence, these DFT studies using the new formulas for the NMR chemical shifts in paramagnetic species yield an insight into the relationship between NMR chemical shifts and the electronic and molecular structures directly and in a systematic way.

3.8. References

1. Moon, S.; Patchkovskii, S. "First-Principles calculations of paramagnetic NMR shifts", *In Quantum Chemical Calculation of NMR and EPR Parameters*, Kaupp, M. et al., Eds.; Wiley-VCH, Weinheim, *submitted*, 2003.
2. Moon, S.; Patchkovskii, S., Salahub; D. R. "Applications of Density Functional Theory to NMR Chemical Shifts in open-shell species", *manuscript in preparation.*
3. Bertini, I.; Luchinat, C.; *NMR of Paramagnetic Molecules in Biological Systems*, Benjamin/Cummings, Menlo Park, CA, 1986.
4. Bertini, I.; Turano, P.; Vila, A. J., *Chem. Rev.* **1996**, 93, 2833.
5. Bertini, I.; Luchinat, C.; Parigi, G., *Solution NMR of Paramagnetic Molecules*, Elsevier, Amsterdam, 2001.
6. Bertini, I.; Luchinat, C., *In Physical Methods: for Chemistrs*, edited by Drago, R. S., 2nd ed., HBJ, 1992, p. 500.
7. Kreilick,R. W., *J. Chem. Phys.* **1967**, 46, 4260.
8. Calder, A.; Forrester, A. R.; Emsley, J. W.; Luckhurst, G. R.; Storey, R. A., *Mol. Phys.* **1970**, 18, 481.
9. Hatch, G. F.; Kreilick, R. W., *J. Chem. Phys.* **1972**, 57, 3696.
10. Kreilick, R. W., *J. Chem. Phys.* **1966**, 45, 1922.
11. Hausser, H. H.; Brunner, Jochim, J. C., *Mol. Phys.* **1966**, 10, 253.
12. McConnell, H. M.; Chesnut, D., B., *J. Chem. Phys.* **1958**, 28, 107.
13. Kurland, R. J.; McGarvey, B. R., *J. Magn. Reson.* **1970**, 2, 286.
14. Lar Mar, G. N.; Horrocks, Jr., W. D., *NMR of Paramagnetic Molecules: Principles and Applications*, Academic Press, New York and London, 1973.
15. McConnell, H. M.; Robertson, R. E., *J. Chem. Phys.* **1958**, 27, 1361.
16. Jesson, J. P., *J. Chem. Phys.* **1967**, 579, 582.
17. Golding, R. M.; Pascual, R. O.; McGarvey, B. R., *J. Magn. Reson.* **1982**, 46, 30.
18. Golding, R. M.; Pascual, R. O.; Vrbrancich, *Mol. Phys.* **1976**, 31, 731.
19. Horrocks, Jr., W. D.; Greenberg, E. S., *Biochim. Biophys. Acta* **1973**, 322, 38.
20. Bohan, T. L., *J. Magn. Reson.* **1977**, 26, 109.

21. McGarvey, B. R., *Coord. Chem. Rev.* **1998**, 170, 75.

22. McGarvey, B. R.; Batista, N. C.; Bezerra, C. W. B.; Schultz, M. S.; Franco, D. W., *Inorg. Chem.* **1998**, 37, 2865.

23. Rinkevivius, Z.; Vaara, J.; Telyatnyk, L.; Vahtras, O., *J. Chem. Phys.* **2003**, 118, 2550.

24. Harriman, J. E., *Theoretical Foundations of Electron Spin Resonance*, Academic Press, New York, 1978.

25. Malkin, V. G.; Malkina, O. L.; Eriksson, L. A.; Salahub, D. R., In *Modern Density Functional Theory: A Tool for Chemistry; Theoretical and Computational Chemistry*; Seminario, J. M., Politzer, P., Eds.; Elsevier, Amsterdam, 1995., Vol. 2.

26. Schreckenbach, G., Ph. D. Thesis, The University of Calgary, Canada, 1996.

27. Helgaker, T.; Jaszuński M.; Ruud, K., *Chem. Rev.* **1999**, 99, 293.

28. Malkina, O. L.; Vaara, J.; Schimmelpfennig, B.; Munzarová, M.; Malkin, V. G.; Kaupp, M., *J. Am. Chem. Soc.* **2000**, 122, 9206.

29 Mao, J.; Zhang, Y.; Oldfield, E., *J. Am. Chem. Soc.* **2002**, 124, 13911.

30. Bertini, I.; Ciurli, S.; Dikiy, A.; Gasanov, R.; Luchinat, C.; Martini, G.; Safarov, N., *J. Am. Chem. Soc.* **1999**, 121, 2037.

31. Bertini, I.; Fernandez, C. O.; Karlsson, B. G.; Leckner, J.; Luchinat C.; Malmstrom, C.; Nersissian, A. M.; Pierattelli, R.; Shipp, E.; Valentine, J. J.; Vila, A. J., *J. Am. Chem. Soc.* **2000**, 122, 3701.

32. Jaszewski, A. R.; Jezierska, J., *Chem. Phys. Lett.* **2001**, 343, 571.

33. Swart, M., Ph. D. Thesis, Materials Science Center, Rijksuniversiteit Groningen (RuG), Nijenborgh 4 (2002).

34. Fujii, H., *J. Am. Chem. Soc.* **2002**, 124, 5936.

35. For high-spin states with significant (compared to *kT*) zero-field splitting (ZFS), each degenerate subset has to be treated separately. For example, a triplet state can be treated as a combination of an effective doublet and an effective singlet [See: A. Abragam, B. Bleaney, *Electron paramagnetic resonance of transition ions*, Clarendon, Oxford, **1970**].

36. Lohr, L. L.; Miller, J. C.; Sharp, R. R. *J. Chem. Phys.* **1999**, 111, 10148.

37. Becke, A. D. *J. Chem. Phys.* **1993**, 98, 5648.

38. Frisch, M. J.; Trucks, G. W.; Schelegel, H. B. et al. GAUSSIAN 98, A.7, Gaussian, Inc., Pittsburgh, PA, 1998.

39. St-Amant, A.; Salahub, D. R. *Chem. Phys. Lett.* **1990**, 169, 387.

40. Perdew, J. P.; Wang, Y. *Phys. Rev. B* **1992**, 45, 13244.

41. (a) Perdew, J. P.; Wang, Y. *Phys. Rev. B* **1986**, 33, 8800. (b) Perdew, J. P.; Wang, Y. *Phys. Rev. B* **1986**, 33, 8822.

42. Becke, A. D. *Phys. Rev. A* **1988**, 38, 3098.

43. Kutzelnigg, W.; Fleischer, U.; Schindler, M. In *NMR-Basic Principles and Progress*, Springer, Heidelberg, **1990**, Vol. 23, p165.

44. (a) Boys, S. F. *In Quantum theory of Atoms, Molecules and the Solid State*; Löwdin, P.-O., Ed., Academic Press, New York, 1966, p253.
(b) Pipek, J.; Mezey, P. Z. *J. Chem. Phys.* **1989**, 90, 4916.

45. Schreckenbach, G.; Ziegler, T. *J. Phys. Chem.* **1995**, *99*, 606-611.

46. Baerends, E. J.; Ziegler, T. et al. ADF 2003.2, Scientific Computing and Modelling NV, Amsterdam, http://www.scm.com/

47. Solomon, E.; Baldwin, M. J.; Lowery, M. D., *Chem. Rev.* **1992**, 92, 521.

48 Munzarova, M.; Kaupp, M. *J. Phys. Chem. A* **1999**, 103, 9966.

49. The X-leap program is distributed with the AMBER (version 6.0) program. (http://www.amber.ucsf.edu/amber/amber.html)

50. (a) Godbout, N; Salahub, D. R.; Andzelm, J.; Wimmer, E. *Can. J. Chem.* **1992**, 70, 560.
(b) Dolg, M.; Wedig. U.; Stoll, H.; Preuss, H. *J. Chem. Phys.* **1987**, 86, 866.

51. Zhang, Y.; Yang, W. *Phys. Rev. Lett.* **1998**, 80, 890.

52. All standard ADF basis sets are available on the Internet at http:// www.scm.com/Doc/atomicdata/.

53 Lenthe, E. van; Avoird, A. van der; Hagen, W. R.; Reijerse, E. J. *J. Phys. Chem. A* **2000**, 104, 2070.

54 Foreman, J. B.; Keith, T. A.; Wiberg, K. B.; Snoonian, J.; Frisch, M. J. *J. Phys. Chem.* **1996**, 100, 16098.

55. Barone, V., in *Recent Advances in Density Functional Methods, Part I*, Chong, D. P., Eds., World Scientific Publ. Co., Singapore, 1996.

Global Conclusions and Perspectives

The goal of this thesis was to develop a density functional approach to predict the NMR chemical shifts of paramagnetic species which play an important role in the study of the geometry and electronic structure of biomolecules. All through this thesis, we tried to keep in balance both theoretical and practical aspects for magnetic resonance simulations related to paramagnetic NMR chemical shifts.

Since unique features of the chemical shifts arise from strong interactions between nuclear and electronic spins, magnetic resonance parameters for both spins should be investigated. Therefore, we started this thesis by introducing general theories related to the parameters. We discussed the unit systems in electromagnetism and the Hamiltonian in a magnetic field (minimal coupling). We reviewed general density functional theories especially for the Kohn-Sham (KS) approach and approximate exchange-correlation functionals. Finally, we investigated magnetic resonance parameters such as NMR chemical shielding tensors, nuclear spin-spin coupling tensors, electron-nuclear hyperfine coupling tensors, and electronic g-tensors, based on density functional theory (DFT). We here focused on one-component methods with all-electron treatment, where the magnetic parameters are expressed as the second derivatives of the total electronic energy with respect to two perturbation parameters and spin-polarization of high-spin systems can be properly treated. In addition, we explained the theories based on the uncoupled DFT (UDFT) method which is independent of a current density. The reasons are as follows: (1) The working equations (3.41-3.44) of paramagnetic NMR shifts are directly related to NMR chemical shielding tensors, ESR A-tensors and g-tensors. To have consistent results, all terms should be treated in the same framework. (2) The shifts are mainly dominated by A-tensors (hyperfine tensors) and the spin-polarization density at the nucleus is, therefore, important. (3) Until now, correct current density functionals have not been developed and their effects on magnetic properties seem to be trivial [1]. (4) The one-component methods based on UDFT can be easily combined with the present QM/MM approach.

Recent experiments for paramagnetic NMR shifts largely focus on biological systems. Thus, in order to simulate the magnetic resonances of realistic models (including several thousand atoms), we used a simple but effective QM/MM method where the QM region is capped by one-electron quantum capping potentials (QCPs) and is electrostatically influenced by MM point charges. We proved that the QCPs and MM charges mainly contribute to the magnetic properties of the QM part through the KS orbitals and corresponding energies which are obtained from the self-consistent solutions of the magnetic field-free KS equations. Test calculations for a range of systems demonstrated that QCPs often reproduce well the chemical shielding tensors of the QM subsystem. Chemical shielding anisotropies (CSA) are much more sensitive to QCPs than isotropic shieldings but the sensitivity quickly disappears as the number of bonds from QCPs increases. For systems without strong electrostatic potentials, the QM/MM results do not show any great improvement for chemical shieldings over the pure QM results with QCPs. On the contrary, the shielding results of the pyrimidine base atoms in CMP which has strong electric fields in the phosphates are greatly improved by the present QM/MM approach. We extended this application to nuclear spin-spin coupling constants (CMP) and hyperfine coupling tensors (blue copper proteins, in this case, whole parts of proteins were included in the calculations). Both magnetic parameters are also greatly improved by the QM/MM approach. Unfortunately, the CSA of the oxygen atom in CMP and the hyperfine structures of β-hydrogen atoms in blue copper models show large deviations from full QM results since they are very close to the domain boundary. In this case, the short-range interactions at the boundary (induction, exchange repulsion, and charge transfer) should be included. From the practical point of view, these interactions can be included by a small increase in the size of the QM part or by expanding one-electron terms in the KS equations which can be achieved by the effective fragment potential (EFP) approach [2]. In the EFP, Coulombic, induction, and repulsive interactions are represented via one-electron terms in the Hamiltonian. However, these additional terms require some fitting procedures and we need code modification to use this approach in DFT frameworks, since the EFP was designed based on *ab initio* methods. On the other hand, from the theoretical point of view, we need to have accurate descriptions of the interactions in the boundary region within DFT frameworks. These can be achieved by

more sophisticated approaches. One of promising approaches is a hybrid QM/QM' method on the basis of DFT and DFT based tight-binding (DFT-TB) [3]. In this approach, we do not need to introduce unphysical boundary conditions such as frozen boundary orbitals and capping potentials. In addition, the short range interactions between the QM subsystems are treated correctly without any fitting parameters.

Finally, we derived the general equations for paramagnetic NMR chemical shifts, which can potentially handle most cases and we gave a short guidance for the way to derive a working equation for each different condition. We also provided working formulas for the implementation of a special case (an isolated Kramers doublet state with no thermally accessible excited states). The final formulas are composed of three terms: orbital shift, Fermi contact shift, and pseudocontact shift. The newly derived Fermi contact term is identical to McConnell's in Eq. (3.2) which exhibits a T^{-1} temperature dependence and mainly depends on the isotropic hyperfine constant A^{iso}. On the other hand, the newly derived pseudocontact term is different from McConnell's in Eq. (3.3) in that hyperfine coupling tensors are obtained by first principles methods without any empirical factors. By the new formula we can handle a strong spin delocalization beyond the limit of a point-dipole approximation. The orbital shifts were approximated by the NMR shifts of diamagnetic molecules which have the same geometries as paramagnetic molecules. For validation of the new equations (Eqs. 3.41-3.44), we have performed test calculations for some nitroxides, blue copper protein models, and heme protein models. we summarize the results as follows: (1) In most cases, the orbital shifts are small but not negligible and can be readily replaced by the chemical shifts of similar diamagnetic systems (2) The Fermi contact term dominates chemical shifts and determines all qualitative trends. (3) The calculated chemical shifts exhibit a strong dependence on structural parameters and, therefore, thermal motion effects should be considered for the paramagnetic NMR study even in an approximation. (4) In most cases, the pseudocontact contributions are small (less than 0.1 ppm for ^{1}H shift in nitroxides; less than 1 ppm ^{13}C shifts in nitroxides and ^{1}H shifts in blue copper proteins) while they are large and not negligible for ^{13}CN in iron porphyrin complexes which exhibit large g-tensor anisotropies. In consequence, it is clear that the present theoretical approach enables us to predict the NMR chemical shifts of

open-shell systems within DFT frameworks and to investigate the direct relationship between the chemical shifts and the electronic and molecular structures.

The present study shows the optimistic future of the DFT calculations for NMR chemical shifts in open-shell systems and at the same time leaves many works to be done. First, the orbital shielding contribution should be included to bring the calculated shifts into a better numerical agreement with experiment. It requires code modifications of ESR g-tensor programs based on one-component methods. In fact, this has already been done by Schreckenbach *et al.* in the ADF program [4] and, very recently, by Rinkevicius *et al.* [5] and also by us in the deMon program. Now, all we need are to apply these methods to various paramagnetic systems. Second, the chemical shifts of nitroxides exhibit a strong dependence on the solvent and motional effects. To predict experimental spectra, it is essential to calculate dynamic paramagnetic NMR shifts. The Car-Parrinello (CP) molecular dynamics (MD) method [6] can be combined with DFT calculations for magnetic properties. The CPMD method is already incorporated into the deMon program and it is possible to obtain motional average of the chemical shifts in DFT frameworks. Third, the active sites in blue copper proteins are surrounded by the other part. The paramagnetic NMR shifts of the active sites must be affected by the environment because they are very sensitive to minute variations of the electronic structure. QM/MM methods can be combined with paramagnetic NMR calculations. The geometry optimization of the active site can be done with the ONIOM type method [7] and the chemical shifts can be calculated with the present QM/MM method (details have explained in Chapter 2). Fourth, in the thesis, all calculations for paramagnetic NMR shifts have been performed using working equations for a special case (an isolated Kramers doublet states with no thermally accessible excited states). On the fundamental side, other working equations, which can treat strong zero-field splittings and thermal Zeeman mixing between ground and excited states within DFT frameworks, should be discussed.

References

1. (a) Lee, A. M.; Handy, N. C.; Colewell, S. M., *J. Chem. Phys.* **1995**, 103, 10095. (b) Schreckenbach, G., Ph. D. Thesis, The University of Calgary, Canada, 1996.
2. Gordon, M. S.; Freitag, M. A.; Banyopadhyay, P. B.; Jensen, J. H.; Kairys, V.; Stevens, W. J. *J. Phys. Chem. A* **2001**, 105, 293.
3. Seifert, G.; Porezag, D.; Frauenheim, TH. *Int. J. Quantum Chem.* **1996**, 58, 185.
4. Schreckenbach, G.; Ziegler, T. *J. Phys. Chem.* **1995**, 99, 606.
5. Rinkevivius, Z.; Vaara, J.; Telyatnyk, L.; Vahtras, O., *J. Chem. Phys.* **2003**, 118, 2550.
6. Car, R.; Parinello, M. *Phys. Rev. Lett.* **1985**, 55, 2471.
7. Maseras, F.; Morokuma, K. *J. Comput. Chem.* **1995**, 16, 1170.